

UNIVERSIDADE FEDERAL DO RIO GRANDE DO SUL
INSTITUTO DE GEOCIÊNCIAS
PROGRAMA DE PÓS-GRADUAÇÃO EM GEOCIÊNCIAS

**MODELO DEPOSICIONAL E EVOLUÇÃO BASEADOS EM
ATRIBUTOS SÍSMICOS DO *CANYON ALMIRANTE*
CÂMARA: NEÓGENO AO QUATERNÁRIO DA BACIA DE
CAMPOS, BRASIL**

SAMUEL APARECIDO DA SILVA CORRÊA

ORIENTADOR – Prof. Dr. Juliano Kuchle

Porto Alegre – 2024

UNIVERSIDADE FEDERAL DO RIO GRANDE DO SUL
INSTITUTO DE GEOCIÊNCIAS
PROGRAMA DE PÓS-GRADUAÇÃO EM GEOCIÊNCIAS

**MODELO DEPOSICIONAL E EVOLUÇÃO BASEADOS EM
ATRIBUTOS SÍSMICOS DO *CANYON ALMIRANTE*
CÂMARA: NEÓGENO AO QUATERNÁRIO DA BACIA DE
CAMPOS, BRASIL**

SAMUEL APARECIDO DA SILVA CORRÊA

ORIENTADOR – Prof. Dr. Juliano Kuchle

BANCA EXAMINADORA

Prof. Dr. Claiton Marlon dos Santos Scherer – Instituto de Geociências,
Universidade Federal do Rio Grande do Sul

Dra. Francyne Bochi do Amarante – Universidade Federal do Rio Grande do
Sul

Dra. Júnia Casagrande – PETROBRAS

Dissertação de Mestrado apresentada
como requisito parcial para a obtenção
do Título de Mestre em Ciências.

Porto Alegre – 2024

UNIVERSIDADE FEDERAL DO RIO GRANDE DO SUL

Reitor: Carlos André Bulhões Mendes

Vice-Reitora: Patrícia Pranke

INSTITUTO DE GEOCIÊNCIAS

Diretor: Nelson Luiz Sambaqui Gruber

Vice-Diretora: Tatiana Silva da Silva

CIP - Catalogação na Publicação

CORRÊA, SAMUEL APARECIDO DA SILVA
MODELO DEPOSICIONAL E EVOLUÇÃO BASEADOS EM
ATRIBUTOS SÍSMICOS DO CANYON ALMIRANTE CÂMARA: NEÓGENO
AO QUATERNÁRIO DA BACIA DE CAMPOS, BRASIL / SAMUEL
APARECIDO DA SILVA CORRÊA. -- 2024.
102 f.
Orientador: Juliano Kuchle.

Dissertação (Mestrado) -- Universidade Federal do
Rio Grande do Sul, Instituto de Geociências, Programa
de Pós-Graduação em Geociências, Porto Alegre, BR-RS,
2024.

1. CANYON SUBMARINO. 2. ATRIBUTOS SÍSMICOS. 3.
TURBIDITOS ADELGAÇADOS. 4. CANYON ALMIRANTE CÂMARA. 5.
GEOMORFOLOGIA SÍSMICA. I. Kuchle, Juliano, orient.
II. Título.

Elaborada pelo Sistema de Geração Automática de Ficha Catalográfica da UFRGS com os dados fornecidos pelo(a) autor(a).

*Esta dissertação é dedicada à minha amada família
e consagrada à Santíssima Virgem Maria,
mãe e intercessora por excelência.*

AGRADECIMENTOS

Primeríssimamente, agradeço a *Deus, Senhor* da minha vida e *Pastor*, que sempre me inspirou e edificou minha sabedoria.

Aos meus pais, Mauricélia e Adilson, que sempre estiveram ao meu lado e por todo o apoio e incentivo inã minha educação.

Aos meus amados irmãos Saulo e Eduardo, por todo o carinho e apoio. Em especial, ao meu irmão Saulo pelas calorosas discussões de geoffísica que muito contribuíram para o trabalho e pelo valoroso auxílio prestado em seu desenvolvimento e preparo.

À minha amada avó, Aurea, pela sua generosidade e afeto.

Agradeço, especialmente, à minha amada noiva e futura esposa, Verónica Ortiz Kaempfer, pelo apoio e companheirismo ao longo desta importante etapa da minha vida. Sua dedicação, carinho e amor são partes fundamentais deste trabalho.

Ao meu orientador e amigo, Juliano Kuchle, pela valiosa orientação, permanente incentivo, pelos ensinamentos e discussões, e, principalmente, pela paciência durante essa jornada de trabalho.

A todos os colegas e amigos do Departamento de Estratigrafia, pelos conhecimentos compartilhados e pelo companheirismo ao longo deste trabalho.

Ao amigo Carlinhos Feijó, pela organização, amizade e pela parceria durante a minha estadia no Departamento de Estratigrafia.

À Universidade Federal do Rio Grande do Sul (UFRGS) e ao Programa de Pós-Graduação em Geociências (PPGGEO) pelo ensino e infra estrutura cedida.

Ao laboratório de Sismoestratigrafia da UFRGS, especialmente ao Rodrigo (o "Alemão"), pelo suporte técnico e computacional cedido à realização deste trabalho.

À Shell Brasil Petróleo Ltda e à Agência Nacional do Petróleo, Gás Natural e Biocombustíveis (ANP) pela concessão dos dados sísmicos utilizados e pelo compromisso com o investimento em pesquisa e desenvolvimento.

Ao Conselho Nacional de Desenvolvimento Científico e Tecnológico (CNPq) pelo fomento e auxílio financeiro a esta dissertação de mestrado.

A todos muito obrigado!

“Educar é promover à prole o estado perfeito do homem como homem, isto é, o estado da virtude”.

São Tomás de Aquino

RESUMO

Canyons submarinos constituem importantes feições geomorfológicas das margens continentais, desempenhando um papel fundamental como condutos para o transporte de sedimentos da plataforma continental para o oceano profundo. Estão associados a praticamente todas as etapas de evolução de um sistema turbidítico, transportando uma grande variedade de tamanhos de grãos (argilas a cascalhos), podendo hospedar reservatórios de hidrocarbonetos. Muitos canyons e preenchimentos de canais correspondentes, frequentemente, possuem uma arquitetura complexa com múltiplas superfícies internas de erosão, resultado da evolução a longo prazo e da interação da erosão do canal, degradação, migração lateral e deposição. O canyon do sistema turbidítico Almirante Câmara desenvolve-se entre as isóbatas de 300 e 1200 m, cuja desembocadura do seu canal turbidítico interior assenta-se sobre o platô de São Paulo, adjacente ao talude da Bacia de Campos. Neste trabalho, combinamos atributos sísmicos complexos e análise espectral para investigar a morfologia, elementos arquiteturais, litologias, padrões de preenchimento, e evolução do Canyon Almirante Câmara da Bacia de Campos. A interpretação de detalhe destas análises permite distinguir quatro superfícies erosivas ao longo da evolução do canyon. Estes canyons têm orientação ENE-SSW, formato em U passando ascendentemente para o formato em V, aproximadamente perpendiculares ao talude continental, e relevo variando entre 350-540m e larguras de 1-7,1 km. Além disso, parece haver uma relação contemporânea entre a atividade das falhas nos estágios iniciais da evolução do Canyon Almirante Câmara. Um modelo evolutivo inédito do canyon é aqui proposto, que é dividido em quatro estágios: Estágio I – Superfície de Base Erosional (EBS), Estágio II – Superfície Almirante Câmara 1 (ACS1), Estágio III – Superfície Almirante Câmara 2 (ACS2), e Etapa IV – Superfície Almirante Câmara (ACS3). As características erosivas destas superfícies permitiram uma correlação interpretativa com a curva global do nível do mar durante o Cenozóico. Estes resultados pretendem esclarecer bem como contribuir para o conhecimento de evolução do canyon.

Palavras-Chave: Canyon submarino, Atributos sísmicos, Turbiditos adelgaçados, *Canyon Almirante Câmara*, Geomorfologia sísmica.

ABSTRACT

Submarine canyons constitute important geomorphological features of continental margins, playing a fundamental role as conduits for transporting sediments from the continental shelf to the deep ocean. They are associated with practically all stages of evolution of a turbidite system, transporting a wide variety of grain sizes (clays to gravels), and can host hydrocarbon reservoirs. Many canyons and corresponding channel fills often have a complex architecture with multiple internal erosion surfaces resulting from long-term evolution and the interaction of channel erosion, degradation, lateral migration, and deposition. The canyon of the Almirante Câmara turbidite system develops between the 300 and 1200 m isobaths, whose mouth of its interior turbidite channel sits on the São Paulo plateau, adjacent to the slope of the Campos Basin. In this work, we combine complex seismic attributes and spectral analysis to investigate the morphology, architectural elements, lithologies, filling patterns, and evolution of the Almirante Câmara Canyon of the Campos Basin. The detailed interpretation of these analyses allows us to distinguish four erosion surfaces along the evolution of the canyon. These canyons have an ENE-SSW orientation, a U-shaped form passing upward to a V-shaped form, approximately perpendicular to the continental slope, and relief varying between 350-540m and widths of 1-7.1 km. Furthermore, there appears to be a contemporaneous relationship between fault activity in the early stages of the Almirante Câmara Canyon evolution. An unprecedented evolutionary model of the canyon is proposed here, which is divided into four stages: Stage I – Erosional Base Surface (EBS), Stage II – Admiral Chamber Surface 1 (ACS1), Stage III – Admiral Chamber Surface 2 (ACS2), and Stage IV – Surface Admiral Chamber (ACS3). The erosion characteristics of these surfaces allowed an interpretative correlation with the global sea level curve during the Cenozoic. These results aim to clarify and contribute to the knowledge of the evolution of the canyon.

Keywords: Submarine canyon, Seismic attributes, Thin-bedded turbidites, *Almirante Câmara Canyon*, Seismic geomorphology.

LISTA DE FIGURAS

Figure 1 – Localização do <i>Canyon Almirante Câmara</i> na Bacia de Campos. a) localização da Bacia de Campos no sudeste da margem leste brasileira; b) mapa da Bacia de Campos mostrando seus limites com a Bacia do Espírito Santo e a Bacia de Santos, respectivamente; c) mapa de detalhe do grupo nordeste de canyons da Bacia de Campos. O <i>Canyon Almirante Câmara</i> está localizado na porção extrema noroeste e a área de estudo destacada por um quadrado amarelo.	20
Figure 2 - Carta cronoestratigráfica do Cenozóico na Bacia de Campos. (Modificado de Winter et al., 2007). A área sombreada cinza compreende o intervalo estratigráfico de interesse deste trabalho, limitado inferiormente pelo Marco Cinza (linha vermelha), e geologicamente correspondente à discordância entre o Mioceno Médio e Superior (Viana et al., 1990; Silva, 1992). A linha azul representa o Marco Azul de idade do Oligoceno Inferior (Rangel et al., 1994; Winter et al., 2007).	24
Figure 3 - a) Mapa de localização de sistemas de leques submarinos modernos. b) Seções transversais comparadas de canyons submarinos com um canyon continental (Grand Canyon). Exagero vertical = 48.5. (Modificado de Normark e Carlson, 2003).	25
Figure 4 – Canyons da margem da Guiné Equatorial. Os canyons Tipo I indentam a margem da plataforma e tem ligação com a bacia onde depositou leques submarinos. Os canyons do Tipo II estão restritos ao talude sem ligação com a quebra da plataforma e a área da bacia profunda (Modificado de Jobe et al., 2011).	26
Figure 5 – Diagramas de blocos esquemáticos de sistemas de leques submarinos de águas profundas de acordo com o tamanho de grão dominante. Elementos arquiteturais: CS: <i>Canyon submarino</i> ; DFM: <i>Depósitos de fluxo de massa</i> ; DM: <i>Dique marginal</i> ; C: <i>Canal submarino</i> ; DCS: <i>Depósitos de crevasse splay</i> , DO: <i>Depósitos de overbank</i> ; LD: <i>Lobo deposicional</i> . (Modificado de http://www.sepmstrata.org/page.aspx?pageid=40).	27
Figure 6 – a) mapa morfobatimétrico de canyons submarinos mostrando a geometria dos canyons em forma de U e V, terraços, voçorocas, movimentos de massa e cabeceiras de canyons. Exagero vertical = 10.0. b) perfis transversais dos canyons (ABd1 e ABd2 = canais distributivos do Canyon Areia Branca). (Modificado de Almeida et al., 2015).	30
Figure 7 – Representação do traço sísmico complexo em um diagrama isométrico. O traço complexo (linha verde) é um vetor que descreve um movimento helicoidal ao longo do eixo do tempo. O traço sísmico (linha azul) e de quadratura (linha vermelha) são representados em planos perpendiculares (Modificado de Taner et al., 1979).	34
Figure 8 – Traço sísmico analítico, mostrando a parte real (linha azul) e a quadratura do traço (linha vermelha).	36
Figure 9 – Modelo evolutivo do <i>Canyon Almirante Câmara</i> e de seu preenchimento. Quatro estágios foram propostos: (a) Estágio I (EBS): erosão inicial proeminente do canyon, com deposição de lóbulos arenosos amalgamados de estratos finos; b) Estágio II (ACS1): canyon de largura média, com depósitos de barras arenosas amalgamadas e lóbulos turbidíticos; c) Estágio III (ACS2): canyon de largura média com bypass de sedimentos transportados para o talude inferior ou planície abissal profunda; e d) Estágio IV (ACS3): canyon amplo e profundo, com deposição de turbiditos de estratos finos arenosos. A agradação desses depósitos representa uma miríade de eventos erosivos, de bypass e deposicionais (<i>waxing-waning cycles</i>), preservando uma complexa história de corte e preenchimento.	39
Figure 10 - Curva eustática tectôno-glacial Neógeno-Quaternário e correção tempo-tempo de superfície. As linhas horizontais (vermelha, laranja, verde e azul) atribuem verticalmente	

a idade de cada superfície. a) Curva de tendências residuais do nível do mar e alterações esquemáticas de amplitude associadas (modificado de van der Meer et al., 2022). b) Diagrama de correlação tempo-tempo. As setas para a esquerda e para a direita indicam a subida e a descida do nível do mar, respectivamente. As letras (x, y, z, a' e b') e o sombreamento destacam as sequências estratigráficas ligadas à discordância. A linha pontilhada é a tendência eustática de longo prazo (>50 milhões de anos)..... 41

Figure 11 - The location of the *Almirante Câmara Canyon* in the Campos Basin. a) Location of the Campos Basin in the southeastern of the Brazilian's eastern margin; b) Map of the Campos Basin showing its limits with Espírito Santo Basin and Santos Basin; c) Detail map of the Northeast Group of canyons in the Campos Basin, the *Almirante Câmara Canyon* is located in the extreme northwestern portion, and the study area highlighted by a yellow square. 53

Figure 12 - Chronostratigraphic chart of the Cenozoic in the Campos Basin. (Modified from Winter et al., 2007). The grayscale-shaded area comprises the stratigraphic interval that is of interest to this work, inferiorly limited by the Gray Marker (red line) and geologically correspondent to the unconformity between the Middle and Upper Miocene (Viana et al., 1990; Silva, 1992). The blue line represents the Blue Mark of the Inferior-Oligocene age (Rangel et al., 1994; Winter et al., 2007). 55

Figure 13 - Schematic workflow showing the stages and implemented methodology in the processing to optimize the seismic analysis and interpretation of the 3D seismic data..... 58

Figure 14 - Idealized seismogram showing the principles and geological significance of the Elementary Seismic-Layer (ESL), a) t_1 and t_2 considered such as the top and base of the layer at a determined interval t ; b) hypothetical period T for the highest frequency observed in the seismic data; c) moving window taking the length M equal to $T/2$ (Modified from Bulhões and Amorim, 2005). 62

Figure 15 - Panoramic view of the co-visualization for the amplitude and complex seismic attributes used for the horizon's interpretation from the 3D seismic data. Inline 8514 shows the cosine of the Instantaneous Phase attribute. The inline 8747 shows the AVT attribute. The cross-line 4278 shows the Instantaneous phase. The z-slice 952 shows the amplitude data. 63

Figure 16 - Power spectral density extracted from each interpreted horizon along the zone-of-interest, showing the central frequencies chosen for each RGB composition: a) 15Hz, 30Hz, and 40Hz; b) 35Hz, 45Hz, and 55Hz; and c); d) with the same frequencies of 30Hz, 45Hz, and 55Hz, respectively. The color below the power spectral density curves represents a relative distribution of Power (dB). 66

Figure 17 - 3D seismic volume showing a summarized view of stacked interpreted horizons. The surfaces show canyon-valley systems that cross the volume. Opacity has been applied in the surfaces ACS1 (pink line), ACS2 (green line), and ACS3 (blue line) to enhance the visualization of its lateral extension, depth, and carved features of the canyon-valley systems. The crossline 4669 is shown in detail in Fig. 18..... 69

Figure 18 - Crossline 4669 shows in detail the interpreted horizons across the seismic amplitude and three other seismic attributes. a) Crossline 4669 of amplitude seismic data showing the EBS, ACS1, AC2, and ACS3 horizons, stacked channel forms (HARs), MTD, and secondary smaller channels. b) Crossline 4669 of Instantaneous Phase attribute showing the EBS, ACS1, AC2, and ACS3 horizons with different phase content on seismic data. c) Crossline 4669 of Cosine of Instantaneous Phase attribute showing the EBS, ACS1, AC2, and ACS3 horizons normalized at a grayscale. d) Crossline 4669 of AVT attribute

showing the EBS, ACS1, AC2, and ACS3 horizons, stacked channel forms (HARs), MTD, and secondary smaller channels. The combined use of the seismic attributes brings out details of the canyons' infill and assists in resolving its internal complexity. 70

Figure 19 - a) 3D topographic map of the Erosional Base Surface (EBS) in TWT [ms]. The perspective view shows a central carved deep canyon, moderately sinuous, with secondary smaller channels. b) 2D view of the EBS topographic map. c) Similarity attribute map of the EBS. d) RGB frequency color blend (15Hz, 30Hz, and 40Hz), showing internal thickness variability throughout the canyon and channel deposits. High-frequency responses indicate thin-thickness deposits. e) Envelope attribute map of the EBS..... 72

Figure 20 - a) 3D topographic map of the Almirante Câmara Surface 1 (ACS1) in TWT [ms]. b) 2D view of the ACS1 topographic map. c) Similarity attribute map of the ACS1. d) RGB frequency color blend (35Hz, 45Hz, and 55Hz), showing internal thickness variability throughout the canyon and channel deposits. High-frequency responses indicate thin-thickness deposits. e) Envelope attribute map of the ACS1. 74

Figure 21 - a) 3D topographic map of the Almirante Câmara Surface 2 (ACS2) in TWT [ms]. b) 2D view of the ACS2 topographic map. c) Similarity attribute map of the ACS2. d) RGB frequency color blend (30Hz, 45Hz, and 55Hz), showing internal thickness variability throughout ACS2. Dark opacity indicates low-frequency responses, due to low tuning thickness. e) Envelope attribute map of the ACS2..... 76

Figure 22 - a) 3D topographic map of the Almirante Câmara Surface 3 (ACS3) in TWT [ms]. b) 2D view of the ACS3 topographic map. c) Similarity attribute map of the ACS3. d) RGB frequency color blend (30Hz, 45Hz, and 55Hz), showing internal thickness variability throughout the canyon and channel deposits. High-frequency responses indicate thin-thickness deposits. e) Envelope attribute map of the ACS3. 78

Figure 23 - 2D view attribute comparison of the EBS: a) Envelope attribute map of the EBS. b) RGB frequency color blend (15Hz, 30Hz, and 40Hz) of the EBS. c) Envelope attribute map of the EBS. d) RGB frequency color blend (15Hz, 30Hz, and 40Hz) of the EBS. High Envelope responses represent amalgamated thin-bedded sandy lobes, crevasse-splay, and LAD. High-frequency responses indicate thin-thickness turbidite and channel deposits. Refer to Figure 17a for a detailed reference location of this figure. 80

Figure 24 - 2D view attribute comparison of the ACS1 and ACS2: a) Envelope attribute map of the ACS1. b) RGB frequency color blend (35Hz, 45Hz, and 55Hz) of the ACS1. c) Envelope attribute map of the ACS2. d) RGB frequency color blend (30Hz, 45Hz, and 55Hz) of the ACS2. High Envelope responses represent amalgamated sandy bars, sandy turbidite lobes, and ancient exposed sandy deposits. High-frequency responses indicate thin-thickness turbidite and channel deposits. Refer to Figs. 18a and 19a for a detailed reference location of this figure..... 82

Figure 25 - 2D view attribute comparison of the ACS3: a) Envelope attribute map of the ACS3. b) RGB frequency color blend (30Hz, 45Hz, and 55Hz) of the ACS3. High Envelope and high-frequency responses represent thin-bedded ribbon-shaped channel deposits. Refer to Figure 20a for a detailed reference location of this figure. 83

Figure 26 - 2D view similarity attribute maps from the initial stage (a) to the late stage (d) throughout the canyon development. From a to d, the horizons show a progressive decrease of faults. (e) shows a composite plan view of the canyon migration process by stacking surfaces. Canyon's limit is represented by red, orange, green, and blue dotted lines, regarding the EBS, ACS1, ACS2, and ACS3. Opacity has been applied to the surfaces to enhance the visualization of faults (yellow)..... 85

Figure 27 - Evolutionary model illustrating the evolution of the Almirante Câmara Canyon and its fill. Four stages have been proposed: (a) Stage I (EBS): Initial prominent erosion of the canyon, with deposition of amalgamated thin-bedded sandy lobes; b) Stage II (ACS1): Medium-wide canyon, with deposits of amalgamated sandy bars and turbidite lobes; c) Stage III (ACS2): Medium-wide canyon, with sediment bypass transported to the lower slope or deep abyssal plain; and d) Modern Stage (ACS3): Wide and over-deepening canyon, with deposition of thin-bedded sandy-prone turbidites. The aggradation of these deposits represents a myriad of erosive, bypass, and depositional events (waxing-waning cycles), preserving a complex cut-and-fill history. Figures (a) to (d) show a multi-attribute composition of Envelope and Similarity. 88

Figure 28 - Neogene-Quaternary tectono-glacial eustatic curve and time-time surface correlation. The horizontal lines (red, orange, green, and blue) assign vertically the age of each surface. a) Curve of residual sea level trends and associated schematic amplitude changes (modified from van der Meer et al., 2022). b) Diagram of time-time correlation. Left-arrows and right-arrows indicate rising sea level and falling sea level, respectively. The letters (x, y, z, a', and b') and shading highlight the unconformity-bound stratigraphic sequences. The dotted line is the long-term (>50Myr) eustatic trend. 90

LISTA DE ABREVIATURAS E SIGLAS

ACS1 – Almirante Câmara Surface 1

ACS2 – Almirante Câmara Surface 2

ACS3 – Almirante Câmara Surface 3

ANP – Brazilian National Agency of Petroleum, Natural Gas and Biofuels/Agência Nacional do Petróleo, Gás Natural e Biocombustíveis

AVT – Amplitude Volume Technique

BP – Before Present

CNPq – National Council for Scientific and Technological Development of Brazil/
Conselho Nacional de Desenvolvimento Científico e Tecnológico

DHI – Direct Hydrocarbon Indicator

DSMF – Dip Steered Median Filter

E – East/Leste

EBS – Erosional Base Surface

ENE – East-northeast/És-nordeste

ESL – Elementary Seismic Layer

FFT – Fast Fourier Transform

HAR – High Amplitude Reflector

LAD – Lateral Accretion Deposits

LGM – Last Glacial Maximum

MTD – Mass Transport Deposits

N – North/Norte

NE – Northeast/Nordeste

NNW – North-northwest/Nor-Noroeste

NW – Northwest/Noroeste

PHHA – Positive High Amplitude Anomalies

RMS – Root Mean Square

S – South/Sul

SD – Spectral Decomposition

SE – Southeast/Sudeste

S_R – Sinuosity ratio

SSE – South-southeast/Su-Sudeste

SSW – South-Southwest/Su-sudoeste

STFT – Short-time Fourier Transform

SW – Southwest/Sudoeste

TGE – Tectono-glacial-eustatic

TWT – Two-Way Travel Time

UFRGS – Universidade Federal do Rio Grande do Sul

W – West/Oeste

LISTA DE UNIDADES

km – quilômetro/kilometer

Km² – quilômetro quadrado/square kilometer

m – metro/meter

Ma – Milhões de anos/*Mega annum*

ms – milissegundo/milisecond

$m \cdot s^{-1}$ – metros por segundo/meters per second

SUMÁRIO

1. INTRODUÇÃO	18
1.1. Objetivos.....	19
1.1.1. Objetivo geral	19
1.1.2. Objetivos específicos.....	19
2. ESTADO DA ARTE	20
2.1. Bacia de Campos.....	20
2.1.1. Localização	20
2.1.2. Arcabouço tectônico.....	21
2.1.3. Arcabouço estratigráfico.....	22
2.2. Canyons submarinos	24
2.2.1. Tipos de canyons submarinos.....	26
2.2.2. Morfologia de canyons submarinos.....	28
2.3. <i>Canyon Almirante Câmara</i>	29
2.4. Análise do traço complexo e atributos sísmicos.....	31
2.4.1. Transformada de Hilbert.....	32
2.4.2. O traço sísmico complexo	34
2.4.3. Atributos sísmicos	37
3. SÍNTESE DOS RESULTADOS	39
4. REFERÊNCIAS BIBLIOGRÁFICAS	42
5. ARTIGO CIENTÍFICO	48
5.1. Comprovante de submissão	48
5.2. CORPO INTEGRAL DO ARTIGO SUBMETIDO – SEISMIC ATTRIBUTE-BASED DEPOSITIONAL MODEL AND EVOLUTION OF LARGE-SIZE CANYON – <i>ALMIRANTE CÂMARA</i> (NEOGENE TO QUATERNARY) OF CAMPOS BASIN, BRAZIL	49
5.3. Abstract.....	49
5.4. Introduction	51
5.5. Geological setting	52
5.5.1. Stratigraphy of the Campos Basin	52
5.5.2. The <i>Almirante Câmara Canyon</i>	55
5.6. Methodology	56
5.6.1. Dataset and Relative Age calibration.....	56
5.6.2. <i>SteeringCube</i> and <i>Dip Steered Median Filter (DSMF)</i>	58
5.6.3. Complex seismic trace attributes.....	59
5.6.4. Advanced seismic attributes.....	65

5.7. Results and Interpretations	68
5.7.1. <i>Erosional Base Surface (EBS)</i>	71
5.7.2. <i>Almirante Câmara Surface 1 (ACS1)</i>	73
5.7.3. <i>Almirante Câmara Surface 2 (ACS2)</i>	75
5.7.4. <i>Almirante Câmara Surface 3 (ACS3)</i>	77
5.7.5. <i>Depositional architecture analysis and sedimentary implications</i>	79
5.7.5.1. Comparison of EBS attribute responses	79
5.7.5.2. Comparison of ACS1 and ACS2 attribute responses	81
5.7.5.3. Comparison of ACS3 attribute responses	83
5.8. Discussions.....	84
5.8.1. <i>Structural control on sea-floor topography</i>	84
5.8.2. <i>Canyon's sediment supply</i>	86
5.8.3. <i>Insights into the canyon's filling and evolution</i>	86
5.8.4. <i>Tie-surfaces and global mean sea level curve</i>	89
5.9. Conclusions	91
5.10. Acknowledgments.....	92
5.11. References	93

ESTRUTURA DA DISSERTAÇÃO

Esta dissertação de mestrado está estruturada e centrada no artigo “*Seismic attribute-based depositional model and evolution of large-size canyon Almirante Câmara (Neogene to Quaternary) of Campos Basin, Brasil*”, submetido ao periódico *Marine and Petroleum Geology*. A sua organização compreende os seguintes capítulos principais:

- i) Capítulo 1 (Introdução): apresenta a introdução sobre o tema central, bem como a descrição dos objetivos da dissertação;
 - ii) Capítulo 2 (Estado da arte): apresenta o contexto geológico da Bacia de Campos, canyons submarinos, o traço sísmico complexo, e os atributos sísmicos,
 - iii) Capítulo 3 (Síntese dos resultados): apresenta de forma breve, sem ser simplista, uma síntese dos resultados obtidos;
 - iv) Capítulo 4 (Referências bibliográficas): contém as referências bibliográficas do estado da arte da dissertação; e
 - v) Capítulo 5 (Artigo científico e corpo principal da dissertação): contém o artigo escrito em língua inglesa, produto de desenvolvimento de pesquisa junto a este programa de pós-graduação;
-

1. INTRODUÇÃO

Canyons submarinos representam um dos principais componentes que contribuem para a modelagem do fundo do mar. Além de constituírem uma feição fisiográfica comum nas margens continentais e atuarem como canais importantes para o transporte de sedimentos da plataforma continental e talude superior para o oceano profundo, representam a principal fonte pontual de sedimentos para sistemas turbidíticos (Shepard, 1981; Droz et al., 1996; Babonneau et al., 2002; Mchug et al., 2002; Canals et al., 2006; Harris and Whiteway, 2011). Normalmente ocorrem como vales estreitos (alguns quilômetros) e profundos (centenas de metros), em forma de V, com paredes íngremes, podendo estar diretamente conectados e atribuídos a grandes sistemas fluviais continentais, que foram capazes de penetrar na margem da plataforma e transportar sedimentos para o fundo do mar (Droz et al., 1996; McHug et al., 1998; Babonneau et al., 2002; Wynn et al., 2007; Jobe et al., 2011). Apesar de constituírem zonas de *bypass* de sedimentos, com pouca acumulação de sedimentos dentro do canyon até que ele deixe de ser um conduto ativo, frequentemente podem hospedar reservatórios de hidrocarbonetos ricos em areia (Stow e Mayall, 2000; Posamentier, 2003; Mayall et al., 2006; Meiburg e Kneller, 2010). Com base em dados sísmicos 3D e o uso combinado de atributos sísmicos, apresentamos neste trabalho um modelo evolutivo e de preenchimento inédito do *Canyon Almirante Câmara* durante o Neógeno ao Quaternário na margem da plataforma continental da Bacia de Campos, ademais de estabelecer uma correlação tentativa dos estágios evolutivos com a curva eustática global.

1.1. Objetivos

A presente dissertação tem como objetivos:

1.1.1. Objetivo geral

Construir um modelo evolutivo deposicional do *Canyon Almirante Câmara* para o intervalo de estudo Neógeno-Quaternário;

1.1.2. Objetivos específicos

(i) reconhecer e mapear as principais superfícies de expressão regional e de significado erosivo;

(ii) mapear a geometria, elementos arquiteturais, distribuição, e padrão de preenchimento dos depósitos arenosos internos ao *Canyon Almirante Câmara* ao longo da sua evolução;

(iii) através da análise espectral e do uso combinado de atributos sísmicos complexos, investigar e correlacionar os tipos litológicos aos depósitos internos e externos ao canyon; e

(iv) correlacionar tentativamente as superfícies mapeadas à uma curva eustática tectôno-glacial global.

2. ESTADO DA ARTE

2.1. Bacia de Campos

2.1.1. Localização

A Bacia de Campos está localizada na margem continental brasileira. Ocupa uma área de cerca de 120.000 km² até a batimetria de 3500 m e, deste total, apenas 500 km² situa-se na parte terrestre (Dias et al., 1990). Limita-se a norte com a Bacia do Espírito Santo, pelo Alto de Vitória, e a sul, com a Bacia de Santos, pelo Alto de Cabo Frio. A área de estudo é mostrada na Fig. 1 abaixo.

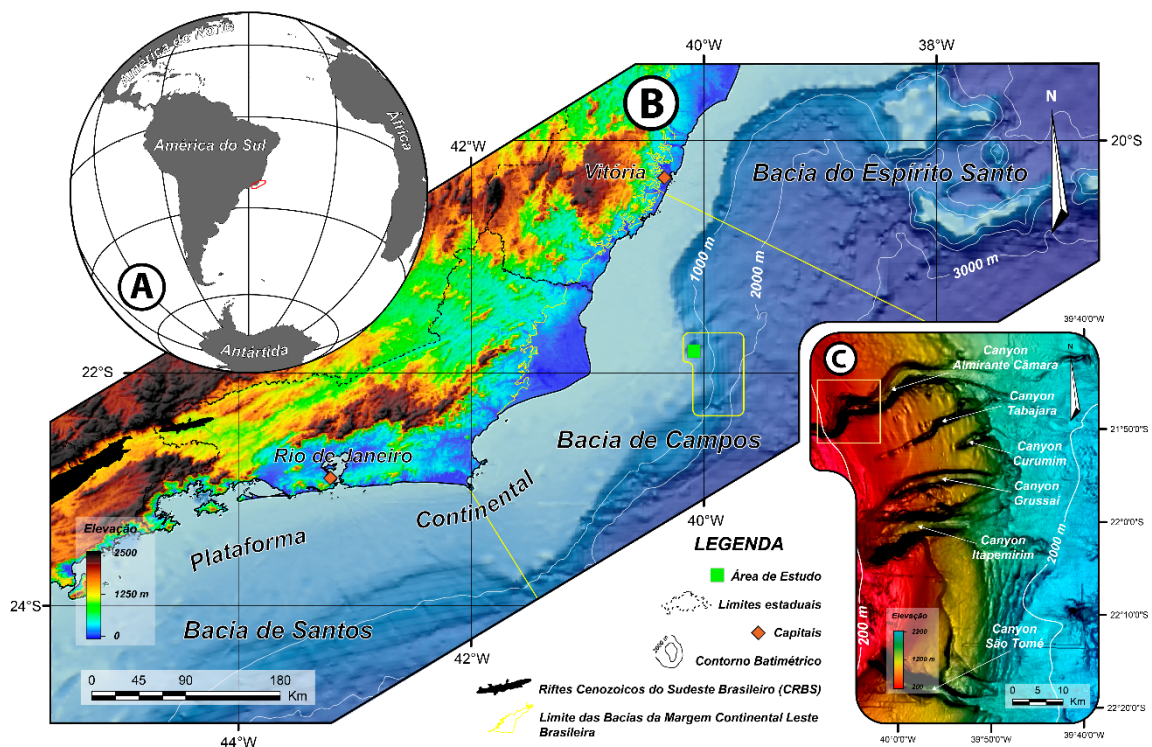


Figure 1 – Localização do *Canyon Almirante Câmara* na Bacia de Campos. a) localização da Bacia de Campos no sudeste da margem leste brasileira; b) mapa da Bacia de Campos mostrando seus limites com a Bacia do Espírito Santo e a Bacia de Santos, respectivamente; c) mapa de detalhe do grupo nordeste de canyons da Bacia de Campos. O *Canyon Almirante Câmara* está localizado na porção extrema noroeste e a área de estudo destacada por um quadrado amarelo.

2.1.2. Arcabouço tectônico

Assim como as bacias da margem leste brasileira, a Bacia de Campos tem sua gênese associada à ruptura do Continente Gondwana e à abertura do Oceano Atlântico Sul, apresentando dois estilos tectônicos distintos (Mohriak et al., 2008; Karner, 2000). O primeiro associado à tectônica diastrófica, que afeta os sedimentos da fase rift, e o segundo associado à tectônica adiastrófica, relacionada à halocinese, que atua sobre os sedimentos da fase transicional e drifte (Chang et al., 1990).

A fase rifte é caracterizada por estruturas do tipo *horst*, *grabens* e *meio-grabens* alongados preferencialmente na direção NE-SW. As falhas sintéticas e antitéticas que limitam essas estruturas possuem rejeitos que variam de dezenas de metros até cerca de 2500 m. As falhas de direção NNW-SSE e E-W são menos expressivas na bacia (Dias et al., 1990). Nesse arcabouço estrutural, destaca-se a Charneira de Campos, que segmenta regiões de embasamento raso e embasamento profundo, cujo bloco baixo se depositou uma espessa seção lacustrina da fase rifte, as quais constituem rochas geradoras da Bacia de Campos (Dias et al., 1990).

A fase pós-rifte é caracterizada por falhas lítrica relacionadas a halocinese, associadas a anticlinais, calhas, domos, e diápiros de sal. Reativações posteriores relacionadas à falhamentos do embasamento também afetaram localmente os sedimentos da fase transicional e drifte da bacia (Chang et al., 1990; Dias et al., 1990).

2.1.3. Arcabouço estratigráfico

O trabalho pioneiro de Schaller (1973) estabelece a primeira carta cronoestratigráfica para a Bacia de Campos, posteriormente sendo modificada pelos trabalhos de Rangel et al. (1994) e Winter et al. (2007). Genericamente, o arcabouço tectonoestratigráfico da Bacia de Campos pode ser caracterizado por três superssequências distintas (Chang et al., 1990; Winter et al., 2007).

A superssequência Rifte corresponde aos basaltos e conglomerados menores da Formação Cabiúnas (Hauteriviano) e da porção inferior do Grupo Lagoa Feia, definido pelas formações Atafona, Coqueiros e Itabapoana (Winter et al., 2007). A Formação Cabiúnas é constituída pro basaltos amigdaloidais interdigitados com conglomerados polimíticos (Rangel et al., 1994). Datações utilizando o método K-Ar indicam idades entre 122 e 134 Ma (Mizusaki et al., 1989). A Formação Atafona de idade Barremiana consiste em siltitos, arenitos, folhelhos lacustres, e calcários finos lacustres intercalados. A Formação Coqueiros sobrejacente é de idade Barremiana Superior a Aptiana Inferior (Rangel e Carminatti, 2000). A Formação Itabapoana, constituída de leques aluviais/deltas proximais e sedimentos lacutres distais, é também de idade Barremiana a Aptiana Inferior, lateralmente equivalente às formações Atafona e Coqueiros (Winter et al., 2007).

A supersequência Pós-Rifte é caracterizada pela deposição de sedimentos siliciclásticos, carbonáticos e evaporíticos, entendendo-se até o Aptiano. A sedimentação clástica ocorreu nas porções proximais da bacia, e padrão deposicional progradacional. De outro modo, a sedimentação carbonática ocorreu na porção superior deste intervalo, em padrão retrogradacional. O topo desta superssequência é representado por um ambiente marinho restrito associado a

condições áridas a semi-áridas, correspondentes aos pacotes evaporíticos da Formação Retiro (Winter et al., 2007).

A superssequência de Drifte, ou superssequência Marinha, iniciou-se após o término dos eventos de rifteamento e a abertura efetiva do Oceano Atlântico Sul. Esta sucessão compreende sedimentos marinhos dos Grupos Macaé e Campos depositados em regime de subdiência térmica associada a tectônica dominada pela gravidade (Winter et al., 2007), ocasionada principalmente pela remobilização de evaporitos. O Grupo Macaé (Albiano Inferior ao Cenomaniano) consiste predominantemente de calcários e margas, enquanto o Grupo Campos (Turoniano ao Recente) consiste predominantemente de sedimentos siliciclásticos, depositados em ambientes marinhos progressivamente mais profundos (Winter et al., 2007).

A partir do Paleoceno Superior (Fig. 2) se instala na bacia uma configuração francamente marinha regressiva, permanecendo até os dias atuais. Esta configuração é marcada por um conjunto de sedimentos clásticos progradantes, e é constituída por sistemas deposicionais de leques costeiros e plataformas carbonáticas (Formação Emborê) até sistemas de talude e bacia profunda (Formação Ubatuba). A proeminente progradação clástica está vinculada à queda eustática global de primeira ordem aliada à baixa taxa de subsidência térmica, además do incremento do volume de sedimentos relacionado ao soerguimento da Serra do Mar durante o Terciário (Zalán e Oliveira, 2005). Esta superssequência contém grandes sistemas turbidíficos e constituem importantes reservatórios de hidrocarbonetos da Bacia de Campos (Guardado et al., 2000; Bruhn, 1998; Bruhn et al., 2003).

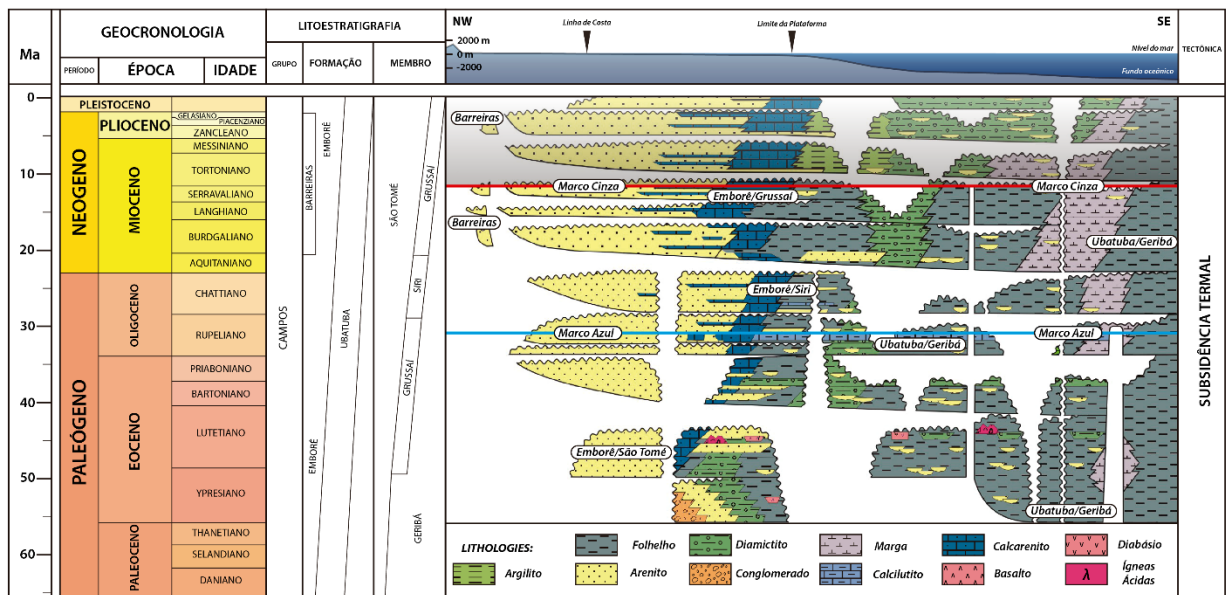


Figure 2 - Carta cronoestratigráfica do Cenozóico na Bacia de Campos. (Modificado de Winter et al., 2007). A área sombreada cinza compreende o intervalo estratigráfico de interesse deste trabalho, limitado inferiormente pelo Marco Cinza (linha vermelha), e geologicamente correspondente à discordância entre o Mioceno Médio e Superior (Viana et al., 1990; Silva, 1992). A linha azul representa o Marco Azul de idade do Oligoceno Inferior (Rangel et al., 1994; Winter et al., 2007).

2.2. Canyons submarinos

Os vales submarinos e, particularmente, os canyons nos taludes continentais são os principais condutos para o transporte de sedimentos do continente para o oceano. Desde o estudo pioneiro de Dana (1863), um grande número de canyons submarinos foram estudados nas margens continentais e que, inicialmente, foram relacionados ao acúmulo de sedimentos transportados a leques submarinos de águas profundas (Fig. 3). Por exemplo, os lobos deposicionais do Amazônias estão localizados a 1100 km da cabeceira do canyon (Jegou, 2008). Estes vales submarinos são profundos e estreitos com paredes íngremes, formados principalmente pela erosão do talude continental e da plataforma externa (Shepard, 1981).

Muitos canyons submarinos mostram um flanco erosivo abrupto e profundo, e um flanco deposicional mais suave, onde se formam terraços. Esta morfologia confere ao canyon uma assimetria. O talvegue não está localizado no meio do canyon, mas sim na lateral do flanco erosivo. Em contraste, canais submarinos retos apresentam um vale simétrico em forma de V (e.g., Shepard et al., 1966) ou um vale em forma de U (e.g., Piper e Savoye, 1993, Lastras et al., 2009).

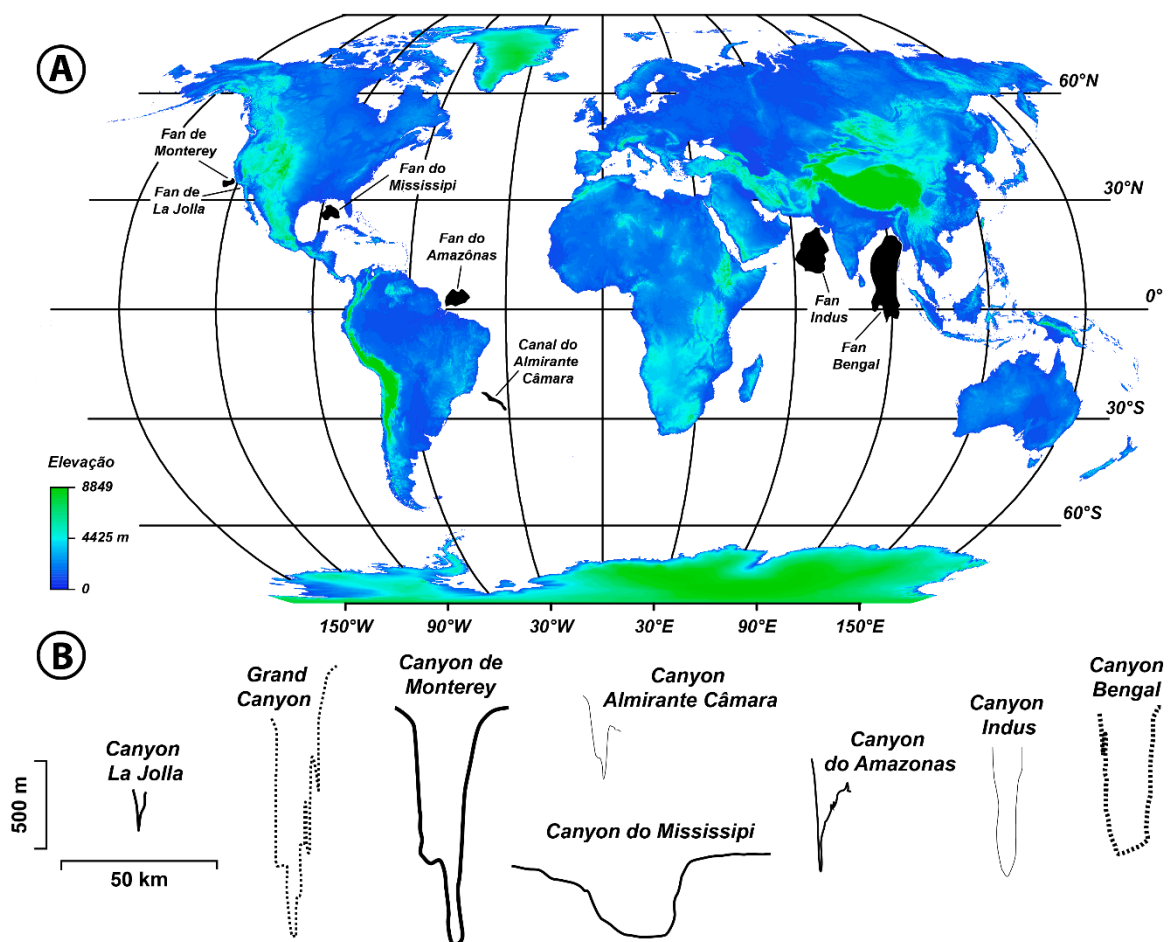


Figure 3 - a) Mapa de localização de sistemas de leques submarinos modernos. b) Seções transversais comparadas de canyons submarinos com um canyon continental (Grand Canyon). Exagero vertical = 48.5. (Modificado de Normark e Carlson, 2003).

2.2.1. Tipos de canyons submarinos

Dados de subsuperfície, estudos análogos de afloramentos e estudos de sistemas modernos resultaram em uma extensa e crescente literatura sobre a natureza de canyons submarinos. Estes estudos numerosos, detalhados e abrangentes centraram-se em aspectos específicos dos processos de transporte, deposição, e da morfologia dos canyons existentes nas margens continentais em todo o mundo, de forma a permitir uma classificação consistente de canyons submarinos em dois tipos (Fig. 4).

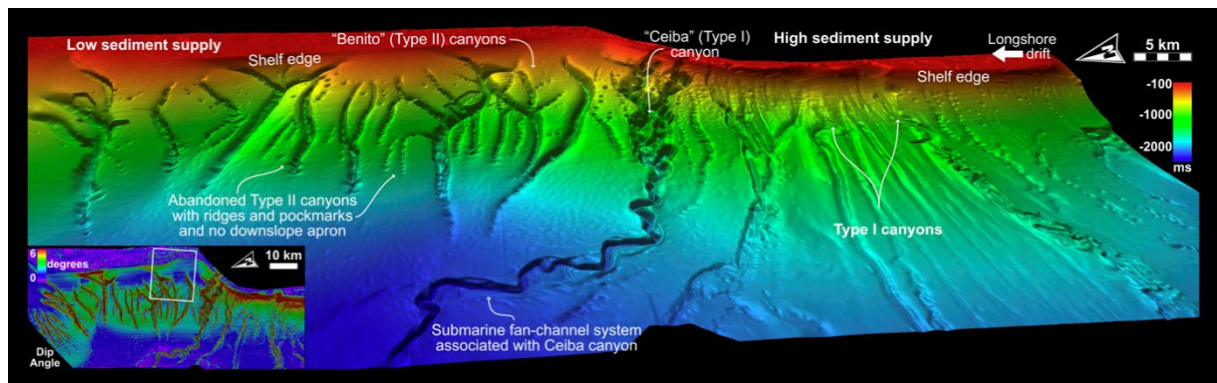


Figure 4 – Canyons da margem da Guiné Equatorial. Os canyons Tipo I indentam a margem da plataforma e tem ligação com a bacia onde depositou leques submarinos. Os canyons do Tipo II estão restritos ao talude sem ligação com a quebra da plataforma e a área da bacia profunda (Modificado de Jobe et al., 2011).

Os canyons do Tipo I (Jobe et al., 2011), correspondem aos canyons erosivos (Carter et al., 2016; Soulet et al., 2016) ou canyons incisos na plataforma (Farre et al., 1983; Mauffrey et al., 2017). Esses canyons possuem uma ligação direta entre a plataforma continental e o ambiente marinho profundo porque a sua reentrância na plataforma permite uma estreita associação com os ambiente fluviais onde os sedimentos são rapidamente fornecidos e, através de canais submarinos erosivos, transferidos para a bacia profunda. Os canyons submarinos erosivos depositam

turbiditos, lóbulos de canais, complexos de diques de canais, e contornitos no fundo das bacias oceânicas (Fig. 5). Frequentemente, contêm uma miríade de complexos de canais, complexos de diques e grandes complexos de transporte de massa. Seus canais interiores são altamente sinuosos e bordejados pelas paredes íngremes do canyon. Com geometria de seção transversal em forma de V, suas complexidades geométricas são consideráveis, variando de um padrão de cabeceira dendrítica a conexões de ravinas, e até mesmo, conexões adjacentes de canyons submarinos mais jovens em vários pontos de confluência. A presença de terraços neste tipo de canyon mostra evidências de significativa erosão, seguida de períodos subsequentes de preenchimento.

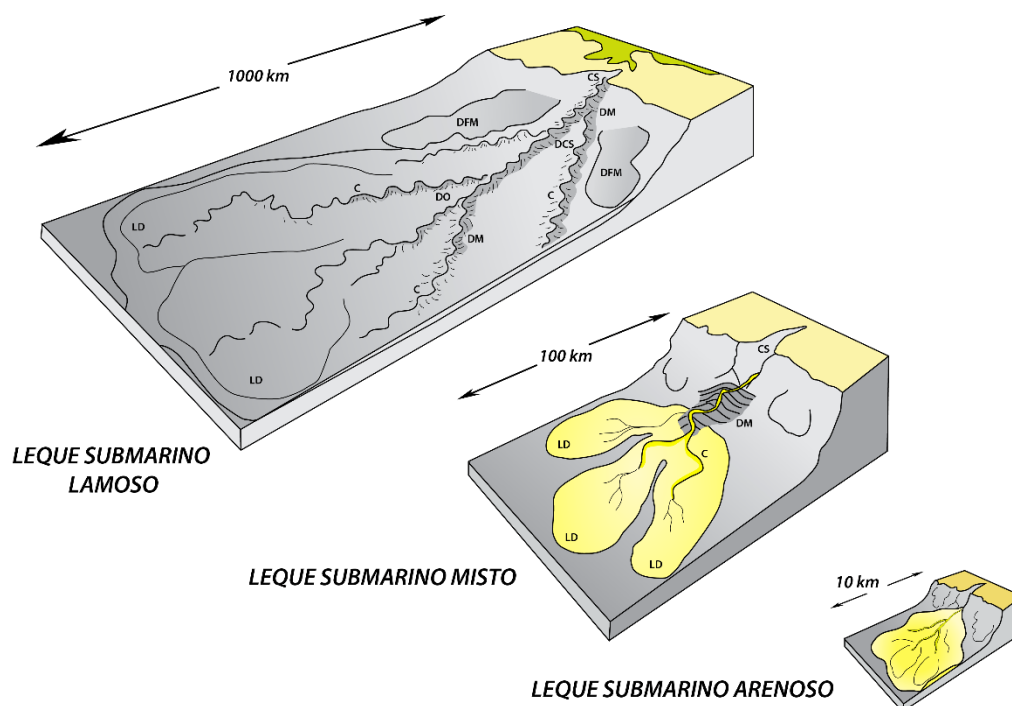


Figure 5 – Diagramas de blocos esquemáticos de sistemas de leques submarinos de águas profundas de acordo com o tamanho de grão dominante. Elementos arquiteturais: CS: *Canyon submarino*; DFM: *Depósitos de fluxo de massa*; DM: *Dique marginal*; C: *Canal submarino*; DCS: *Depósitos de crevasse splay*, DO: *Depósitos de overbank*; LD: *Lobo deposicional*. (Modificado de <http://www.sepmstrata.org/page.aspx?pageid=40>).

Os canyons do Tipo II (Jobe et al., 2011), também chamados de canyons de talude (Farre et al., 1983) ou canyons confinados em talude (Brothers et al., 2013; Li et al., 2013; Mauffrey et al., 2017), correspondem aos canyons agradacionais. Esses canyons não têm conexão com a plataforma e nem com os ambientes oceânicos profundos, porque estão restritos às regiões de talude, sendo sua formação geralmente atribuída a atividades de falhas e dobramentos. Podendo ser encontrados nas margens continentais passivas e ativas, são considerados carentes de sedimentos devido à desconexão com sistemas fluviais alimentadores. A maioria dos sedimentos depositados no canyon são gerados a partir de falhas nas paredes dos canyons submarinos.

2.2.2. Morfologia de canyons submarinos

A morfologia dos canyons depende do padrão de deposição de sedimentos que impulsiona a construção prolongada das margens continentais (Gerber et al., 2009), embora a manutenção a longo prazo dos canyons ainda seja pouco compreendida (Lo Iacono et al., 2014). Considerando-se as diferenças geomorfológicas de uma ampla gama de canyons submarinos, tem-se que os mecanismos de vanguarda responsáveis pela sua formação e desenvolvimento podem ser resumidos em termos de processos descendentes e ascendentes (Shepard, 1981; Twichell e Roberts, 1982). Os processos descendentes referem-se aos fluxos hiperpicnais e correntes de turbidez que ocorrem ao longo da margem da plataforma, criando uma incisão axial (Fig. 6) das regiões superiores até o talude em arquitetura erosiva e deposicional variada (Baztan et al, 2005, Almeida et al., 2015). Os processos ascendentes, por sua vez, são desenvolvidos pela ruptura da parede do talude, produzindo fluxos de detritos e fluxos de massa, ao mesmo tempo que aumenta a

largura do canyon (Pratson et al., 1994). Esses processos geralmente estão ativos em áreas carentes de sedimentos, taludes continentais tectonicamente ativos e íngremes (Lo lacono et al., 2014; Biscara et al., 2013; Micalleff et al., 2014).

De acordo com Twichell e Robert (1982), os canyons podem variar de retos a sinuosos. Os canyons com eixos sinuosos, criados pelo mecanismo descendente, cortam a quebra plataforma e são frequentemente mais antigos que os canyons do talude superior, enquanto os mecanismos ascendentes criam canyons submarinos de eixos lineares e parecem ser mais jovens que os canyons que indentam a plataforma.

2.3. Canyon Almirante Câmara

O *Canyon Almirante Câmara*, pertence ao Grupo Nordeste de canyons da Bacia de Campos (Viana et al., 1998; Viana et., 1999; Almeida e Kowsmann, 2014). Em planta, possui 28 km de comprimento, 4 km de largura, 340 m de relevo, com morfologia meandrante, indicando um forte condicionamento estrutural. É o único canyon maduro da Bacia de Campos caracterizado por um entalhe profundo, perfil em V, um canal muito sinuoso em seu talvegue e uma acentuada reentrância de sua cabeceira na plataforma continental (Farre et al., 1983, Machado et al. , 2004).

Inicialmente o canyon desenvolveu um típico perfil em U da fase juvenil, através de colapsos progressivos de sua cabeceira superior, resultando em movimentos de massa depositados predominantemente no Planalto Paulista. Na fase madura o canyon indentava a plataforma continental, capturando o Rio Paraíba do Sul onde a corrente fluvial descendente erodiu uma profunda calha sinuosa dentro do fundo lamacento do perfil em U da fase juvenil (Machado et al., 2004; Almeida e Kowsmann, 2014).

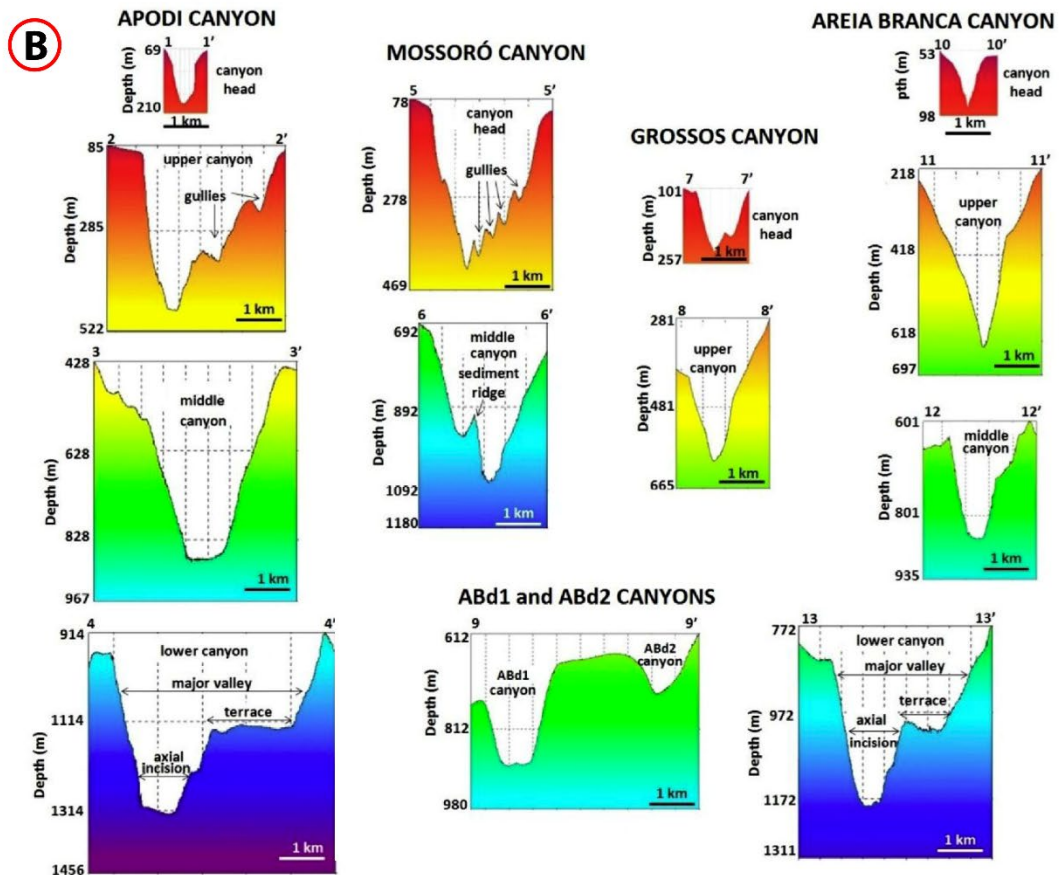
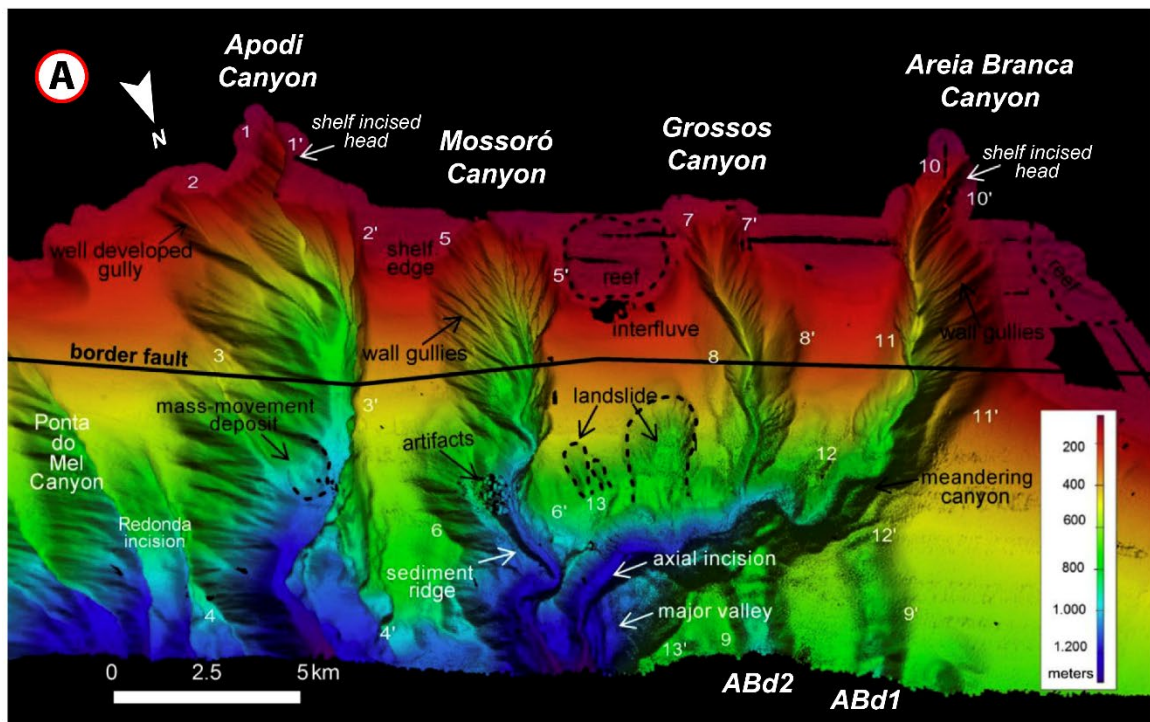


Figure 6 – a) mapa morfobatimétrico de canyons submarinos mostrando a geometria dos canyons em forma de U e V, terraços, voçorocas, movimentos de massa e cabeceiras de canyons. Exagero vertical = 10.0. b) perfis transversais dos canyons (ABd1 e ABd2 = canais distributivos do Canyon Areia Branca). (Modificado de Almeida et al., 2015).

2.4. Análise do traço complexo e atributos sísmicos

A análise do traço sísmico complexo, bem como a análise de atributos sísmicos em geral, foi fomentada em um importante momento da descoberta das zonas de gás (*bright-spots*) entre 1960 e 1970, iniciando novos horizontes para o estudo do traço sísmico complexo.

O uso de atributos sísmicos foi integrado à interpretação sísmica no início da década de 1970 por Anstey (Chopra e Marfurt, 2007), quando os primeiros estudos foram desenvolvidos a partir da implementação da coloração das amplitudes das seções sísmicas (Balch, 1971), baseando-se na análise espectral dos eventos sísmicos associados à variação da forma de onda com o tempo. O seu uso extensivo dá-se no final da década de 1970 e início da década de 1980, quando Taner e Koehler retomam as investigações iniciadas por Anstey no início de 1970 (Chopra e Marfurt, 2007). Motivados pela descrição do sinal analítico, descobrem que o traço complexo (ou sinal analítico) oferece uma medida superior do traço, do envelope do traço, ademais de outras informações como a fase instantânea e a frequência instantânea. Essa nova abordagem de cálculo de atributos sísmicos foi denominada como *Análise do Traço Sísmico Complexo*, culminando na publicação de dois artigos: Sheriff e Taner (1977) e Taner et al. (1979).

No campo da exploração sísmica, são muitos os atributos sísmicos disponíveis, alguns utilizados como indicadores de hidrocarbonetos, outros como indicadores de estruturas geológicas (e.g., canais e falhas). O tipo de análise deverá determinar o atributo sísmico mais adequado a ser utilizado, de forma que o atributo escolhido seja diretamente sensível ao recurso geológico desejado ou propriedade do reservatório de interesse (Brown, 2001).

2.4.1. Transformada de Hilbert

Antes do tratamento matemático do traço sísmico complexo, faz-se necessário a compreensão da Transformada de Hilbert, que aplica uma rotação de $-\pi/2$ ao dado sísmico.

O filtro de quadratura é o operador matemático que atua na fase do traço de quadratura, por vezes conhecida como Transformada de Hilbert do traço sísmico de entrada. Definindo-se o ângulo de rotação de $\pi/2$, está implicado aqui na troca do sinal do traço de quadratura resultante. Esta definição é objeto de convenção.

Tem-se que no domínio da frequência, o operador que provoca uma rotação de fase constante θ em um sinal, mas não modifica seu espectro de amplitude, pode ser representado por

$$R(\omega, \theta) = \begin{cases} e^{i\theta}, & \omega > 0 \\ e^{-i\theta}, & \omega < 0 \\ \cos \theta, & \omega = 0 \end{cases} \quad (1)$$

onde i é a unidade imaginária.

O operador de Hilbert, no domínio da frequência, é obtido substituindo-se o valor do ângulo de rotação na equação acima.

$$H(\omega) = -sng(\omega) = \begin{cases} e^{-i\frac{\pi}{2}} = -i, & \omega > 0 \\ e^{i\frac{\pi}{2}} = i, & \omega < 0 \\ 0, & \omega = 0 \end{cases} \quad (2)$$

onde

$$\text{sgn}(\omega) = \begin{cases} 1, & \omega > 0 \\ -1, & \omega < 0 \\ 0, & \omega = 0 \end{cases} \quad (3)$$

Realizando-se a operação da Transformada de Fourier inversa, este operador é expresso no domínio do tempo como

$$h(t) = \frac{i}{\pi t} \quad (4)$$

Dessa forma, o traço sísmico $x(t)$ e seu traço de quadratura $y(t)$ estão relacionados pela equação

$$y(t) = h(t) * x(t) \quad (5)$$

Podemos expressar um operador que subtrai um ângulo θ da fase de um sinal em termos de um filtro de quadratura do domínio da frequência, dado por

$$R(\omega, \theta) = \begin{cases} e^{i\theta} = \cos \theta - i \sin \theta, & \omega > 0 \\ e^{-i\theta} = \cos \theta + i \sin \theta, & \omega < 0 \\ \cos \theta, & \omega = 0 \end{cases} \quad (6)$$

Reorganizando-se as equações (6) e (2), podemos escrever a seguinte expressão

$$R(\omega, \theta) = \cos \theta + H(\omega) \sin \theta \quad (7)$$

cuja Transformada de Fourier inversa é

$$r(t, \theta) = \delta(t) \cos \theta + h(t) \sin \theta \quad (8)$$

$\delta(t)$ é a função Delta de Dirac.

2.4.2. O traço sísmico complexo

A análise do traço sísmico complexo (ou analítico) permite discretizar as informações de amplitude e fase, sem ocasionar a perda de variações locais (Taner et al., 1979).

Um traço sísmico $x(t)$ pode ser decomposto segundo a equação

$$x(t) = A(t) \cos \theta(t) \quad (9)$$

onde $A(t)$ é a amplitude instantânea e $\theta(t)$ a fase instantânea, ambas funções dependentes do tempo (Fig.7).

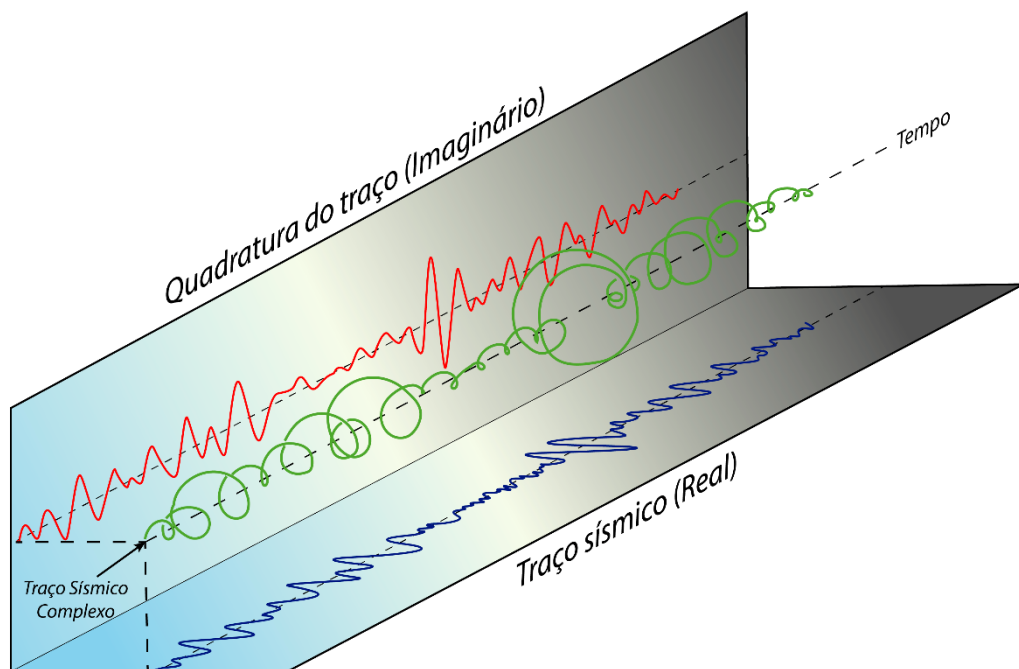


Figure 7 – Representação do traço sísmico complexo em um diagrama isométrico. O traço complexo (linha verde) é um vetor que descreve um movimento helicoidal ao longo do eixo do tempo. O traço sísmico (linha azul) e de quadratura (linha vermelha) são representados em planos perpendiculares (Modificado de Taner et al., 1979).

O traço complexo $Z(t)$ é calculado tomando o traço sísmico de entrada $x(t)$ como sua parte real e o traço de quadratura $y(t)$ como sua parte imaginária. Desse modo, temos que

$$Z(t) = x(t) + iy(t) \quad (10)$$

O operador que realiza a rotação no domínio do tempo pode ser expresso pela equação (8). Realizando-se a operação de convolução de $h(t)$ com o traço sísmico de entrada $x(t)$, obtemos o traço de quadratura $y(t)$. Se aplicarmos o operador $r(t, \theta)$ em $x(t)$, obtemos o traço rotacionado

$$\hat{x}(t) = r(t, \theta) * x(t) = x(t) \cos \theta(t) + y(t) \sin \theta(t) \quad (11)$$

Sendo $\theta(t)$ o ângulo de rotação que em um instante de tempo t maximiza o valor tomado para \hat{x} , temos por definição que o conjunto desses valores é a envoltória do traço sísmico, dada por

$$A(t) = x(t) \cos \theta(t) + y(t) \sin \theta(t) \quad (12)$$

Se tomamos a derivada parcial com relação ao ângulo de rotação é igual a zero, temos

$$\frac{\partial A(t)}{\partial \theta(t)} = -x(t) \sin \theta(t) + y(t) \cos \theta(t) = 0 \quad (13)$$

Assim, temos que

$$x(t) \sin \theta(t) = y(t) \cos \theta(t) \quad (14)$$

Tomando-se os quadrados das equações (12) e (14), e somando-se membro a membro, teremos a expressão da envoltória do traço $x(t)$ em termos das componentes reais e de quadratura

$$A(t) = |Z(t)| = \sqrt{x^2(t) + y^2(t)} \quad (15)$$

A fase pode ser obtida reorganizando-se os termos da equação (14):

$$\theta(t) = \arctan [Z(t)] = \arctan \left[\frac{y(t)}{x(t)} \right] \quad (16)$$

A amplitude instantânea do traço pode ser escrita em termos do traço sísmico complexo $Z(t)$ e seu conjugado $\bar{Z}(t)$, dado por

$$A(t) = \sqrt{Z(t) \cdot \bar{Z}(t)} = |Z| \quad (17)$$

Através das relações matemáticas do traço sísmico analítico, a amplitude e a fase instantânea podem ser calculadas na forma trigonométrica que segue

$$Z(t) = A(t) \cos \theta(t) + iA(t) \sin \theta(t) = A(t)e^{i\theta(t)} \quad (18)$$

A Fig. 8 mostra a representação da parte real e a parte imaginária do traço sísmico complexo. Dessa forma, o traço sísmico pode ser representado como funções analíticas separáveis e independentes entre si, a amplitude e a fase instantânea. Isso constitui a base da análise do traço sísmico complexo, isto é, poder separar a informação de amplitude sísmica da informação de fase do dado (Barnes, 2007).

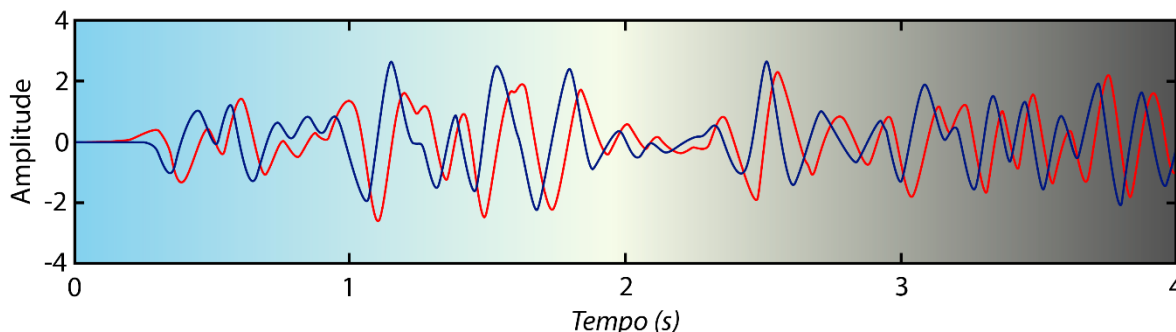


Figure 8 – Traço sísmico analítico, mostrando a parte real (linha azul) e a quadratura do traço (linha vermelha).

Além disso, o traço sísmico complexo $Z(t)$ guarda as informações espectrais do traço sísmico real. Assim, no domínio da frequência, temos:

$$Z(\omega) = X(\omega) + iY(\omega) \quad (19)$$

onde,

$$Y(\omega) = H(\omega)X(\omega) \quad (20)$$

Reorganizando-se as equações (18) e (19), temos que

$$Z(\omega) = X(\omega) + iH(\omega)X(\omega) \quad (21)$$

Substituindo-se o operador de Hilbert $H(\omega)$ no domínio da frequência, dado pela equação (2), temos que

$$Z(\omega) = \begin{cases} 2X(\omega), & \omega > 0 \\ 0, & \omega \leq 0 \end{cases} \quad (22)$$

Assim, temos que o sinal analítico complexo e a sua parte real é idêntico ao sinal original, apenas rotado de $-\pi/2$.

2.4.3. Atributos sísmicos

A atributos sísmicos são quaisquer informações obtidas através de dados sísmicos, seja por meio de medições diretas, lógicas ou baseadas na experiência de conhecimentos anteriores (Taner et al., 1979). Os atributos sísmicos são gerados para enfatizar a característica desejada, a qual não é diretamente identificada nos dados, podendo ainda serem obtidos a partir de dados sísmicos ainda não empilhados, como por exemplo, o atributo de variação de amplitude com o

afastamento da fonte, *AVO - Amplitude Variation with Offset*, ou obtidos a partir de dados já empilhados.

Existe uma grande variedade de atributos sísmicos e sua utilização se dá segundo o tipo de análise e interesse de investigação. Para este trabalho, duas categorias definidas por Taner (2001) são importantes:

(i) *Atributos físicos*: se relacionam com qualidades e quantidades físicas. A magnitude do envelope do traço sísmico é proporcional ao contraste de impedância acústica, a frequência instantânea relaciona-se com a espessura das camadas, dispersão e absorção da onda. Logo, esses atributos são usados principalmente para classificação litológica e classificação de reservatórios; e

(ii) *Atributos geométricos*: descrevem a relação espacial e temporal de todos os outros atributos. A similaridade do traço sísmico permite determinar a continuidade lateral das camadas, densidade de fraturas, bem como as bordas de estruturas (Chopra, 2002). Esses atributos foram inicialmente desenvolvidos para ajudar na interpretação estratigráfica.

Neste trabalho foram utilizados os atributos sísmicos de amplitude, fase instantânea, cosseno da fase instantânea, TecVa (Bulhões e Amorim, 2005), envelope, similaridade, e decomposição espectral (RGB blend). O seu detalhamento matemático é tratado na seção 5.6.3 e 5.6.4 desta dissertação.

3. SÍNTESE DOS RESULTADOS

A evolução do Canyon Almirante Câmara é marcadamente complexa, resultado de uma miríade de ciclos de erosão, bypass e de preenchimento agradacional em ciclos de alta frequência (Machado et al., 2004).

O uso de atributos sísmicos complexos permitiu a interpretação de quatro superfícies erosivas ao longo da evolução do canyon: EBS, ACS1, ACS2, e ACS3 (Fig. 9). Cada uma dessas superfícies apresenta uma gênese interpretativa vinculada com quedas do nível do mar (Fig. 10), embora não seja o único fator controlador do evento erosivo.

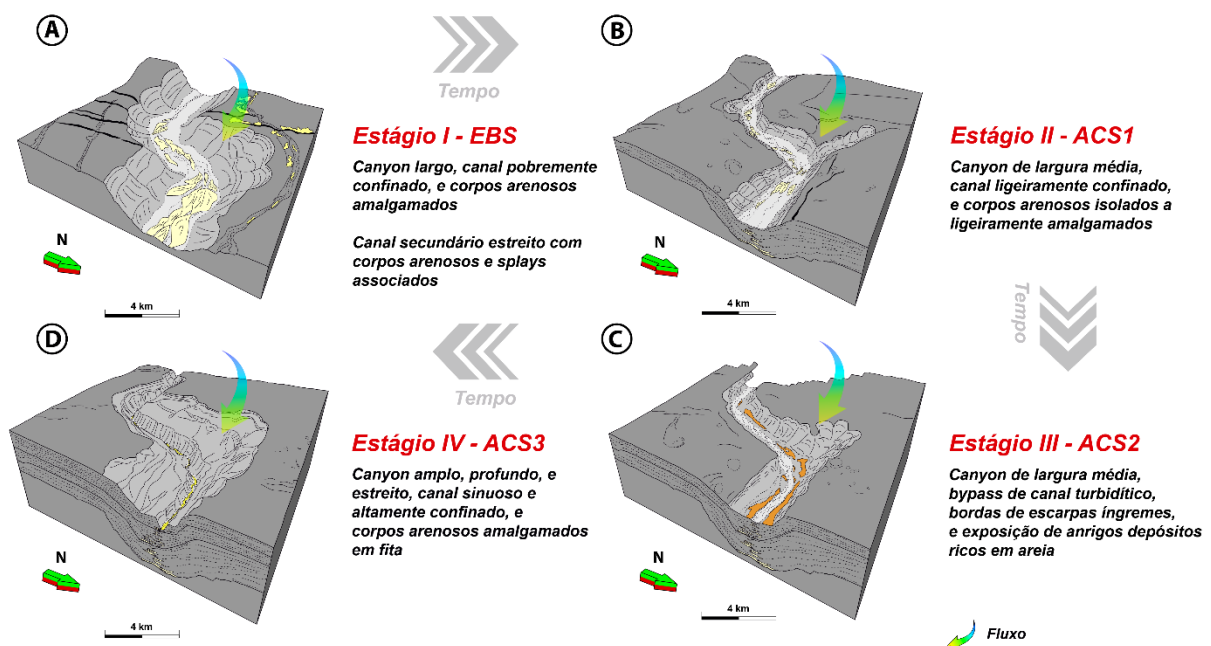


Figure 9 – Modelo evolutivo do Canyon Almirante Câmara e de seu preenchimento. Quatro estágios foram propostos: (a) Estágio I (EBS): erosão inicial proeminente do canyon, com deposição de lóbulos arenosos amalgamados de estratos finos; b) Estágio II (ACS1): canyon de largura média, com depósitos de barras arenosas amalgamadas e lóbulos turbidíticos; c) Estágio III (ACS2): canyon de largura média com bypass de sedimentos transportados para o talude inferior ou planície abissal profunda; e d) Estágio IV (ACS3): canyon amplo e profundo, com deposição de turbiditos de estratos finos arenosos. A agradacão desses depósitos representa uma miríade de eventos erosivos, de bypass e deposicionais (*waxing-waning cycles*), preservando uma complexa história de corte e preenchimento.

Também parece haver uma relação contemporânea da evolução do canyon com as falhas normais, direção N-S e NNW-SSE que interceptam a porção média do canyon, ao menos nos estágios evolutivos iniciais (EBS e ACS1, Fig.9a-b), levando-o a uma deflexão abrupta do canyon e do seu canal interior (cerca de 90°).

O seu preenchimento é constituído de lóbulos turbidíticos de camadas finas, lóbulos amalgamados e barras amalgamadas arenosas, bem como depósitos de fluxos de massa (MTD) que também alimentaram o canyon durante o seu desenvolvimento. A combinação dos atributos de refletividade (envelope e similaridade), decomposição espectral e RGB Blend ajudaram a identificar esses corpos arenosos em resposta à mudança na espessura de sintonia (*tuning thickness*), impedância acústica, bem como espessamento e afinamento relativos. As correntes de fundo oceânicas parecem também haver contribuído para o preenchimento do canyon, conferindo a este um perfil em V assimétrico. Um modelo evolutivo do canyon foi proposto, que é dividido em quatro estágios: Estágio I – EBS, Estágio II – ACS1, Estágio III – ACS2, e Estágio IV – ACS3 (Fig. 9).

Embora o estudo realizado neste trabalho não tenha implicações diretas para a exploração de hidrocarbonetos, o modelo evolutivo-deposicional proposto contribui, sobremaneira, para o entendimento como ambiente análogo de canyons submarinos com potenciais alvos exploratórios, através do detalhamento de preenchimento complexo por eventos erosivos interiores ao canyon e interação de amplos tipos de elementos deposicionais.

Para trabalhos futuros, sugere-se a incorporação de dados geofísicos de poços para a área de trabalho, de modo a minimizar erros verticais de estimativas de espessuras (*well-seismic tie*), bem como tornar mais robusta a correspondência entre a informação de perfis geofísicos com a interpretação dos dados sísmicos 3D.

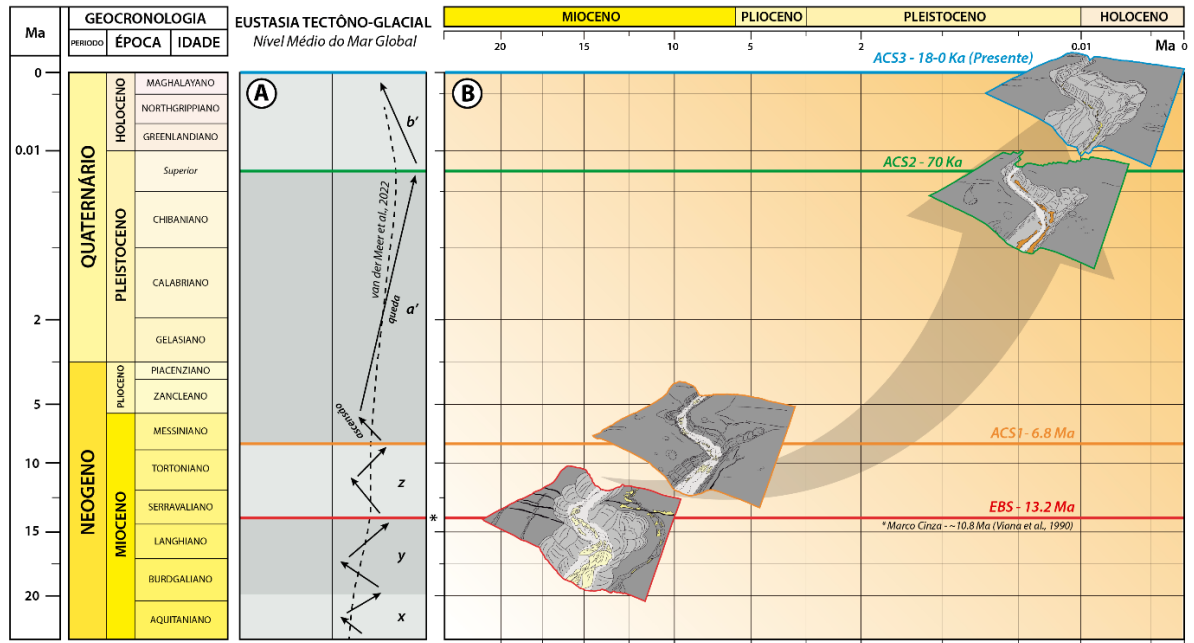


Figure 10 - Curva eustática tectôno-glacial Neógeno-Quaternário e correção tempo-tempo de superfície. As linhas horizontais (vermelha, laranja, verde e azul) atribuem verticalmente a idade de cada superfície. a) Curva de tendências residuais do nível do mar e alterações esquemáticas de amplitude associadas (modificado de van der Meer et al., 2022). b) Diagrama de correlação tempo-tempo. As setas para a esquerda e para a direita indicam a subida e a descida do nível do mar, respectivamente. As letras (x, y, z, a' e b') e o sombreamento destacam as sequências estratigráficas ligadas à discordância. A linha pontilhada é a tendência eustática de longo prazo (>50 milhões de anos).

4. REFERÊNCIAS BIBLIOGRÁFICAS

- Almeida, A. G. & Kowsmann, R. O., 2014. Geomorfologia do Talude Continental e do Platô de São Paulo. In: Kowsmann, R. O. (Ed.). *Geologia e Geomorfologia*. Rio de Janeiro: Elsevier. Habitats Series, v. 1, pp. 33-66.
- Almeida, N.M.de, Vita, H., Gomes, M.P., 2015. Morphology of submarine canyons along the continental margin of the Potiguar Basin, NE Brazil, *Marine and Petroleum Geology*, n. 68(A), pp. 307-324. <https://doi.org/10.1016/j.marpetgeo.2015.08.035>.
- Babonneau, N., Savoye, B., Cremer, M., Klein, B., 2002. Morphology and architecture of the present canyon and channel system of the Zaire deep-sea fan. *Marine and Petroleum Geology*, 194, pp. 445–467. [https://doi.org/10.1016/S0264-8172\(02\)00009-0](https://doi.org/10.1016/S0264-8172(02)00009-0).
- Balch, A.H., 1971, Color sonagrams – a new dimension in seismic data interpretation: *Geophysics*, 36, v.36, n. 6, pp. 1074- 1098. <https://doi.org/10.1190/1.1440233>.
- Barnes, A.E., 2007. A tutorial on complex seismic trace analysis. *Geophysics*, v. 72(6), W33-W43. <https://doi.org/10.1190/1.2785048>.
- Baztan, J., Berné, S., Olivet, J.L., Rabineau, M., Aslanian, D., Gaudin, M., Réhault, J.P., Canals, M., 2005. Axial incision: The key to understanding submarine canyon evolution (in the western Gulf of Lion), *Marine and Petroleum Geology*, 22(6–7), pp. 805– 826. <https://doi.org/10.1016/j.marpetgeo.2005.03.011>.
- Biscara, L., Mulder, T., Hanquiez, V., Marieu, V., Crespin, J-P., Braccini, E., Garlan, T., 2013. Morphological evolution of Cap Lopez Canyon (Gabon): Illustration of lateral migration processes of a submarine canyon. *Marine Geology*, n. 340(9), pp. 49-56. <http://dx.doi.org/10.1016/j.margeo.2013.04.014>.
- Brothers, D.S., ten Brink, U.S., Andrews, B.D., Chaytor, J.D., Twichell, D.C., 2013. Geomorphic process fingerprints in submarine canyons, *Marine Geology*, n.337, pp. 53-66. <https://doi.org/10.1016/j.margeo.2013.01.005>.
- Brown, A., 2001. Understanding seismic attributes. *Geophysics*, 66 (1), pp. 47–48. <https://doi:10.1190/1.1444919>.
- Bruhn, C. H. L. 1998. Deep-Water reservoirs from the eastern Brazilian rift and Passive margin basins. *Petroleum Geology of Rift and Passive Margin Turbidite Systems: Brazilian and Worldwide Examples*. In: 1998 AAPG International Conference & Exhibition, Rio de Janeiro, Course #6.
- Bruhn, C., Gomes, J., Lucchese, C., Johann, P., 2003. Campos Basin: Reservoir Characterization and Management - Historical Overview and Future Challenges: In:

- Offshore Technology Conference, 2003, Houston, Texas, OCT No. 15220, Expanded Abstracts, pp. 1-14. doi.org/10.4043/15220-MS
- Bulhões, E.M., Amorim, W.N., 2005. Princípio da SismoCamada Elementar e sua aplicação à Técnica Volume de Amplitudes (tecVA). In: 9th International Congress of the Brazilian Geophysical Society, Salvador.
- Canals, M., Puig, P., de Madron, X.D., Heussner, S., Palanques, A., Fabres, J., 2006. Flushing submarine canyons. *Nature*, n. 444, pp. 354-357. <https://doi.org/10.1038/nature05271>.
- Carter, R.C., Gani, M.R., Roesler, T., Sarwar, A.K.M., 2016. Submarine channel evolution linked to rising salt domes, Gulf of Mexico, USA, *Sedimentary Geology*, n.342, pp. 237–253. <https://doi.org/10.1016/j.sedgeo.2016.06.021>.
- Chang, H. K.; Bender, A. A.; Kowsmann, R. O., Mello, U. T. 1990. Origem e evolução termomecânica de bacias sedimentares. In: Guilherme Pederneiras Raja Gabaglia e Edison José Milani. Origem e Evolução de Bacias Sedimentares. PETROBRAS, Rio de Janeiro. pp. 49-71.
- Chopra, S., 2002. Coherence Cube and beyond. *EAGE, First Break*, 20(1), pp. 27-33. <https://doi.org/10.1046/j.1365-2397.2002.00225.x>.
- Chopra, S., Marfurt, K.J., 2007. Seismic attributes for prospect identification and reservoir characterization. *Geophysical Developments Series*, n. 11, 481 p. <https://doi.org/10.1190/1.9781560801900>.
- Dana. J. D., 1863. *Manual of Geology*. London. 1st Edition, Trubner, 798p.
- Dias, J.L., Scarton, J.C., Esteves, F.R., Carminatti, M., Guardado, L.R. 1990. Aspectos da evolução tectono-sedimentar e a ocorrência de hidrocarbonetos na Bacia de Campos. In: Gabaglia, G.P.R., Milani, E.J. (coords.). Origem e evolução de bacias sedimentares, PETROBRAS, CENSUD, Rio de Janeiro, p. 333-360.
- Droz, L., Rigaut, F., Cochonat, P., Tofani, R., 1996. Morphology and recent evolution of the Zaire turbidite system (Gulf of Guinea). *GSA Bulletin* 108 (3), pp. 253-269. [https://doi.org/10.1130/0016-7606\(1996\)108<0253:MAREOT>2.3.CO;2](https://doi.org/10.1130/0016-7606(1996)108<0253:MAREOT>2.3.CO;2).
- Farre, J. A.; McGregor, B. A.; Ryan, W. B. F.; Robb, J. M., 1983. Breaching the shelf break: passage from youthful to mature phase in canyon evolution. In: Stanley, D. J.; Moore, G. T., (Eds.). *The shelf break: critical interface on Continental Margins*. Tulsa: Society of Economic Paleontologists and Mineralogists, 1983. pp. 25-39.
- Gerber, T.P., Amblas, D., Wolinsky, M.A., Pratson, L.F., Canals, M., 2009. A model for the long profile shape of submarine canyons. *Journal of Geophysical Research-Earth Surface*, n.114(3).
-

- Guardado, L.R., Spadini, A.R., Brandão, J.S.L., Mello, M.R., 2000. Petroleum Systema of the Campos Basin Brazil. In: Mello, M.R., Katz, B.J. (Ed.). Petroleum system of south Atlantic margins. American Association of Petroleum Geologists. AAPG Memoir 73, v. 72, pp. 317-324.
- Harris, P.T., Whiteway, T., 2011. Global distribution of large submarine canyons: geomorphic differences between active and passive continental margins. *Marine Geology* 285, pp. 69-86.
- Jegou, I., 2008. Etude de la transition chenal/levee/lobe dans les syste`mes turbiditiques re`cents. Application a` l'e`ventail turbiditique de l'Amazone et au ne´ofan du Petit-Rho`ne. Unpubl. Tese de Doutorado, Univinsersité Bretagne Occidentale 1, 351p.
- Jobe, Z.R., Lowe, D.R., Uchytíl, S.J., 2011. Two fundamentally different types of submarine canyons along the continental margin of Equatorial Guinea. *Mar. and Petr. Geology*, n.28, pp. 843-860. <https://doi.org/10.1016/j.marpetgeo.2010.07.012>.
- Karner, G.D., 2000. Rifts of the Campos and Santos basins, Southeastern Brazil: distribution and timing, in: Mello, M.R. and Katz, B.J. (Eds.), *Petroleum systems of South Atlantic margins*. AAPG memoir. 73. pp. 301-315.
- Lastras, G., Arzola, R.G., Masson, D.G., Wynn, R.B., Huvenne, V.A.I., Hühnerbach, V., Canals, M., 2009. Geomorphology and sedimentary features in the Central Portuguese submarine canyons, Western Iberian margin. *Geomorphology* 103, pp. 310-329.
- Li, X., Fairweather, L., Wu, S., Ren, J., Zhang, H., Quan, X., Jiang, T., Zhang, C., Su, M., He, Y., Wang, D., 2013. Morphology, sedimentary features and evolution of a large palaeo submarine canyon in Qiongdongnan basin, Northern South China Sea, *Journal of Asian Earth Sciences*, n.62, pp. 685-696. <https://doi.org/10.1016/j.jseaes.2012.11.019>.
- Lo Iacono, C., Sulli, A., Agate, M., 2014. Submarine canyons of north-western Sicily (Southern Tyrrhenian Sea): Variability in morphology, sedimentary processes and evolution on a tectonically active margin, *Deep-Sea Research Part II: Topical Studies in Oceanography*, n. 104, pp. 93–105. <https://doi.org/10.1016/j.dsr2.2013.06.018>.
- Machado, L.; Kowsmann, R.; Almeida Jr. W.; Murakami, C.; Schreiner, S; Miller, D.; Piauilino, P., 2004. Geometria da porção proximal do sistema deposicional turbidítico moderno da Formação Carapebus, Bacia de Campos; modelo para heterogeneidades de reservatório. *Boletim de Geociências da Petrobrás*, Rio de Janeiro, v. 12, n. 2, p.287-315.
-

- Mauffrey, M-A., Urgeles, R., Berné, S., Canning, J., 2017. Development of submarine canyons after the Mid-Pleistocene Transition on the Ebro margin, NW Mediterranean: The role of fluvial connections, *Quaternary Science Reviews*, n. pp. 77–93. <https://doi.org/10.1016/j.quascirev.2017.01.006>.
- Mayall, M., Jones, E., Casey, M., 2006. Turbidite channel reservoirs—key elements in facies prediction and effective development: *Marine and Petroleum Geology*, v. 23, p. 821–841. <https://doi.org/10.1016/j.marpetgeo.2006.08.001>.
- McHugh, C.M.G., Damuth, J.E., Mountain, G.S., 2002. Cenozoic mass-transport facies and their correlation with relative sea-level change, New Jersey continental margin. *Mar. Geol.* 184, pp. 295-334. [https://doi.org/10.1016/S0025-3227\(01\)00240-7](https://doi.org/10.1016/S0025-3227(01)00240-7).
- McHugh, C.M.G., Ryan, W.B.F., Eittrheim, S., Reed, D., 1998. The influence of the San Gregorio fault on the morphology of Monterey canyon. *Marine Geology* 146 (1-4), pp. 63-91. [https://doi.org/10.1016/S0025-3227\(97\)00118-7](https://doi.org/10.1016/S0025-3227(97)00118-7).
- Meiburg, E., Kneller, B., 2010. Turbidity currents and their deposits. *Annual Review of Fluid Mechanics*, 42, pp. 135–156. <http://dx.doi.org/10.1146/annurev-fluid-121108-145618>.
- Micallef, A., Ribó, M., Canals, M., Puig, P., Lastras, G., Tubau, X., 2014. Space-for-time substitution and the evolution of a submarine canyon-channel system in a passive progradational margin. *Geomorphology*, 221, pp. 34–50. <http://dx.doi.org/10.1016/j.geomorph.2014.06.008>.
- Mizusaki, A.M.P.; Piccirillo, E.M.; Dias, J.L.; Chiaramonti, P.C.; Roisember, A.; Bellieni, G.; Giaretta, A., 1989. Petrologia, Geoquímica e Geocronologia do vulcanismo básico do Neomiano da Bacia de Campos. Rio de Janeiro, Petrobrás. Rel. interno.
- Mohriak, W.U., Nemčok., N., Enciso.,G., 2008. South Atlantic divergent margin volution: rift border uplift and salt tectonics in the basins of SE Brazil. *Geological Society, London, Special 865 Publications 2008*, v. 294, pp. 365-398.
- Normark, W.R., Carlson, P.R., 2003. Giant Submarine Canyons: Is Size Any Clue to Their Importance in the Rock Record? *Geological Society of America. Special Paper 370*. <https://doi.org/10.1130/0-8137-2370-1.175>.
- Piper, D.J.W., Savoye, B., 1993. Processes of late Quaternary turbidity current flow and deposition on the Var deep-sea fan, north-west Mediterranean Sea. *Sedimentology* 40, pp. 557–583.
-

-
- Posamentier, H.W., 2003. Depositional elements associated with a basin floor channel-levée system: case study from the Gulf of Mexico. *Marine and Petroleum Geology* 20, p. 677-690. <https://doi.org/10.1016/j.marpetgeo.2003.01.002>.
- Pratson, L.F., Ryan, W.B.F., Mountain, G.S., Twichell, D.C., 1994. Submarine canyon initiation by downslope-eroding sediment flows: evidence in late Cenozoic strata on the New Jersey continental slope. *Geological Society of America Bulletin*, 106(3), 395–412. [https://doi.org/10.1130/0016-7606\(1994\)106<0395:SCIBDE>2.3.CO;2](https://doi.org/10.1130/0016-7606(1994)106<0395:SCIBDE>2.3.CO;2).
- Rangel, H.; Martins, F.; Esteves, F.; Feijó, F., 1994. Bacia de Campos: Carta Cronoestratigráfica. *Boletim de Geociências da Petrobras, Rio de Janeiro*, v. 8, n. 1, pp. 203-219.
- Rangel, H.D., Carminatti, M., 2000. Rift lake stratigraphy of the Lagoa Feia Formation, Campos Basin, Brazil. In: Gierlowski-Kordesch, E.H., Kelts, K.R. (Eds.), *Lake Basins Through Space and Time: American Association of Petroleum Geology Studies in Geology*, 46, pp. 225–244
- Schaller, H. Estratigrafia de Bacia de Campos. 1973. In: *Congresso Brasileiro de Geologia* 27, Aracaju. v. 3, pp.247-258.
- SEPM STRATA – SEPM Stratigraphy Web. Deepwater Source and Settings: Depositional settings, source terrains of deepwaters fans and mass transport debris. Disponível em: <http://www.sepmstrata.org/page.aspx?pageid=40>. Acesso em: 16 de dezembro de 2023.
- Shepard, F.P., 1981. Submarine canyons: multiple causes and long-time persistence. *AAPG Bull.* 65, pp. 1062-1077.
- Shepard, F.P., Dill, R.F., von Rad, U., 1966. Physiography and sedimentary processes of La Jolla submarine fan and fan valley, California. *Am. Assoc. Pet. Geol. Bull.* 53, pp. 390–420. <https://doi.org/10.1306/5D25C615-16C1-11D7-8645000102C1865D>.
- Sheriff, R.E., Taner, M.T. (1977) Application of amplitude, frequency, and other attributes to stratigraphic and hydrocarbon exploration, *AAPG*, v. 26, pp. 301–327.
- Silva, A. 1992. Evolução sedimentar pós-miocênica na área nordeste da bacia de Campos. Rio de Janeiro, Universidade Federal do Rio de Janeiro. Dissertação de Mestrado. 120 p.
- Soulet, Q., Migeon, S., Gorini, C., Rubino, J-L., Raison. F., Bourgues, P., 2016. Erosional versus aggradational canyons along a tectonically-active margin: The northeastern Ligurian margin (western Mediterranean Sea), *Marine Geology*, n.382, pp. 17–36. <https://doi.org/10.1016/j.margeo.2016.09.015>.
-

- Stow, D.A.V., Mayall, M., 2000. Deep-water sedimentary systems: new models for the 21st century. *Marine and Petroleum Geology*, 17(2), pp.125-135. [http://doi:10.1016/S0264-8172\(99\)00064-1](http://doi:10.1016/S0264-8172(99)00064-1).
- Taner, M. T., 2001, Seismic attributes, CSEG Recorder, September Issue, pp. 48-56
- Taner, M.T., Koehler, F., Sheriff, R.E., 1979. Complex Seismic Trace Analysis, *Geophysics*, 44(6), pp. 1041-1063. <http://dx.doi.org/10.1190/1.1440994>.
- Twichell, D. C., Roberts, D.G., 1982. Morphology, distribution, and development of submarine canyons on the United States Atlantic continental slope between Hudson and Baltimore Canyons, *Geology*, 10(8), pp. 408-412. [https://doi.org/10.1130/0091-7613\(1982\)10<408:MDADOS>2.0.CO;2](https://doi.org/10.1130/0091-7613(1982)10<408:MDADOS>2.0.CO;2).
- van der Meer, D.G., Scotese, C.R., Mills, B.J.W., Van den Berg van Saparoea, A.-P., Sluijs, A., van de Weg, R.M.B., 2022. Long-Term Phanerozoic Global Mean Sea Level: Insights from Strontium Isotope Variations and Estimates of Continental Glaciation. *Gondwana Research*, 111, pp. 103-121. <https://doi.org/10.1016/j.gr.2022.07.014>.
- Viana, A.R., Almeida, W., Machado, L.C. 1999. Different styles of canyon infill related to gravity and bottom current processes: examples from the upper slope of the SE Brazilian margin. 6th International Congress of the Brazilian Geophysical Society; Rio de Janeiro, Brasil. Rio de Janeiro: Sociedade Brasileira de Geofísica. Expanded Abstract 01499. <https://doi.org/10.3997/2214-4609-pdb.215.sbgf014>.
- Viana, A.R.; Faugères, J.C., Stow, D.A.V., 1998. Bottom-current-controlled sand deposits – a review of modern shallow – to deep-water environments. *Sedimentary Geology*, v.115, pp. 53-80.
- Viana, A.R.; Kowsmann, R.O.; Castro, D.D., 1990. A discordância do Mioceno Médio/Superior: Um Marco regional no talude da bacia de Campos. In: 36º Congresso da Sociedade Brasileira de Geologia, Natal. Anais... Natal, SBG.1: p. 313-323.
- Winter, W.R.; Jahnert, R.J.; França, A.B., 2007. Bacia de Campos. *Boletim de Geociências da Petrobras*, Rio de Janeiro, v. 15, n. 2, pp. 511-529.
- Wynn, R.B., Cronin, B.T., Peakall, J., 2007. Sinuous deep-water channels: genesis, geometry and architecture. *Marine and Petroleum Geology* 24 (6-9), pp. 341-387. <https://doi.org/10.1016/j.marpetgeo.2007.06.001>.
- Zalán P.V.; Oliveira J.B.A., 2005. Origem e Evolução Estrutural do Sistema de Riftes Cenozóicos do Sudeste do Brasil. *Boletim de Geociências da Petrobras*, Rio de Janeiro, v. 13, n. 2, pp. 269-300.
-

5. ARTIGO CIENTÍFICO

5.1. Comprovante de submissão



Samuel Correa <scorrea.strat@gmail.com>

Track the status of your submission to Marine and Petroleum Geology

1 message

Track your Elsevier submission <no-reply@submissions.elsevier.com> Tue, Dec 26, 2023 at 6:42

To: scorrea.strat@gmail.com

Manuscript Number: JMPG-D-23-01633

Manuscript Title: Seismic attribute-based depositional model and evolution of large-size canyon – Almirante Câmara (Neogene to Quaternary) of Campos Basin, Brazil

Journal: Marine and Petroleum Geology Dear

Samuel Aparecido da Silva Correa,

Your submitted manuscript is currently under review. You can track the status of your submission in Editorial Manager, or track the review status in more detail using Track your submission here: <https://track.authorhub.elsevier.com?uid=cd5fe394-01bc-45da-bc3a-eb39db11c867>

This page will remain active until the peer review process for your submission is completed. You can visit the page whenever you like to check the progress of your submission. The page does not require a login, so you can also share the link with your co-authors.

If you are a WeChat user, then you can also receive status updates via WeChat. To do this please click the following link; you will be taken to Elsevier China's website where further instructions will guide you on how to give permission to have your submission's details made visible in WeChat. Note that by clicking the link no submission data is transferred to the WeChat platform. If you have any questions about using Track your submission with WeChat please visit 在线咨询 https://cn.service.elsevier.com/app/chat/chat_launch/supporthub/publishing/session/ - Journal Article Publishing 支持中心

<https://webapps.elsevier.cn/st-wechat/subscribe?signature=1703622413-c3ff2ab517925c943709a84024421e4b&uid=cd5fe394-01bc-45da-bc3a-eb39db11c867>

<https://webapps.elsevier.cn/st-wechat/subscribe?signature=1703622413-c3ff2ab517925c943709a84024421e4b&uid=cd5fe394-01bc-45da-bc3a-eb39db11c867>

We hope you find this service useful. Kind

regards,
Journal Office of Marine and Petroleum Geology
Elsevier B.V.

5.2. CORPO INTEGRAL DO ARTIGO SUBMETIDO – SEISMIC ATTRIBUTE-BASED DEPOSITIONAL MODEL AND EVOLUTION OF LARGE-SIZE CANYON – ALMIRANTE CÂMARA (NEOGENE TO QUATERNARY) OF CAMPOS BASIN, BRAZIL

Samuel Aparecido da Silva Correa ^{a,*}, Juliano Kuchle ^a, Saulo Aparecido da Silva Correa ^b

a *Programa de Pós-Graduação em Geociências, Universidade Federal do Rio Grande do Sul, Bento Gonçalves Avenue, Building 43137, Agronomia, 91501-970, Porto Alegre, RS, Brazil.*

b *Programa de Pós-Graduação em Dinâmica dos Oceanos e da Terra, Instituto de Geociências, Universidade Federal Fluminense, Avenida General Milton Tavares de Souza, s/nº, 4th floor, 24210-346, Niterói, RJ, Brazil.*

* *Corresponding author (e-mail address: scorrea.strat@gmail.com, +5517981205187)*

5.3. Abstract

Submarine canyons represent the most common erosive features occurring on the continental slopes. They cut deeply all continental margins, acting as important conduits for the transfer of sediment from continents to the lower slope and abyssal plains, with a critical role in understanding deep-sea sedimentation. Further, they can constitute an important storage source of hydrocarbon reservoirs linked to turbidite channels. In this paper, we combine the use of complex seismic attributes and spectral analysis to investigate the morphology, architectural elements, lithology, fill patterns, and evolution of Almirante Câmara Canyon, developed at the continental shelf margin in the Campos Basin, southeastern Brazilian margin. A detailed interpretation of these analyses distinguishes four erosive canyon-valley surfaces throughout the canyon's evolution,

allowing an interpretative correlation with the global sea level curve. These canyons have ENE-SSW orientation, U-shaped form passing upward to V-shaped form, roughly perpendicular to the continental slope, with relief ranging from 350-540 m and 1-7.1 km widths. Also, there appears to be a contemporary relationship between faults activity at the initial stages of the Almirante Câmara Canyon evolution. Lastly, an unprecedented evolutionary canyon model was proposed, which is divided into four stages: Stage I - *Erosional Base Surface* (EBS), Stage II - *Almirante Câmara Surface 1* (ACS1), Stage III - *Almirante Câmara Surface 2* (ACS2), and Stage IV - *Almirante Câmara Surface* (ACS3). These results aim to shed light and contribute to understanding the canyon's evolution.

Keywords: Submarine canyon, Seismic attributes, thin-bedded turbidite, *Almirante Câmara Canyon*, Seismic geomorphology.

5.4. Introduction

Submarine valleys or submarine canyons represent one of the most common features on continental margins that contribute to the sea-bottom modeling, considered an important primary conduit of large sediment transport from the continental shelf and upper slope to the deep oceanic basins (Shepard, 1972, 1981; Babonneau et al., 2002; Normark and Carlson, 2003). Also, submarine canyons, sometimes tightly linked to fluvial channels, are linked to large submarine turbidite channels and frequently are associated with sand-rich hydrocarbon reservoirs (Stow and Mayall, 2000; Posamentier, 2003; Normark and Carlson, 2003; Mayall et al., 2006; Meiburg and Kneller, 2010). It is known the most common process responsible for canyon initiation is slope failure, although there is no single origin for submarine canyons. Likewise, gravity-driven processes at continental margins, which occur at different scales, are trigger factors in the origin of canyons, producing a wide spectrum of products and styles (Butler and Turner, 2010; Scarselli, 2020). Commonly, many canyons present a complex internal fill architecture with successive inner-erosive surfaces, resulting from a long-term evolution and interplay of erosion and deposition (Greene et al., 1991; Deptuck et al., 2007; Kane et al., 2013; Mayall et al., 2006).

The Almirante Câmara turbidite system is compounded by three major physiographic elements: a) continental slope with its mature canyon; b) turbidite depositional trough (essentially sand-prone); and c) mass-wasting deposits (Machado et al., 2004). This system belongs to the Carapebus Formation, a relevant Brazilian post-salt petroleum reserve (Machado et al., 1997; Machado et al., 1998). The importance of this modern system is given by its similar conditions of development with ancient turbidite reservoir levels of the Carapebus Formation (Rangel et al., 1994). The observation *in situ* of these reservoir-like sediments consolidates an excellent exploratory and depositional model for the turbidite reservoirs of the Campos Basin (Bruhn et al., 2003; Machado et al., 2004).

In this study, we use complex seismic attributes analysis to investigate and describe the morphology, architectural elements, lithology, fill patterns, and evolution of the Almirante Câmara Canyon throughout its development from Neogene to Quaternary. The results should improve and also shed some light on Almirante Câmara Canyon as a new model of its evolution.

5.5. Geological setting

5.5.1. Stratigraphy of the Campos Basin

The Campos Basin is located on the southeast portion of Brazilian's eastern margin (Fig. 11a). It is limited to the north by the Espírito Santo Basin, by the Vitória High, and the south, by the Santos Basin, by Cabo Frio High, respectively (Fig. 11b). Occupies an area around of 120.000 km² until the bathymetry of 3500 m, where of this total, 500 km² are located at the onshore part.

The tectonic-sedimentary framework of the Campos Basin can be characterized by three distinct Supersequences: A Rift Supersequence deposited under a regime of extensional tectonic and pronounced mechanic subsidence, and the Sag and Passive Margin Supersequences both deposited under a regime of thermal subsidence associated with the cooling of the asthenospheric thermal anomaly and non-diastrophic tectonism (Mohriak et al., 1990; Winter et al., 2007).

The Rift Supersequence is marked by the occurrence of amygdaloidal tholeiitic basalts (Cabiúnas Formation), at the base of the sedimentary column, with radiometric dating between 134 and 122 Ma (Mizusaki et al., 1988). The continental sediments of the Lagoa Feia Formation correspond to a mixed carbonate-siliciclastic sequence predominantly lacustrine, including on the superior part a pack of pelecypods' coquinas (Coqueiros Member), interbedded with carbonaceous black shales, comprising the main

hydrocarbon reservoir of Campos Basin (Pereira et al., 1984; Dias et al., 1988; Guardado et al., 1989; Abrahão and Warme, 1990; Alvarenga et al., 2021).

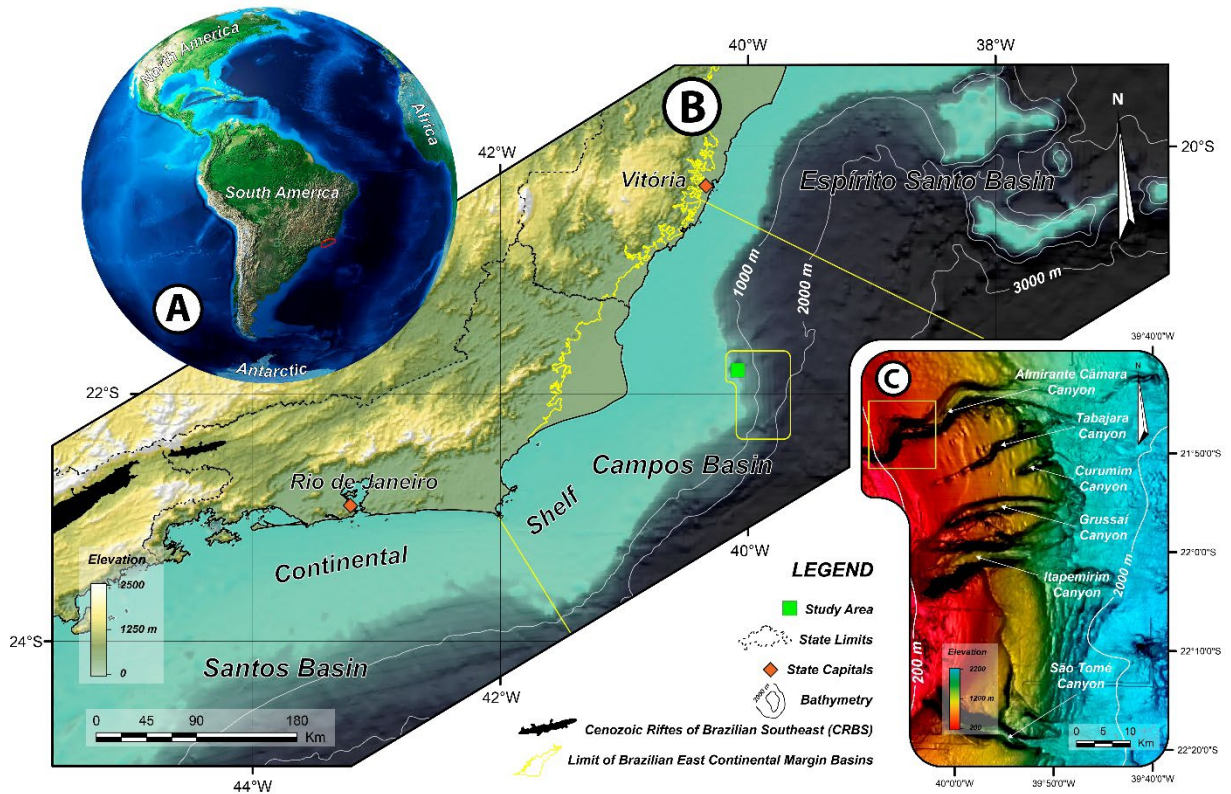


Figure 11 - The location of the *Almirante Câmara Canyon* in the Campos Basin. a) Location of the Campos Basin in the southeastern of the Brazilian's eastern margin; b) Map of the Campos Basin showing its limits with Espirito Santo Basin and Santos Basin; c) Detail map of the Northeast Group of canyons in the Campos Basin, the *Almirante Câmara Canyon* is located in the extreme northwestern portion, and the study area highlighted by a yellow square.

The Sag (or Transitional Supersequence) is characterized by a period of relative tectonic quiescence, registering Aptian siliciclastic deposits and by evaporite deposits of Retiro Member, comprising a thermal-controlled crustal adjustment phase that precedes the end of the rifting process (Pérez-Gussinyé et al., 2020), as part of the Lagoa Feia Formation (Winter et al., 2007).

The Passive Margin Supersequence (or Marine Supersequence) is initially represented by shallow water carbonates of the Macaé Formation during the Albian-Cenomanian (Winter et al., 2007), with sandy facies (Goitacá Member) and calcarenites (Quissamã Member) with a progressive upward and basinward gradation to a sequence of marl and shales (Outeiro Member). The Tamoios Formation corresponds to pelitic sediments of the Turonian age to the Upper Cretaceous, marking a transgressive marine phase. From the Upper-Cretaceous to Lower Miocene is characterized by a marine regressive phase, with the deposition of siliciclastic sediments of the Campos Group, that includes a proximal sequence (Emborê Formation), a carbonate shelf (Grussaí Formation), a distal sequence with slope muds (Ubatuba Formation), besides of turbidite sandstone deposits (Carapebus Formation) interbedded with bathyal shales (Schaller, 1973; Rangel et al., 1994; Winter et al., 2007).

The tectonic of salt is marked on the continental shelf mainly by small escape features, such as domino faults related to the burden-driven escape zone, showing large salt diapirs and walls in the region beyond the shelf break, slope, and abyssal basin, influencing strongly younger sequences, originating anticlines, roll-lovers faults, depocenters localized between salt diapirs (mini-basins), with compressional features next to the crustal limit (Figueiredo and Martins, 1990; Demercian et al., 1993; Cobbold et al., 1995; Amarante et al., 2021).

During the Cenozoic two important stratigraphic marks are recognized in the Campos Basin (Fig 12). The first one originated in the Inferior-Oligocene (Rupelian), denominated by the Blue Mark, which occurs almost throughout the basin, composed of calcilutites rich in nanoplankton *Braarudosphaera bigelowii*, that represents an important event of flooding in the basin - a Maximum Flooding Surface (Rangel et al., 1994; Winter et al., 2007). The second one was formed between the Middle and Upper Miocene through a significant fall in sea level, originating an important erosional unconformity, denominated

by Gray Marker (Viana, et al., 1990; Silva, 1992). Above this unconformity, with *onlap* features, present a carbonate shelf sequence of the Emborê Formation and Grussaí Member (Viana et al., 1998).

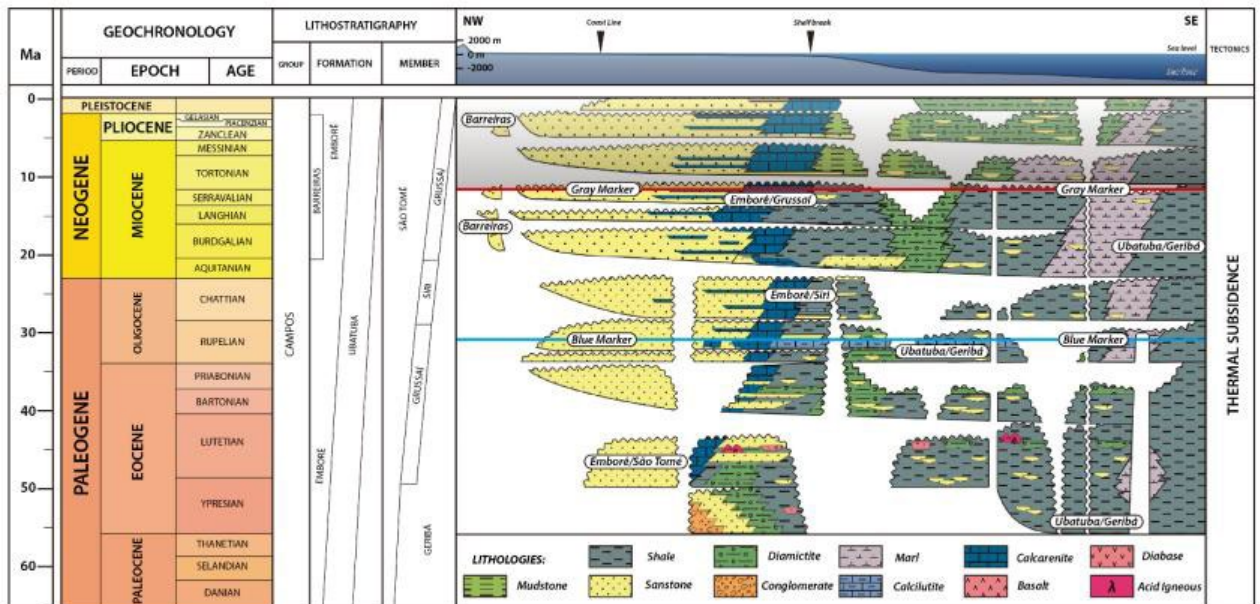


Figure 12 - Chronostratigraphic chart of the Cenozoic in the Campos Basin. (Modified from Winter et al., 2007). The grayscale-shaded area comprises the stratigraphic interval that is of interest to this work, inferiorly limited by the Gray Marker (red line) and geologically correspondent to the unconformity between the Middle and Upper Miocene (Viana et al., 1990; Silva, 1992). The blue line represents the Blue Mark of the Inferior-Oligocene age (Rangel et al., 1994; Winter et al., 2007).

5.5.2. The *Almirante Câmara Canyon*

Belonging to the Northeast Group of canyons of the Campos Basin, together with the canyons Tabajara, Grussaí, Itapemirim, and São Tomé (Almeida and Kowmann, 2014), the *Almirante Câmara Canyon* has 28 km length, 4 km of width, 340 m of relief, with a general and highly sharp-end sinuous tracing, indicating strong structural conditioning (Fig. 11c). Is the only mature canyon in the Campos Basin characterized by a deep carving "V" profile, a very sinuous channel on its thalweg and a pronounced indentation of its headboard on the continental shelf (Farre et al., 1983; Machado et al., 2004).

Initially, the canyon developed a typical "U" section of the juvenile phase, through progressive collapses of its headboard slope above, resulting in mass movements deposited predominantly on the São Paulo Plateau. In the mature phase the canyon meshed the continental shelf, capturing the Paraíba do Sul River where the fluvial underflow current eroded a deep sinuosity gutter within the muded bottom of the U-shape of the juvenile phase. In this way, there are rigorously two agents of canyon excavation, one eroding into the carving of the other, and it is by the V-shape of the mature phase that the sands are transferred to deep waters (Machado et al., 2004; Almeida and Kowsmann, 2014).

Lastly, the geometry of *Almirante Câmara Canyon* is an indicative factor that the depositional lobe did not form at one time, but in multiple episodic events during a long geological time once that it is not possible to pass the gigantic volume of sand of the depositional lobe (deeper) throughout the narrow canyon of 340 m (Machado et al., 2004).

5.6. Methodology

5.6.1. Dataset and Relative Age calibration

The seismic data utilized is a full-stack 3D seismic cube located in the central portion of the Campos Basin (see the yellow square in Fig. 11c) with a surface coverage of approximately 12.6 x 11.6 km². The data volume consists of 1000 inlines and 932 crosslines spaced both spaced 25 m and a vertical extent of 0-2000 ms, with a 4 ms standard sample rate. The 3D seismic survey was processed and migrated through the numerical technique of finite-difference migration (MIG FIN) (Yilmaz, 2001).

Precise age control for the stratigraphic interval studied in this work is not available due to the lack of well data in the study area. For this reason, was established a relative age calibration for the interval of investigation to provide only a rough estimate of its age from

the collection of the available data extensively documented in the literature, leading to the recognition of a reliable correlation between the most basal interpreted surface (i.e. the Erosional Base Surface-EBS) to the limit between the Middle-Miocene and the Upper-Miocene (Barker et al., 1983a, 1983b; Gambôa et al., 1983; Castro, 1992; Mézerais et al., 1993; Alves, 1999; Viana et al., 2003). This surface is characteristically erosive and irregular, marked by a high-amplitude reflector with regional distribution along the Brazilian eastern margin dated at 10.8 Ma and corresponding to the Gray Mark of the Campos Basin (Viana, et al.; 1990; Silva, 1992; Artusi, 2004; Pellizon, 2005). Moreover, the age of the surfaces overlaid to EBS is speculative, except the age of the most recent surface.

The seismic analysis and interpretation were carried out in the open-source software OpendTect Pro® (Version 6.2). The seismic reflectors were picked and tied manually (2D auto-track) throughout the 3D seismic volume to ensure much more accuracy of interpreted surfaces, with a grid increment on inlines and crosslines of 25 x 25 (i.e., 300 x 300 m). Four horizons were interpreted, namely the *Erosional Base Surface (EBS)*, *Almirante Câmara Surface 1 (ACS1)*, *Almirante Câmara Surface 2 (ACS2)*, and *Almirante Câmara Surface 3 (ACS3)*. An integrated methodology was employed to optimize the horizons interpretation in this work and the workflow is summarised in Fig. 13.

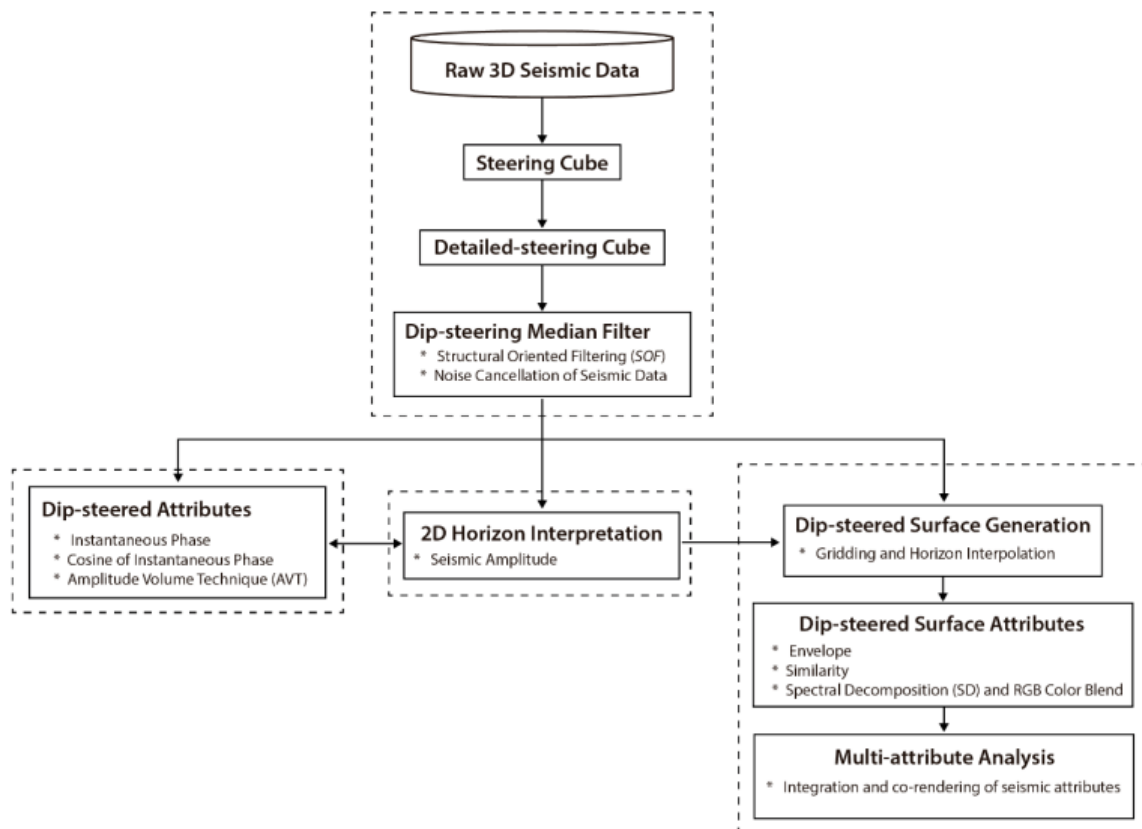


Figure 13 - Schematic workflow showing the stages and implemented methodology in the processing to optimize the seismic analysis and interpretation of the 3D seismic data.

5.6.2. *SteeringCube* and *Dip Steered Median Filter (DSMF)*

Before the application of a *Dip-steered Median Filter* to seismic data, is required to create a *SteeringCube* that consists of a volume computed from seismic data by the extraction of every sample position information about the local dip and azimuth, composing the principal foundation for the structurally oriented filtering (Tingdahl, 1999; Tingdahl et al., 2001; Höcker and Fehmers, 2002; Iacopini et al., 2012). A *Detailed SteeringCube* is calculated by taking sufficiently close samples to preserve details and obtain the improvement in the observation of faults, flexures, and local stratigraphic features of small scale (Brouwer, 2007; Brouwer and Huck, 2011).

For the computation of the Detailed SteeringCube was applied the Fast Fourier Transform (FFT) based algorithm that uses seismic frequency and amplitude attributes, and is chosen as a method that preserves geologic details such as fault dips and stratigraphy. (Qayyum and de Groot, 2012; Jaglan et al., 2015). Lastly, a *Dip-steered Median Filter* was applied to *SteeringCube* to improve the quality of the raw 3D seismic data by the enhancement of signal-to-noise ratio (Chopra and Marfurt, 2007).

The calculation *a priori* of the *SteeringCube* allows the immediate use of the dip-steered attributes that always have an advantage over the non-steered attributes, improving the multi-trace attributes by extraction attributes input along reflectors (Jaglan et al., 2015). This process will produce more accurate geological features such as geomorphology, faults, and channels rather than artifacts (Qayyum and de Groot, 2012).

5.6.3. Complex seismic trace attributes

The analysis of the complex seismic trace allows a natural separation between the amplitude and the phase content of the seismic data, from which the instantaneous complex attributes are calculated without losing sight of local variations (Taner et al., 1979). Once complex seismic attributes are sensitive to changes in acoustic impedance and, thus, sensitive to lithology, porosity, content of fluids (hydrocarbons), and tuning bed thickness, they can provide and improve geological information that sometimes cannot be directly identified in a zero-offset seismic data (Taner et al., 1979; Barnes, 2016). The appropriate choice of the horizons interpreted in this work was mediated by the seeking of high-amplitude continuous reflectors, aiming to avoid the phase change during their tracking and that had crucial stratigraphic significance.

Three complex attributes were utilized in an integrated way for the interpretation of horizons on the 2D seismic sections to optimize and impart rigor to the process: the

Instantaneous Phase, the Cosine of Instantaneous Phase, and the Amplitude Volume Technique (Taner et al., 1979; Bulhões and Amorim, 2005).

The instantaneous Phase emphasizes the continuity of events, allowing a better definition of events with low amplitude and low coherence. It is effective in showing discontinuities, faults, pinchouts, angularities, and stratigraphic patterns of onlap and downlap, especially helpful in recognizing sequence boundaries (Taner et al., 1979; Mitchum Jr. et al., 1977). Mathematically is calculated taking the argument of the seismic complex trace, where $f^*(t)$ ¹ is the quadrature of the seismic trace and $f(t)$ is the real part of the seismic trace and it is expressed as:

$$\theta(t) = \tan^{-1} \left(\frac{f^*(t)}{f(t)} \right) \quad (23)$$

As long as both $f^*(t)$ and $f(t)$ are in phase, the displayed color is the same for -180° and 180°. Once the instantaneous phase assumes the value of zero whenever there is a local maximum of seismic amplitude, this attribute effectively is taken as a good indicator of seismic events (Taner et al., 1979).

The Cosine of Instantaneous Phase has no amplitude information. Since it rescales the output data in a range of -1.0 to 1.0, this attribute can be described as a normalization of the seismic trace and it is expressed by:

$$\cos[\theta(t)] = \cos \left[\tan^{-1} \left(\frac{f^*(t)}{f(t)} \right) \right] \quad (24)$$

¹ Although not demonstrated, the quadrature of the seismic trace is calculated by taking the Hilbert Transform ($H(u)(t)$) on the seismic trace, given by $f^*(t) = H\{f(t)\}$

The normalization effect enhances the continuity of reflections, commonly applied to guide interpretation in areas with low resolution of amplitude to optimize geological features like faults and to delineate stratigraphic patterns of terminations (Taner et al., 1979; Barnes, 2016). According to Barnes (2016), this attribute represents the seismic data with all contrasts of amplitude removed, acting like a strong automatic gain.

The Amplitude Volume Technique (AVT) is based on the Elementary Seismic-Layer Principle. The Elementary Seismic-Layer (ESL) represents the smallest layer thickness or set of layers that seismic data can solve, as an approximation of the limit resolution defined by Rayleigh in the Yilmaz vertical seismic resolution approach. (Kallweit and Wood, 1982; Yilmaz, 2001; Bulhões and Amorim, 2005; Vernengo and Trincherro, 2015).

The *ESL* is a key element of ponderation for the calculation of the AVT attribute, and its obtention is based on the observation of the smallest period T related to the highest frequency, in time or depth, where the thickness M of *ESL* will be the half of the observed period (Bulhões and Amorim, 2005).

Assuming a seismic trace at a determined interval of time t with period T , and t_1 , t_2 correspondents to the top and base of the layer, respectively. The *ESL* is the window that will correspond to the number of samples to be used in the calculation of the moving average along the seismic trace (Fig. 14).

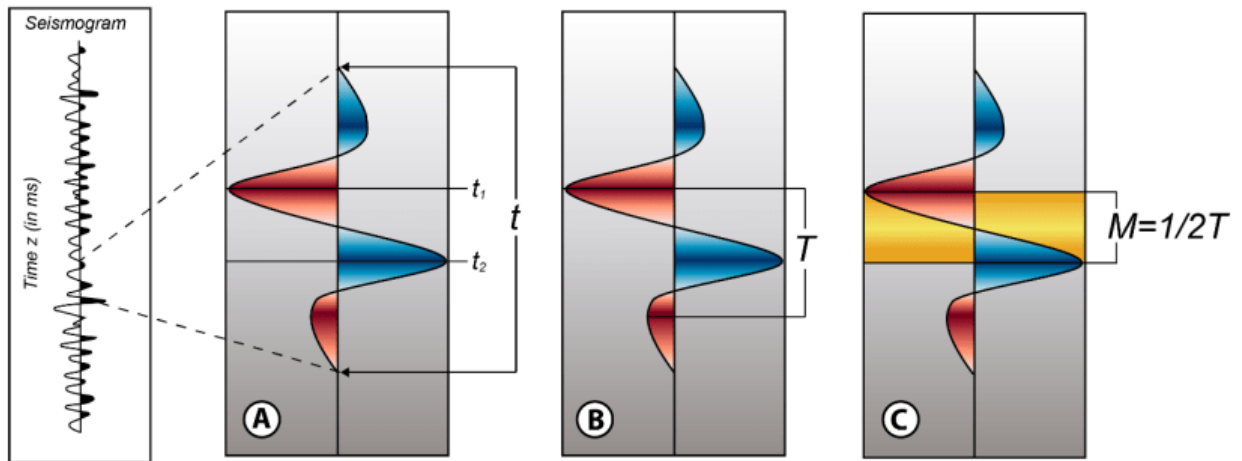


Figure 14 - Idealized seismogram showing the principles and geological significance of the Elementary Seismic-Layer (ESL), a) t_1 and t_2 considered such as the top and base of the layer at a determined interval t ; b) hypothetic period T for the highest frequency observed in the seismic data; c) moving window taking the length M equal to $T/2$ (Modified from Bulhões and Amorim, 2005).

The first step in the construction of the AVT attribute is the calculation of the RMS Amplitude, modulated by a scale factor proportional to the defined moving window (ESL).

The RMS Amplitude is given by the equation:

$$A_{RMS_j} = \sqrt{\frac{1}{M} \sum_{j=i-\frac{M}{2}}^{j=i+\frac{M}{2}} a_j^2} \quad (25)$$

Where M is the length of the moving window (in ms), j is the position of the sample, $i = 1, 2, 3, 4, \dots, (n-2), (n-1), n$ is the step of the moving window centered at the sample j , and a_j is the amplitude of the sample.

After the calculation of RMS Amplitude, the next proceeding is to apply a phase rotation of $-\pi/2$ on the resultant seismic trace. Analytically, this operation corresponds to an Inverse Hilbert Transform on the trace, given by:

$$A_{RMS} \left(\frac{\pi}{2} \right)_j = H^{-1} \{ A_{RMS_j} \} \quad (26)$$

To evaluate the amplitudes throughout the 3D seismic survey, the power spectral density was extracted, for which the maximum frequency of 125Hz was observed, whose period of 0.002 ms is the thickness M found for the ESL, used in the calculation of the AVT attribute.

Using alternately the co-visualization of multiple seismic attributes previously described with the amplitude seismic data, it was possible to enhance the delineation and lateral continuity, as well as reveal more detail for the interpreted surfaces across the 3D seismic cube (Fig. 15).

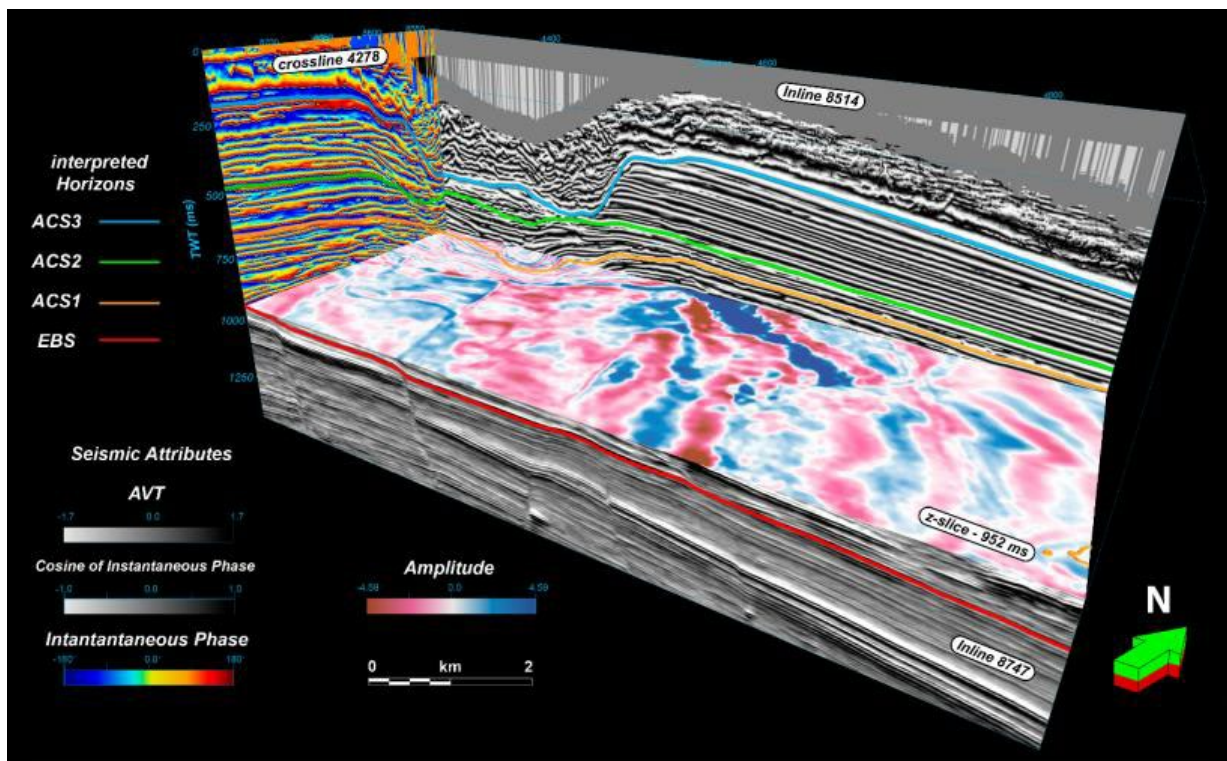


Figure 15 - Panoramic view of the co-visualization for the amplitude and complex seismic attributes used for the horizon's interpretation from the 3D seismic data. Inline 8514 shows the cosine of the Instantaneous Phase attribute. The inline 8747 shows the AVT attribute. The cross-line 4278 shows the Instantaneous phase. The z-slice 952 shows the amplitude data.

Other seismic attributes adopted in this work include Instantaneous Amplitude and Similarity within the interpreted horizons aiming to reveal more details of sedimentary features, structures, and seismic amplitude anomalies.

Instantaneous Amplitude or Envelope is the total energy of the complex seismic trace at a determined instant. The Envelope is phase-independent, which means that the maximum values of the Envelope cannot be in the same position of peaks or troughs when compared with the zero-offset seismic section (Taner et al., 1979).

High values of Envelope are often associated with major lithologic changes between adjacent rock layers, such as sequence boundaries associated with sharp changes in sea level or depositional environments. Also, can be associated with gas accumulations as bright spots and it is a good Direct Hydrocarbon Indicator (DHI) (Taner et al., 1979; Chopra and Marfurt, 2005; Barnes, 2016). The Envelope is mathematically expressed by:

$$E = \sqrt{f^2(t) + f^{*2}(t)} \quad (27)$$

The Similarity attribute is a form of coherence that expresses how much two or more traces look alike. Assuming two vectors x_i and y_i , where i is the number of the samples. The similarity is defined as the Euclidean distance between the amplitude vectors, normalized over the sum of the length vectors (Jaglan et al., 2015). Mathematically is expressed as:

$$S_{im} = 1 - \frac{\sqrt{\sum_{i=1}^N (x_i - y_i)^2}}{\sqrt{\sum_{i=1}^N x_i^2} + \sqrt{\sum_{i=1}^N y_i^2}} \quad (28)$$

Seismic discontinuities can be generated from faults and stratigraphic features, which change the characteristics around these seismic traces promoting a loss of similarity between the seismic traces sampled (Bahorich and Farmer, 1995). High values of similarity mean that the segments are completely identical in waveform and amplitude, while null values mean that they are completely dissimilar (Chopra, 2002). The time-gate window used for the calculation of the Similarity attribute was -28.0 to 28.0 ms.

5.6.4. Advanced seismic attributes

The use of advanced seismic attributes allows the seismic interpretation process to improve the quality and confer reliability to the interpreted seismic data, considered an important stage to aid especially in quantifying subsurface reservoirs heterogeneities such as permeability, porosity, lateral continuity, elastic properties, reducing the risk analysis in exploratory frontier, and more recently, for the assessment of reservoirs for CO₂ sequestration (Baranova and Mustaqeem, 2010; Liner et al., 2010; Marfurt et al., 2011).

In this scenery, the Spectral Decomposition method is summarily important for generating and analyzing maps of seismic attributes, and that allows a suitable definition to determine stratigraphic sequences, as well as to reveal channel systems and structural characteristics of the reservoirs (Partyka et al., 1999; Henderson et al., 2007; Barnes, 2016).

Time-frequency decomposition or Spectral Decomposition (SD) is a data analysis process that breaks down the seismic signal into its narrow bandwidth discrete-frequency components (Partyka et al., 1999; Partyka et al., 2011). The computing algorithm used to realize the SD in this study was the Short-time Fourier Transform (STFT), in which a time-frequency spectrum is produced by taking the Fourier Transform over a chosen short time window (Cohen, 1995; Partyka et al., 1999).

To optimize the SD analysis, the concept of "Tuning Cube" was used according to the approach proposed by Partyka et al. (1999). The "Tuning Cube" consists of a frequency domain representation where a short temporal window is extracted from the target zone of interest within the 3D seismic data and is transformed from the time domain into the frequency domain (Partyka et al., 1999). For each interpreted horizon the bounds of zone-of-interest correspond to a temporal window of -24.0-24.0 ms, which were extracted from the power spectrum, and chosen the best results in terms of the different magnitude frequencies (Fig. 16).

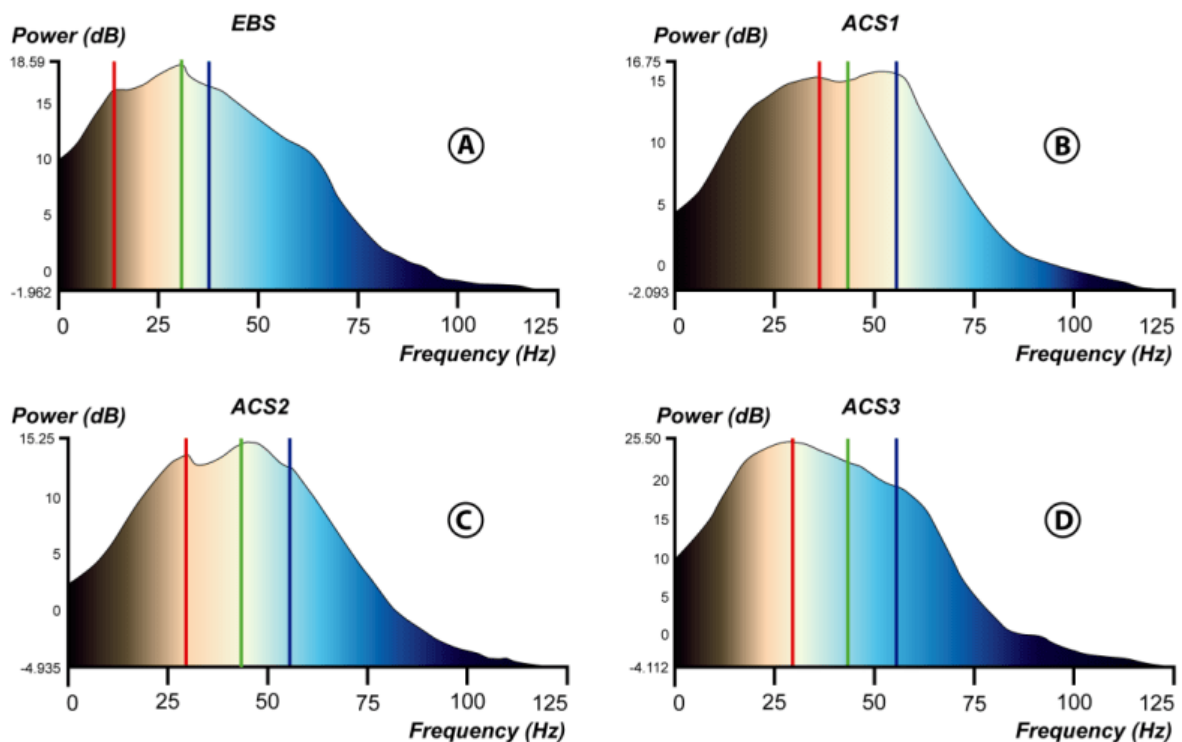


Figure 16 - Power spectral density extracted from each interpreted horizon along the zone-of-interest, showing the central frequencies chosen for each RGB composition: a) 15Hz, 30Hz, and 40Hz; b) 35Hz, 45Hz, and 55Hz; and c); d) with the same frequencies of 30Hz, 45Hz, and 55Hz, respectively. The color below the power spectral density curves represents a relative distribution of Power (dB).

According to the generated power spectrums shown in Fig. 16, were selected the central frequencies at 15Hz, 30Hz, and 40Hz to EBS; 35Hz, 45Hz, and 55Hz to ACS1; and 30Hz, 45Hz, and 55Hz to surfaces ACS2 and ACS3, respectively.

The Red-Green-Blue (RGB) color blending was performed to combine the three spectral components representing low, intermediate, and high frequencies (Henderson et al., 2007; Henderson, 2012). The resulting composite RGB image shows variation in color and intensity that correlates with the change in magnitude response at the different frequencies (McArdle and Ackers, 2012; Gilani and Gomes, 2015). Thus, the RGB color blend can show qualitative variations in lithology, bed thickness, and pore fill, where generally thinner beds will be better displayed with higher frequency components as blue; green suggests moderately thick features and thicker beds with lower frequency showed as red (Barnes, 2016). White indicates features that have strong response at all frequencies, such as solitary bright spots reflections, and black indicates features that have weak amplitudes at all frequencies, such as faults and weak reflections (Castagna et al., 2003; McArdle and Ackers, 2012; Gilani and Gomes, 2015).

The resultant RGB color blended cube is expressed as:

$$I_{RGB}(\mathbf{x}) = S \left[I_R(\mathbf{x}), I_G(\mathbf{x}), I_B(\mathbf{x}) \right] \quad (29)$$

where $x = (x, y, z)$ is the position within the 3D volume, and S defines the linear transformation applied to each of the three input volumes $I_R(\mathbf{x})$, $I_G(\mathbf{x})$ and $I_B(\mathbf{x})$ to fit the input data into the 3D $I_{RGB}(\mathbf{x})$ color blended space. The linear transformation S assigns a color to each point in an output volume (i.e., a voxel) based on the values in each of the three input volumes (Henderson et al., 2008; McArdle and Ackers, 2012).

5.7. Results and Interpretations

The use of complex seismic attributes and multi-attribute analysis was performed in order to assess as well as reveal geometric and sedimentological details from the interpreted surfaces, focusing on the canyon's fill and evolution throughout the stratigraphic interval (Middle-Upper Miocene to Holocene) studied in this work (Fig. 17).

All surfaces were picked as a zero-phased normal SEG polarity, corresponding to a local maximum peak with high reflectivity and amplitude seismic response (Fig. 18a). As shown in the crossline 4669 (Fig. 18b-d), the combined use of complex seismic attributes (i.e., the Instantaneous Phase, Cosine of Instantaneous Phase and AVT) brings out the lateral continuity and aid principally in the mapping of the surfaces as well as support to resolve the internal architectural complexity of the canyons. By simplification, we assume that *Almirante Câmara Canyon* fills for the stratigraphic interval is composed of multiple cycles of waxing energy followed by waning flow energy (waxing-waning cycles) at multiple scales (McHargue et al., 2011). However, each cycle has not been systematically mapped given its complexity. In turn, these cycles are made up of a myriad of erosive, by-passing, and depositional events of high-frequency cyclicity during a long geological time (Machado et al., 2004).

It can be seen that the canyon-valley systems are strongly influenced by a basal and primary carved deep canyon with secondary smaller peripheral channels associated (Fig.17 and 18a,d). The canyons' infill comprises a series of vertical to sub-vertical stacked channel forms, with discrete lateral step-wise shifts of the channels, internally characterized by cut-and-fill architecture. This aggradational pattern creates on the thalweg of the canyons, seismic facies with narrow zones of high-amplitude reflectors (HARs) dying out laterally that appear as continuous and horizontal seismic reflections (e.g., Deptuck et al., 2003). These laterally extensive sheets with high amplitudes are interpreted here as channel-axis deposits infilling the canyons (Fig. 18a,d). HARs width

ranges from 140-200 m with a thickness of deposits that ranges from 12.0-15.0 ms (TWT), and represents a maximum thickness of ca. 10.8-13.5 m, assuming an internal velocity wave propagation of $1800 \text{ m} \cdot \text{s}^{-1}$ (adequate according to Viana et al., 2003).

Zones of chaotic and weak to moderate seismic amplitudes can also be seen immediately above the EBS, and are interpreted as Mass-Transport Deposits (MTD). The chaotic amplitude reflectors can be associated with rotational slump blocks, while the weak to moderate amplitude reflectors are associated with rotational slide blocks given the preservation of its internal stratal architecture (Fig 18a,d). Although MTD is often an important component of canyon-valley worldwide systems' infilling and at multiple scales (Mayall and Stewart, 2000; Posamentier and Kolla, 2003; Mayall et al., 2006), in this work we will not discuss these deposits carefully. The interpreted surfaces are described below.

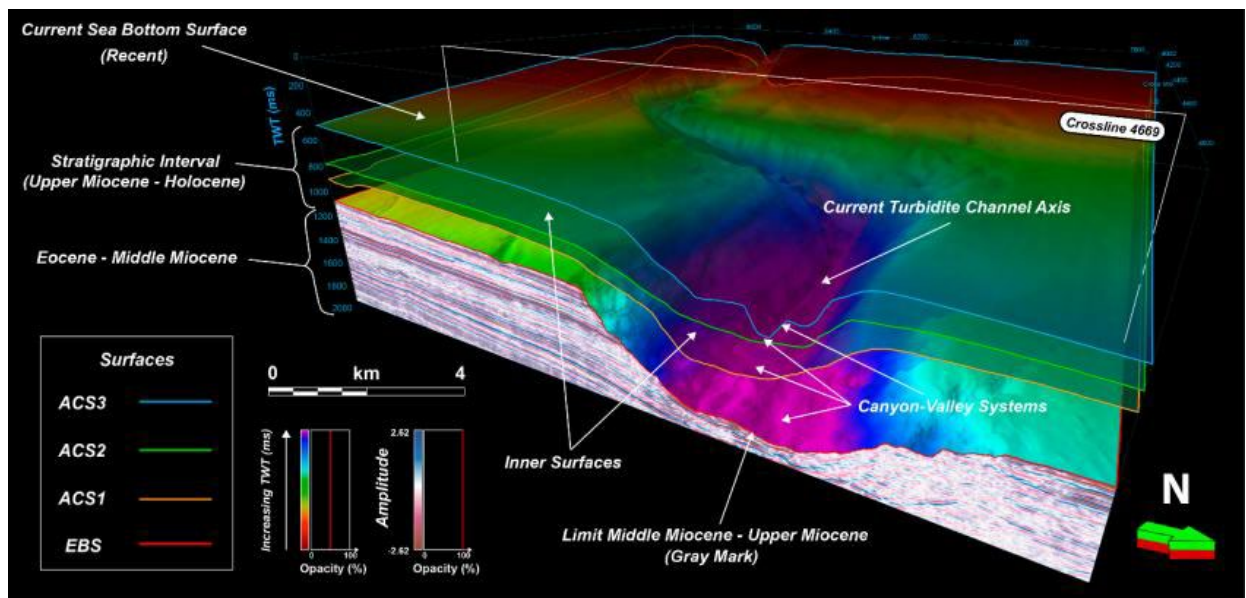


Figure 17 - 3D seismic volume showing a summarized view of stacked interpreted horizons. The surfaces show canyon-valley systems that cross the volume. Opacity has been applied in the surfaces ACS1 (pink line), ACS2 (green line), and ACS3 (blue line) to enhance the visualization of its lateral extension, depth, and carved features of the canyon-valley systems. The crossline 4669 is shown in detail in Fig. 18.

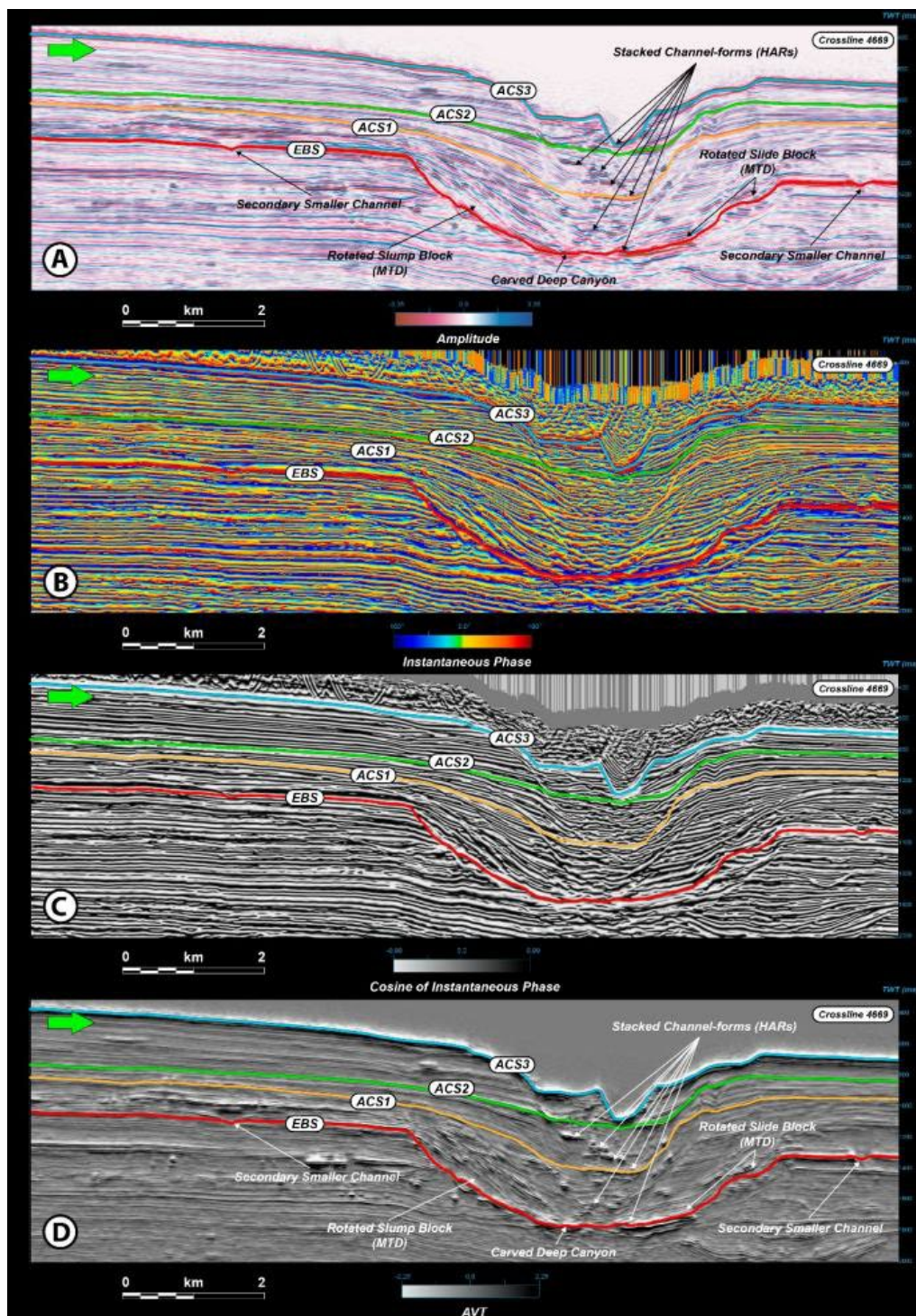


Figure 18 - Crossline 4669 shows in detail the interpreted horizons across the seismic amplitude and three other seismic attributes. a) Crossline 4669 of amplitude seismic data showing the EBS, ACS1, AC2, and ACS3 horizons, stacked channel forms (HARs), MTD, and secondary smaller channels. b) Crossline 4669 of Instantaneous Phase attribute showing the EBS, ACS1, AC2, and ACS3 horizons with different phase content on seismic data. c) Crossline 4669 of Cosine of Instantaneous Phase attribute showing the EBS, ACS1, AC2, and ACS3 horizons normalized at a grayscale. d) Crossline 4669 of AVT attribute showing the EBS, ACS1, AC2, and ACS3 horizons, stacked channel forms (HARs), MTD, and secondary smaller channels. The combined use of the seismic attributes brings out details of the canyons' infill and assists in resolving its internal complexity.

5.7.1. Erosional Base Surface (EBS)

The Erosional Base Surface is the most basal mapped surface, with a depth (TWT) ranging from 510 to 1881 ms (Fig. 19a,b). This surface is marked by its strongly erosive characteristic of regional distribution, corresponding to a maximum amplitude peak and a strong continuous reflector regarding the successive surfaces (Fig. 18a).

The Erosional Base Surface shows a moderately sinuous U-shaped canyon, ranging in width from 4 km to 7.2 km, with a relief of ca. 540 m and east-western direction. It is interpreted as a juvenile stage of canyon development. Due to the strongly erosive characteristics, this development stage of the EBS surface indicates that it is related to a relative sea-level fall (Fig. 19a).

The use of the Similarity attribute (Fig.19c) enhances details and highlights the boundaries of the canyon, as well as slide scars and rotated slide block features that constitute canyon fill deposits. Slump deposits (MTD) can be identified on the canyon's northern and southern flanks, characterized by low similarity values. Thin-turbidite deposits inside the canyon have high similarity values (Fig.19c). The north and south canyon margins show normal faults, ranging from ca. 5 km-12 km, and north-south structural trend, which likely conditioned the development of this structure. Likewise, three smaller channels develop in the northern and southern flanks outside the canyon (Fig.19c). The RGB frequency blend shows lateral and internal variability of the canyon and channel deposits, where thin bed deposits below seismic resolution present high-frequency responses (brightness zones, Fig. 19d). In turn, areas with high-frequency responses correspond to high Envelope, supporting the presence of thin bed sandy deposits inside the canyon and associated channels (Fig. 19d,e).

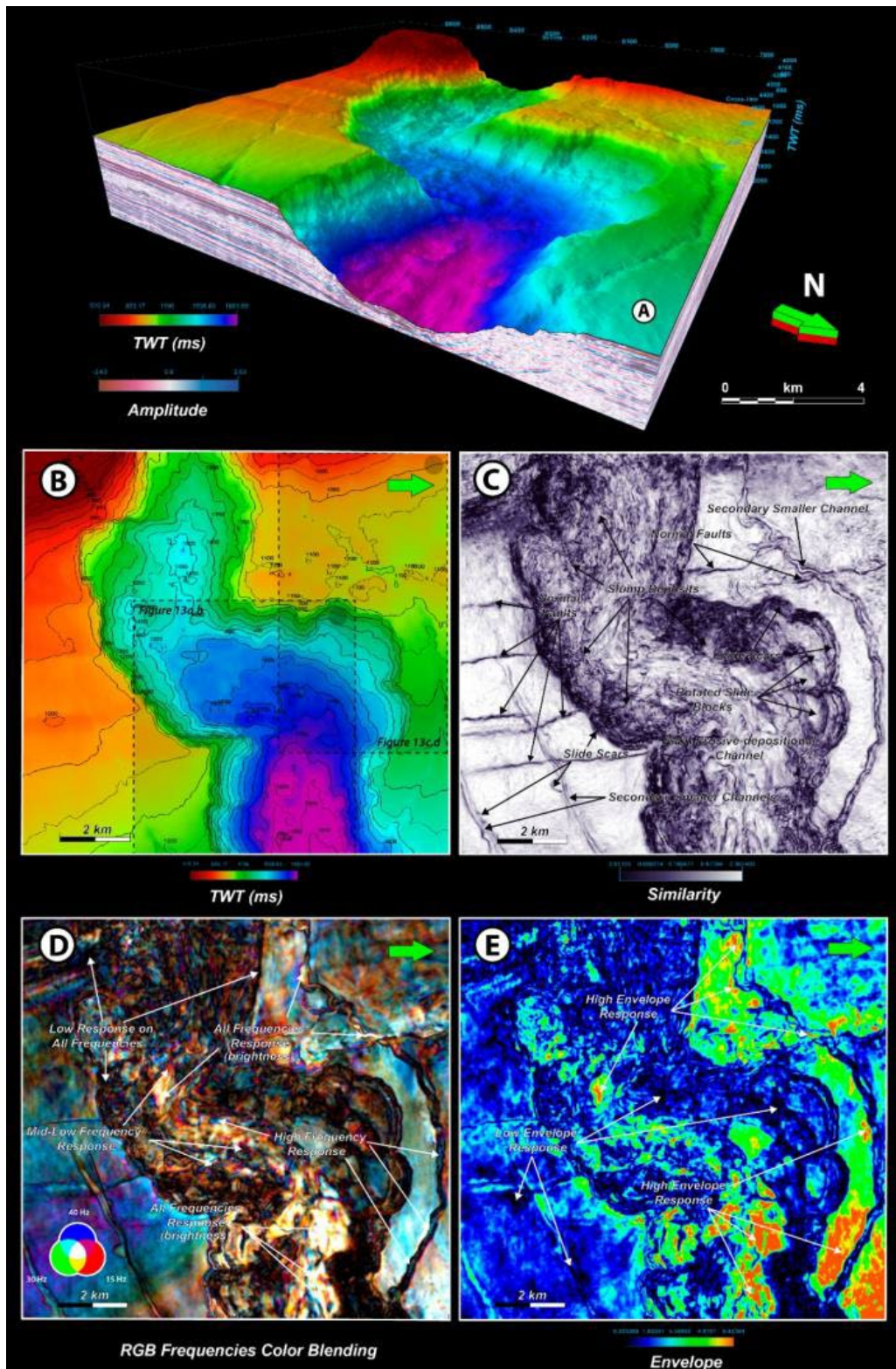


Figure 19 - a) 3D topographic map of the Erosional Base Surface (EBS) in TWT [ms]. The perspective view shows a central carved deep canyon, moderately sinuous, with secondary smaller channels. b) 2D view of the EBS topographic map. c) Similarity attribute map of the EBS. d) RGB frequency color blend (15Hz, 30Hz, and 40Hz), showing internal thickness variability throughout the canyon and channel deposits. High-frequency responses indicate thin-thickness deposits. e) Envelope attribute map of the EBS.

5.7.2. *Almirante Câmara Surface 1 (ACS1)*

The Almirante Câmara Surface 1 is the mapped surface superimposed on EBS, with a surface depth (TWT) ranging from 251 to 1499 ms (Fig. 20a,b). This surface presents a southwest-northeastern downdip gradient with regional distribution, corresponding to a maximum peak with a moderate and continuous amplitude reflector (Fig. 18a).

The ACS1 shows a moderate erosive sinuous U-shaped canyon with an east-western trend, a width ranging from 1.2 km to 2.5 km, and a relief of 360 ms (heights ca. 325 m). It is interpreted as a canyon juvenile phase, driven by progressive collapses of the headboard slope above (Fig. 20a).

The Similarity attribute (Fig. 20c) brings out a set of normal faults with a north–southern and west–east trend, ranging from ca. 0.6 km–2.7 km. Slide scars and landslide deposits (MTD) features show low similarity values, playing a role as a permanent feeding mechanism throughout the canyon development. It is observed an undeveloped feeder tributary channel with a northwest–southeastern trend, as well as incipient channels on the canyon's inner terrace (Fig. 20c). Pockmarks present as circular to sub-circular anomalies and can be identified on the canyon edge neighborhood, ranging from 70 m to 580 m, and heights of ca. 15 ms–83 ms (13 m–73 m; Fig. 20c,d). They are geo-spatially associated with shallow depressions geometries and appear on envelope maps as strong and sharply bounded high amplitude regions - *positive high amplitude anomalies* (PHAAs). These PHAAs are often interpreted as the result of gas chimneys due to gas accumulation in older strata units (Andresen et al., 2008; Ho et al., 2012). The RGB frequency blend shows lateral thickness variation throughout the ACS1 and its canyon-inner channel deposits, with high-frequency responses indicating thin-bedded sandy deposits (Fig. 20d). The Envelope map shows high values amplitudes for these deposits (Fig. 20e).

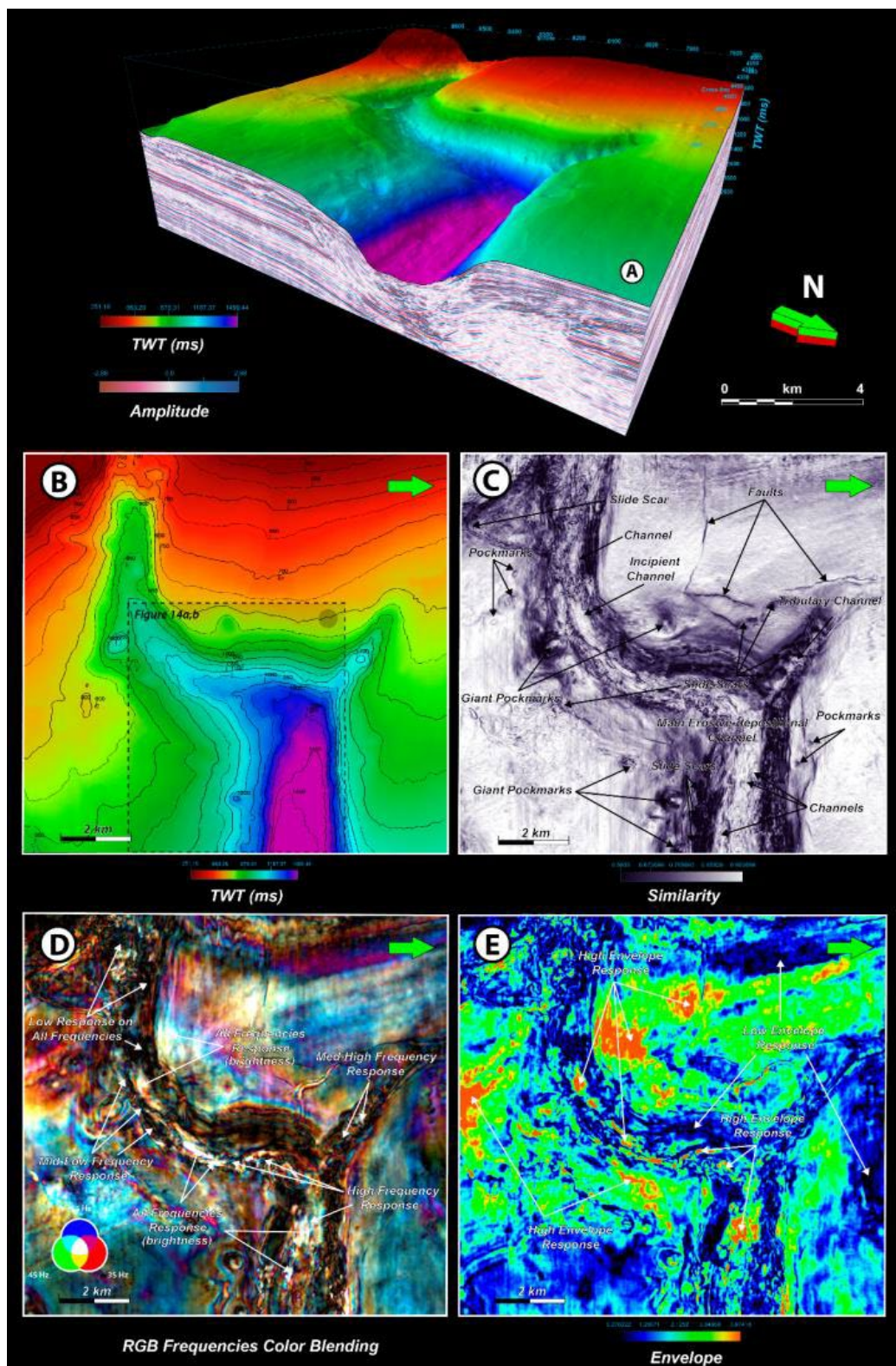


Figure 20 - a) 3D topographic map of the Almirante Câmara Surface 1 (ACS1) in TWT [ms]. b) 2D view of the ACS1 topographic map. c) Similarity attribute map of the ACS1. d) RGB frequency color blend (35Hz, 45Hz, and 55Hz), showing internal thickness variability throughout the canyon and channel deposits. High-frequency responses indicate thin-thickness deposits. e) Envelope attribute map of the ACS1.

5.7.3. *Almirante Câmara Surface 2 (ACS2)*

The Almirante Câmara Surface 2 mapped superimposes the ACS1, with a depth (TWT) ranging from 305 to 1246 ms (Fig. 21a,b). This surface also shows a regional distribution with a southwest-northeastern downdip gradient and is eroded in the southwest portion of the study area. It corresponds to the maximum of a peak with a moderate and continuous reflector, becoming disrupted when approaching its eroded zone (Fig. 21a).

The Almirante Câmara Surface 2 maintains the moderate erosive sinuous U-shaped canyon with an east-western trend, a width ranging from 1.3 km to 2.5 km, and a relief of 260 ms (ca. 234 m). According to its erosive characteristics, ACS2 is interpreted as a canyon transitional phase, with continental shelf exposure and subsequent erosion on its headboard by a relative sea-level fall (Fig. 21a).

The similarity attribute (Fig.21c) highlights the canyon's edge and slide scar features, showing an erosive-dominated channel on the canyon thalweg. A terrace slightly higher than the main channel develops on its interior, with incipient channels cutting through this relief. Also, an undeveloped feeder tributary channel with a northwest–southeastern trend is observed, likely fed by autochthonous landslides. Pockmarks present as circular anomalies at the canyon edge neighborhood, ranging from 170 m to 500 m, and heights of ca. 15 ms-63 ms (13 m-57 m, Fig. 21c,d). An incipient mass flow (MTD) and a frontal pressure ridge can be seen in the outer southern portion of the canyon (Fig. 21c). The RGB frequency blend shows internal thickness variability of the ACS2 and the lack of thin-bedded deposits in the canyon thalweg (Fig. 21d). High Envelope values on the inner canyon terrace are interpreted as exposure and erosion events of older strata units. Otherwise, canyon thalweg with low Envelope values, unresponsive to any frequency (black values), are interpreted as bypass sediments towards the deep basin (Fig. 21d,e).

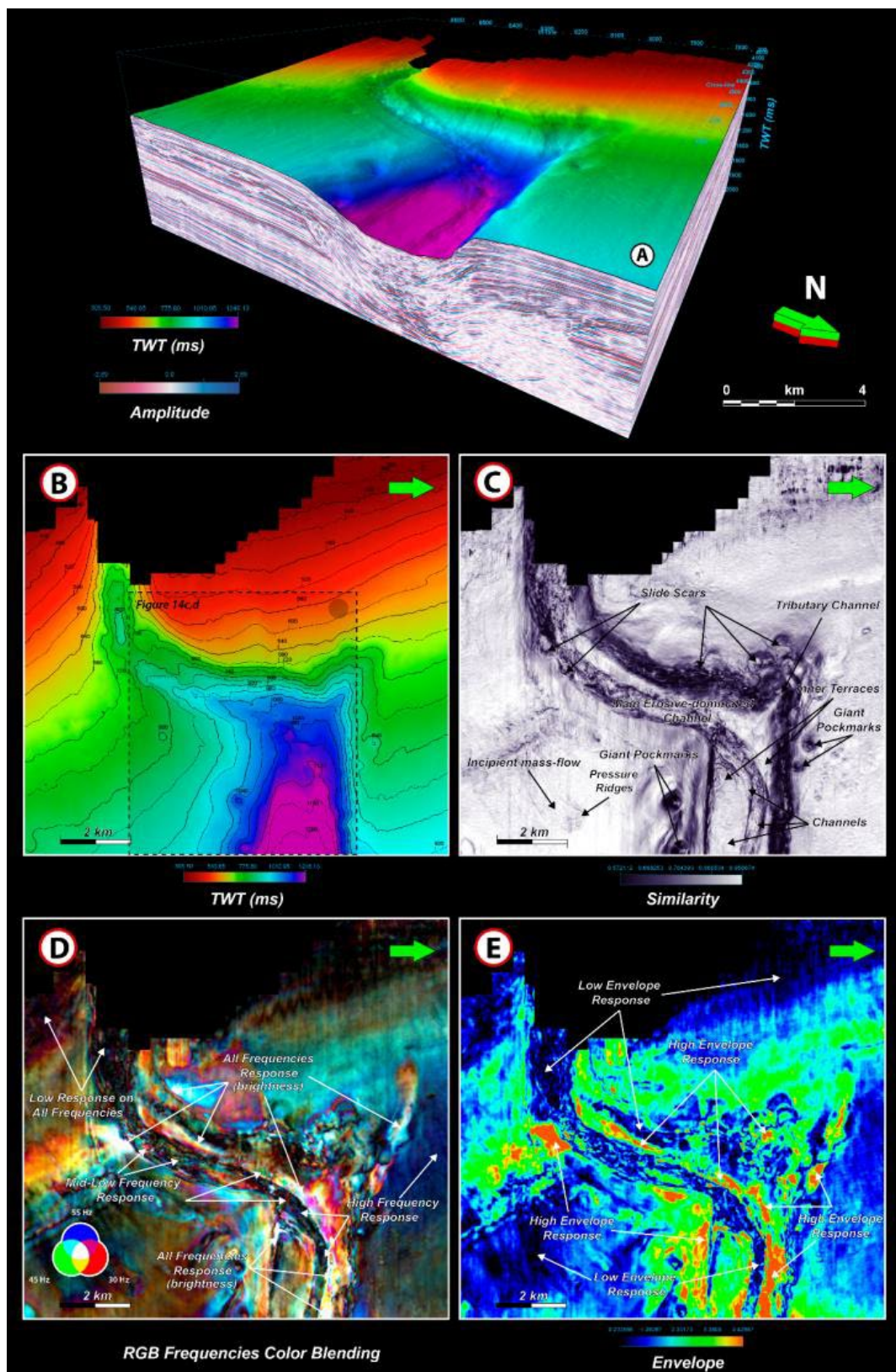


Figure 21 - a) 3D topographic map of the Almirante Câmara Surface 2 (ACS2) in TWT [ms]. b) 2D view of the ACS2 topographic map. c) Similarity attribute map of the ACS2. d) RGB frequency color blend (30Hz, 45Hz, and 55Hz), showing internal thickness variability throughout ACS2. Dark opacity indicates low-frequency responses, due to low tuning thickness. e) Envelope attribute map of the ACS2.

5.7.4. *Almirante Câmara Surface 3 (ACS3)*

The Almirante Câmara Surface 3 is the mapped surface superimposed to ACS2 and corresponds to the current sea bottom, with a surface depth ranging from 111 to 1194 ms (Fig. 22a,b). This surface preserves a southwest-northeastern downdip gradient with wide distribution, corresponding to a maximum amplitude peak and a strong continuous amplitude reflector throughout the area (Fig. 18a).

The Almirante Câmara Surface 3 shows a sinuous and deep carved V-shaped canyon with an east-western trend. Its width ranges from 1 km to 5.5 km, and a relief of 375 ms (heights ca. 350 m). The ACS3 is interpreted as a canyon mature stage, showing a narrow canyon and a marked retreat of its headwall on the continental shelf (Fig. 22b).

The similarity attribute (Fig.22c) highlights the canyon's edge, as well as normal faults with amphitheater-shaped headwall, which occur genetically related to slumps and slide blocks, most abundant on the north flank of the canyon. An inner terrace is also well-developed within the canyon. The roughness of the outer area on the canyon's south-eastern flank is interpreted as sediment waves, with a wavelength ranging from 60 m to 85 m. The pockmarks present a circular geometry and not-so-clear recognizing, ranging from 95 m-105 m, and heights of about 13 ms (11.7 m) located in the north flank, outside the canyon. An incipient pressure ridge is shown at the canyon's northeast flank (Fig. 22c). A meandering channel ($S_R = 1.63$; *Sinuosity ratio*) is shown in the canyon's thalweg, with high values of similarity, indicating high continuity (ribbon-shaped channels) of these sandy deposits. The RGB frequency blend shows a thickness variability through the ACS3, where the sandy channel deposits have a distinguishable frequency response (brightness zones, Fig. 22d). The Envelope map shows high values for the slide areas adjacent to the canyon and is interpreted as exposure of the older

strata. Otherwise, high Envelope values for the inner-canyon channel are interpreted as thin-bedded sandy deposits (Fig. 22d,e).

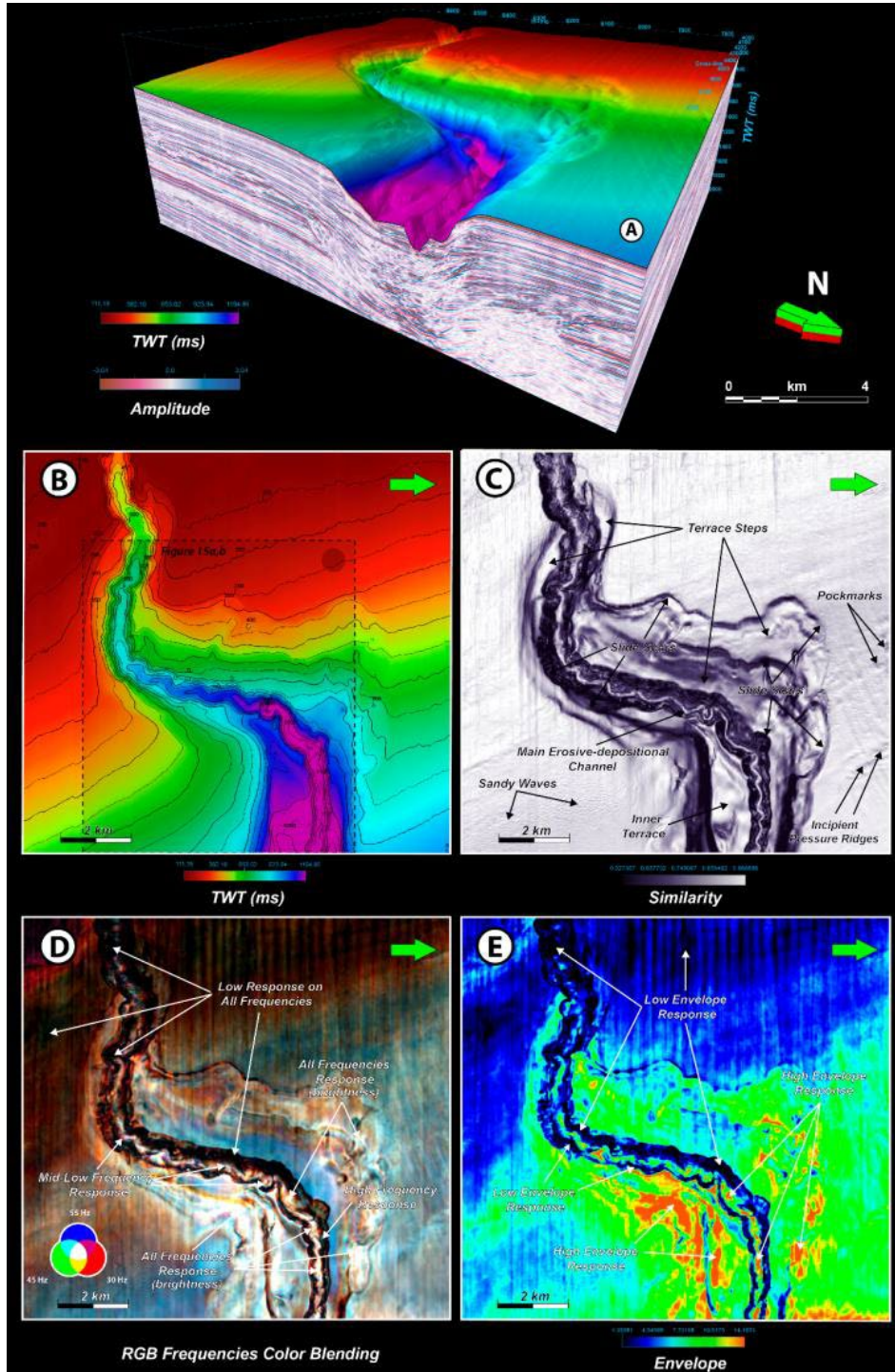


Figure 22 - a) 3D topographic map of the Almirante Câmara Surface 3 (ACS3) in TWT [ms]. b) 2D view of the ACS3 topographic map. c) Similarity attribute map of the ACS3. d) RGB frequency color blend (30Hz, 45Hz, and 55Hz), showing internal thickness variability throughout the canyon and channel deposits. High-frequency responses indicate thin-thickness deposits. e) Envelope attribute map of the ACS3.

5.7.5. Depositional architecture analysis and sedimentary implications

5.7.5.1. Comparison of EBS attribute responses

The EBS is presented in Fig. 23 to show the amplitude, tuning, and RGB frequency variability. The EBS has a high and isolated Envelope response throughout the surface and occurs mainly on the canyon's thalweg (Fig. 23a,b), as well as at the outer northern flank adjacent to the canyon (Fig. 23c,d). The RGB frequency blend brings out details related to the thickness variability response and petrophysical properties of the horizon and its deposits.

The Envelope response of EBS is not constant, showing high amplitude values on the canyon's thalweg, with semi-continuous transitioning to continuous stacked lobe geometry towards the canyon's down dip, interpreted as amalgamated thin-bedded sandy lobes. The Envelope extraction differentiates the sandy bodies (orange to green colors) from the surrounding shales (blue to dark colors, Fig. 23a). Its superficial area ranges from ca. 0.22 to 1.60 km². The outer channel to the canyon has adjacent zones with high Envelope responses with irregular-to-fan geometry, and the inner channel with high Envelope shows ribbon-shaped geometries. High values outer to the channel are interpreted as crevasse-splay channels, unlike internal values, interpreted as inner-channel sandy and lateral accretion deposits (LAD, Fig. 23a,c). These deposits have areas ranging from ca. 0.036 to 1.7 km².

The RGB frequency color blend shows low variability for these thin-bedded deposits. The crevasse-splay and LAD show high-frequency response, transitioning from blue to white, indicating areas of thin-thickness (Fig. 23b,d). Compared to the Envelope attribute, the RGB frequency blend enhances the heterogeneity of these sandy bodies below the tuning thickness.

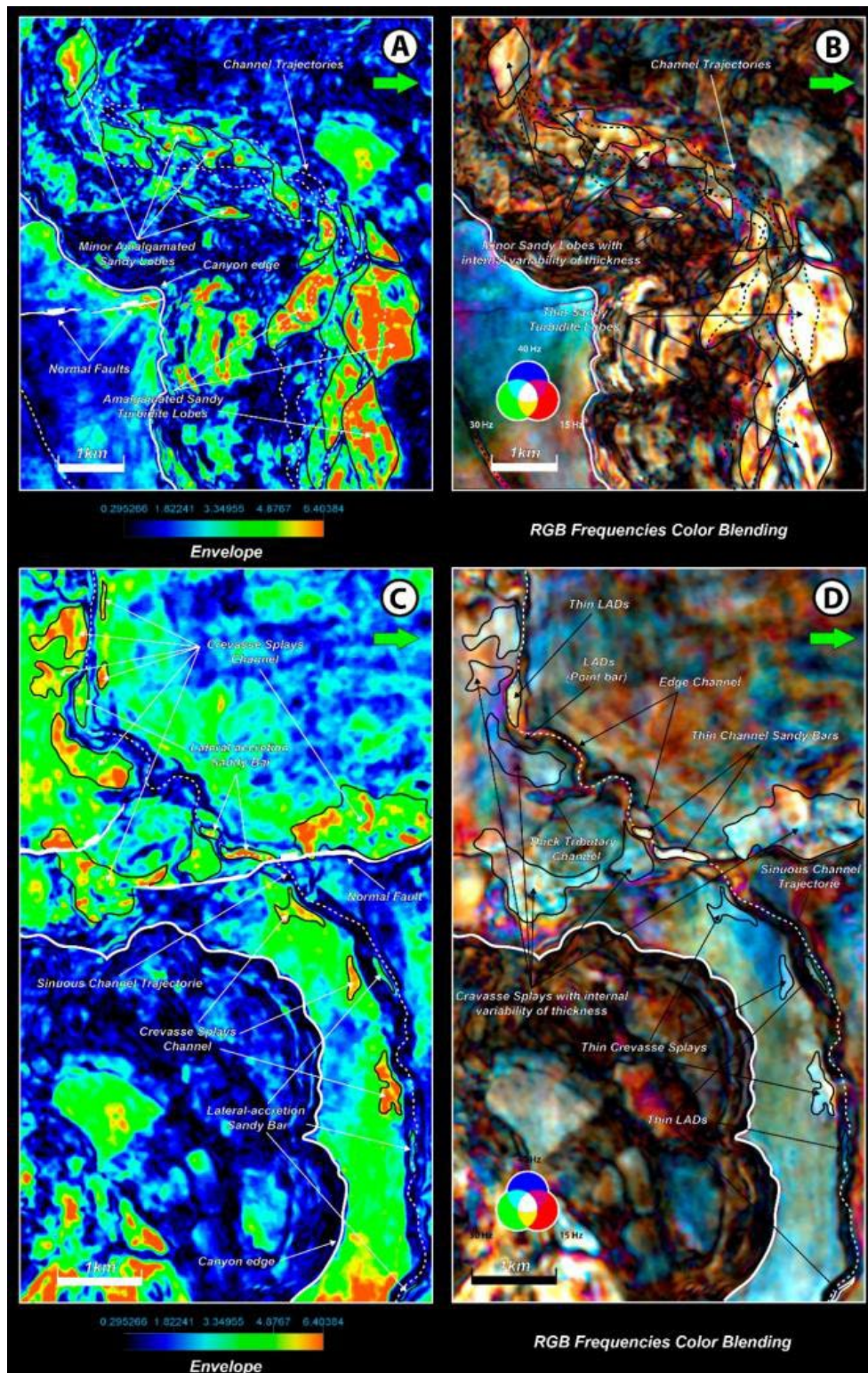


Figure 23 - 2D view attribute comparison of the EBS: a) Envelope attribute map of the EBS. b) RGB frequency color blend (15Hz, 30Hz, and 40Hz) of the EBS. c) Envelope attribute map of the EBS. d) RGB frequency color blend (15Hz, 30Hz, and 40Hz) of the EBS. High Envelope responses represent amalgamated thin-bedded sandy lobes, crevasse-splay, and LAD. High-frequency responses indicate thin-thickness turbidite and channel deposits. Refer to Fig. 19a for a detailed reference location of this figure.

5.7.5.2. Comparison of ACS1 and ACS2 attribute responses

The two horizons, ACS1 and ACS2, are presented in Fig. 24 to show the amplitudes, tuning, and RGB frequency variability.

The ACS1 has a high Envelope response across the surface, also not uniform, with high values centered especially in the continental shelf-to-slope limit, adjacently to the canyon's edge, and the inner canyon. High Envelope response areas on the canyon's thalweg here interpreted can be associated with amalgamated sandy bars and amalgamated turbidite lobes (Fig. 24a). Its superficial area ranges from ca. 0.063 to 0.66 km². These deposits have a good correlation with the attribute of RGB frequency color blend, where areas of high Envelope values always correspond to areas with a high-frequency response (blue-to-white transitioning, Fig. 24b), likely associated with thin-bedded sandy bodies.

The ACS2 also has high Envelope values similar to the ACS1 horizon. Otherwise, the areas of the inner canyon with high Envelope responses do not occur on its thalweg, but in its inner terraces, interpreted as ancient exposed sandy deposits (Fig. 24c). The canyon's thalweg presents low Envelope values, indicating sedimentary bypass towards the deep basin. The area of these erosive features can range from ca. 0.045 to 1.60 km². The RGB frequency analysis highlights these areas with high-frequency responses as white brightness zones (Fig. 24d), which could indicate the thin-thickness features of these deposits.

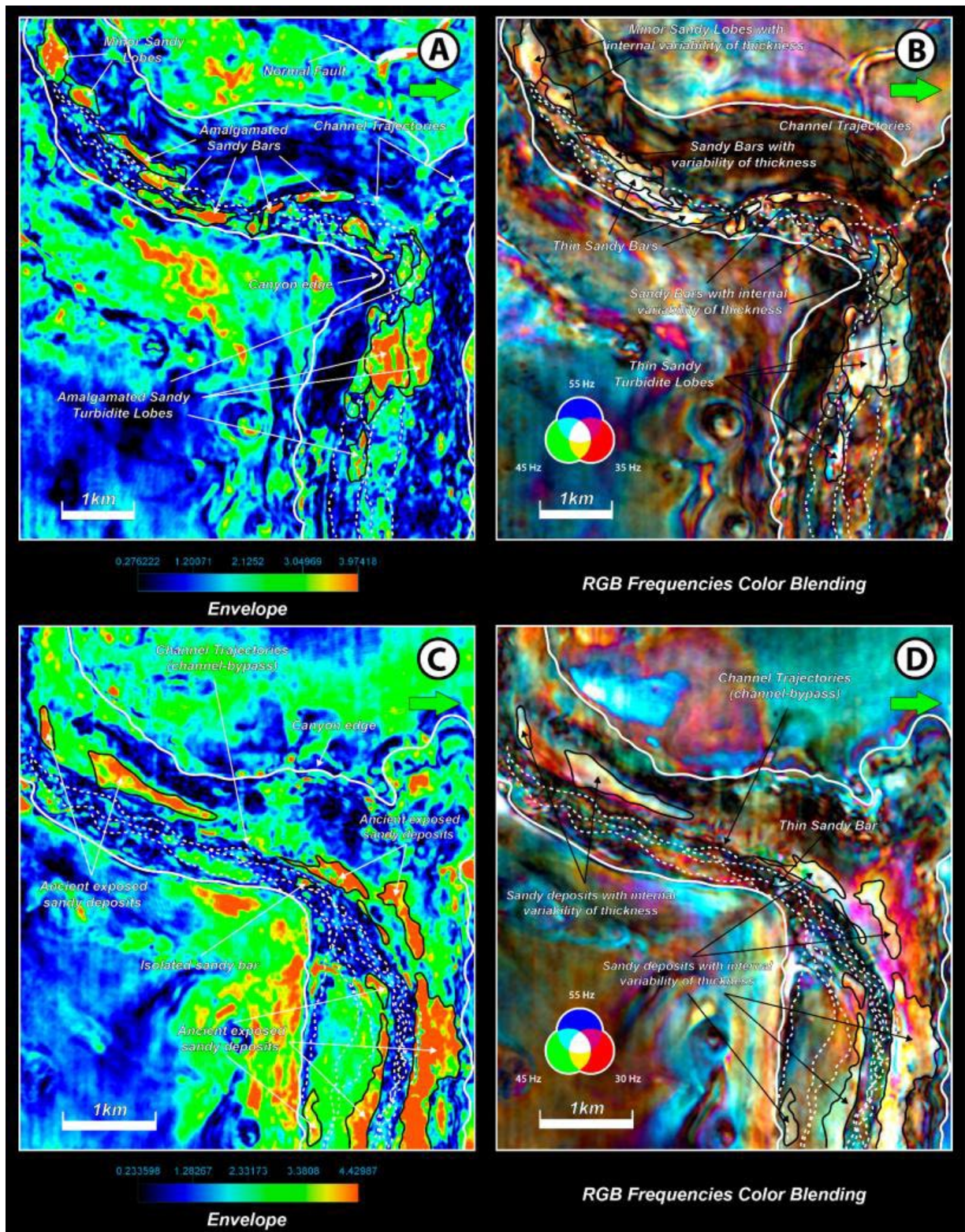


Figure 24 - 2D view attribute comparison of the ACS1 and ACS2: a) Envelope attribute map of the ACS1. b) RGB frequency color blend (35Hz, 45Hz, and 55Hz) of the ACS1. c) Envelope attribute map of the ACS2. d) RGB frequency color blend (30Hz, 45Hz, and 55Hz) of the ACS2. High Envelope responses represent amalgamated sandy bars, sandy turbidite lobes, and ancient exposed sandy deposits. High-frequency responses indicate thin-thickness turbidite and channel deposits. Refer to Figs. 20a and 21a for a detailed reference location of this figure.

5.7.5.3. Comparison of ACS3 attribute responses

The ACS3 is shown in Fig. 25 with amplitude and RGB frequencies. The ACS3 has high Envelope values, which occur on the inner walls near the canyon edge (Fig. 25a). Low Envelope responses can be seen in the continental shelf-to-slope limit and on the vertical wall that limits the current canyon channel. High Envelope responses are interpreted as modern thin-bedded sand-prone infilling the highly sinuous and confined channel. (Fig. 25a). The superficial area of these deposits can range from 0.15 to 0.7 km². The RGB frequency color blend brings out low variability and thin-bedded deposits (white brightness zones), showing ribbon-shaped geometry (Fig. 25b).

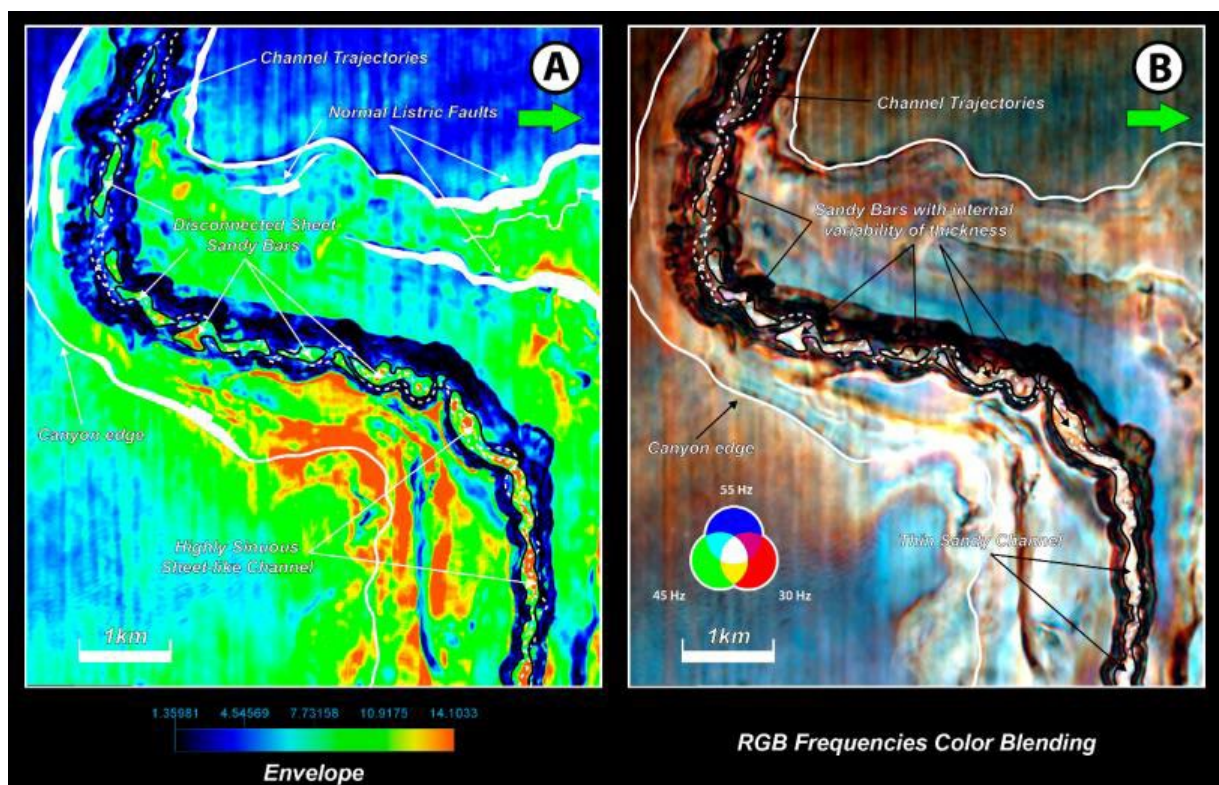


Figure 25 - 2D view attribute comparison of the ACS3: a) Envelope attribute map of the ACS3. b) RGB frequency color blend (30Hz, 45Hz, and 55Hz) of the ACS3. High Envelope and high-frequency responses represent thin-bedded ribbon-shaped channel deposits. Refer to Fig. 22a for a detailed reference location of this figure.

5.8. Discussions

To investigate the features of the Almirante Câmara Canyon in different stages of its history evolution, we have carefully interpreted the stratigraphy outlined by the amplitude, phase, and frequency content of seismic data. The use of instantaneous phase and cosine of instantaneous phase attributes provides the improvement of the seismic interpretation in zones of discontinuous seismic reflectors (Bitrus et al., 2016), especially those of the canyon walls associated with landslides. Likewise, the combined results allowed us to delineate as well as discuss some features of the canyon's structuration, sediment supply, and evolution.

5.8.1. *Structural control on sea-floor topography*

The rift phase of the Campos Basin initiates in the Lower Cretaceous (Barremian, ca. 130 Ma), with NE-SW faults and less significant NNW-SSE and E-W orientation. Major faulting and tectonic activity ceased before the Pre-Alagoas unconformity (ca. 124 Ma), assuming this horizon as the limit of the rift phase (Dias et al., 1990). Nevertheless, during the Miocene, the basin was also strongly influenced by salt tectonics, which gave rise to the reactivation and origin of new growth faults of large tailings, caused by the load of a thick sedimentary progradation (Reis, 1994). The canyons of the northeast group of the Campos Basin have strong structural control of these faults, especially the Itapemirim Canyon, which has its walls controlled by faults with E-W passing to NE-SW and tend to join with NW-SE faults that control the São Tomé Canyon (Cobbold and Szatimari, 1991). As shown in Fig. 26a-b, major faults are well-developed in the study area, with fault throws generally of less than 30 ms (ca. 27m). However, there may be evidence of a contemporaneous relationship between faults activity and at least in the initial stages of the Almirante Câmara Canyon (Fig. 26a-b). These N-S to NNW-SSE faults, throwing down to the ENE, generally intersect the mid-portion of the canyon (Fig. 26a), which presents a prominent bend in the same direction. This abrupt deflection was

likely influenced by local accommodation of these faults. As described by Mayall et al. (2006), the repeated coincidence of prominent channel bends and the location of faults, especially those associated with diapirism, seems to indicate a genetic link and control of their geometry. Fig. 26b shows faults closer to the headwall of the canyon's tributary channel. Otherwise, at this time, the faults seem not to have direct implications in the bend of the canyon, although they may have contributed to generating sediment gravity flows (MTD) that flowed down the canyon.

Likewise, assessing the planform geometry of successive horizons drawn from similarity volume (Fig. 26a-d) can verify the Almirante Câmara Canyon shows a unidirectional migration with a likely fixed and slightly sinuous axis through its evolution. The stacked mapped surfaces show that Almirante Câmara Canyon becomes narrow over time. On the other hand, the aggradation of these deposits slowly and progressively softens the morphology of the underlying canyon (Fig. 26e).

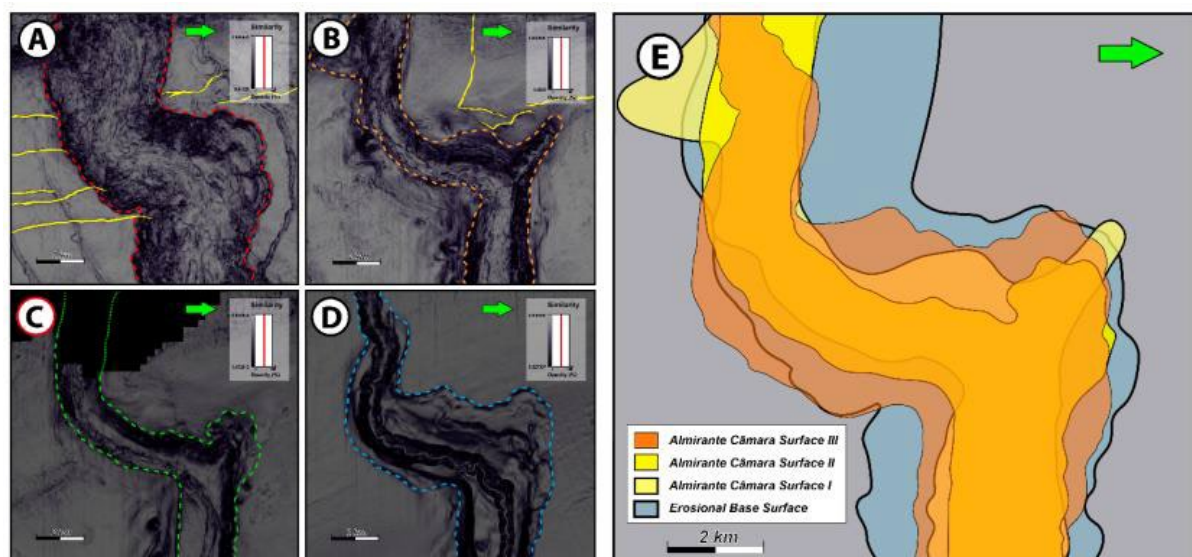


Figure 26 - 2D view similarity attribute maps from the initial stage (a) to the late stage (d) throughout the canyon development. From a to d, the horizons show a progressive decrease of faults. (e) shows a composite plan view of the canyon migration process by stacking surfaces. Canyon's limit is represented by red, orange, green, and blue dotted lines, regarding the EBS, ACS1, ACS2, and ACS3. Opacity has been applied to the surfaces to enhance the visualization of faults (yellow).

5.8.2. Canyon's sediment supply

The asymmetry of canyons and channels can be generated by differential sediment supply of either flank, forcing them to migrate towards the other flank, particularly, when canyons and channels are oblique to the slope (Kertzus and Kneller, 2009). However, the Almirante Câmara Canyon is NE-SW oriented along its entire length, oriented approximately perpendicular to the slope. An analogous case of this canyon migration architecture is described by He et al. (2013) for the Qiongdongnan Basin canyons.

Canyons are frequently zones of sediment bypass during low stand sea level (Posamentier, et al., 1991). Therefore, the Almirante Câmara shows up to be typical of canyons with remaining long-lived turbidite conduits for deep-sea sediments, hence preserving a complex cut-and-fill history. The asymmetry of its transverse profile is attributed to contourite deposits with a sigmoidal stacking pattern, deposited from the Miocene to the Recent by bottom currents, with progradation from the left flank to the interior of the canyon (Viana et al., 1999; Souza Cruz, 1995).

A plausible hypothesis is that the internal sands of Almirante Câmara Canyon have fluvial origin by run-off in hyperpycnal flows, with a transport and deposition process by subaqueous grain flow composed of grain shock, drag, traction, and subaqueous saltation. Regional seismic data indicates (Machado et al., 2001; Machado et al., 2002) that the Paraíba do Sul River physically continues in the incised valley, fitting into the Almirante Câmara Canyon and connecting to the deep turbidite system.

5.8.3. Insights into the canyon's filling and evolution

This study has documented four major surfaces, defining the geometry of the canyon and influencing its fill history through the development of stratigraphic cycles. Furthermore, the surfaces documented the evolution of fill from amalgamated sandy bars and turbidity lobes to thin-bedded sandy turbidite channels. The filling of the Almirante

Câmara Canyon occurred for a long time from the Upper Miocene, punctuated by a series of aggradational phases interrupted by erosional phases and sediment bypass throughout the canyon to the slope or deep abyssal plain. The canyon's fill by turbidite channels may reflect a sandy-prone delta for the sediment supplied to the canyon. In this case, namely, the ancient Rio Paraíba do Sul (or proto-river). Delta-fed systems generally show a dominance of fine to sandy-grained material, with the potential to maintain a continuous hyperpycnal flow regime (Normark and Piper, 1991).

Based on the surfaces mapped, seismic attributes, and the depositional architecture elements assessment, an evolutionary model for the Almirante Câmara Canyon has been proposed (Fig. 27). In this model, the canyon's evolution is divided into four stages: Stage I (EBS), Stage II (ACS1), Stage III (ACS2), and Stage IV (ACS3). At Stage I, the initial canyon's morphology presents a prominent erosion due to a Middle-Upper Miocene sea-level fall (Gray Marker). Amalgamated thin-bedded sandy lobes were deposited (Fig. 27a). In Stage II, a medium-wide canyon comes out, with deposition of amalgamated sandy bars and turbidity lobes (Fig. 27b). In Stage III, the medium-wide canyon stays, when the deposition of sediments along the canyon was extremely limited or absent, bypassing the sediments to the slope or deep abyssal plain (Fig. 27c). Corresponding to the modern sea floor, Stage IV shows a wide and over-deepening canyon, with the deposition of thin-bedded turbidites. At this stage, a highly sinuous and confined channel leads the modern sediments to down-slope locations (Fig. 27d). Likewise, MTD was developed throughout all stages due to the canyon head and margin failure, playing a role as a major source of sediment for the canyon, particularly mud-prone sediments (Posamentier, 2003; Mayall et al., 2006; Deptuck et al., 2007). The interplay between turbidite currents and ancient bottom currents led to the vertical aggradation and lateral migration of these canyons.

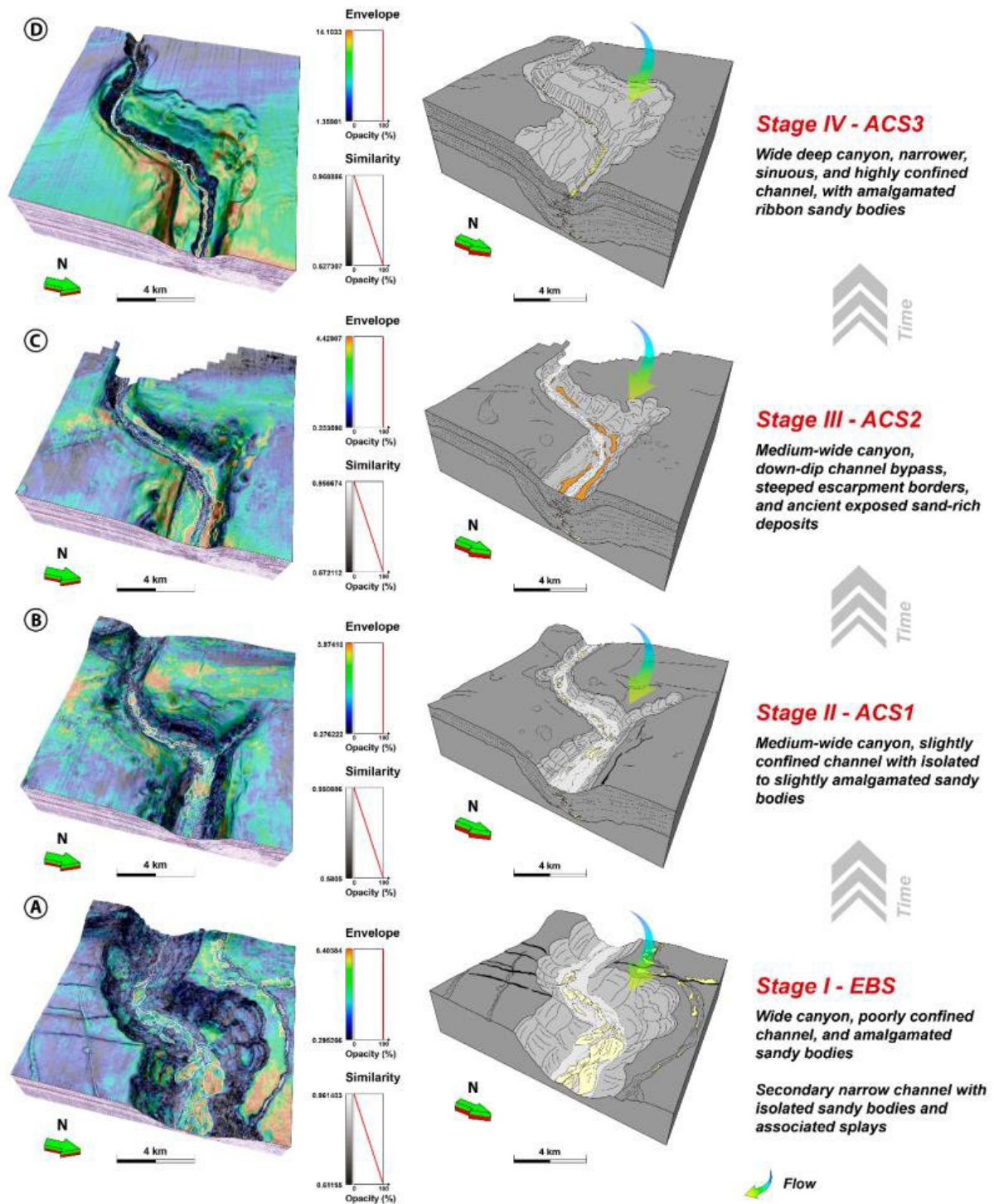


Figure 27 - Evolutionary model illustrating the evolution of the Almirante Câmara Canyon and its fill. Four stages have been proposed: (a) Stage I (EBS): Initial prominent erosion of the canyon, with deposition of amalgamated thin-bedded sandy lobes; b) Stage II (ACS1): Medium-wide canyon, with deposits of amalgamated sandy bars and turbidite lobes; c) Stage III (ACS2): Medium-wide canyon, with sediment bypass transported to the lower slope or deep abyssal plain; and d) Modern Stage (ACS3): Wide and over-deepening canyon, with deposition of thin-bedded sandy-prone turbidites. The aggradation of these deposits represents a myriad of erosive, bypass, and depositional events (waxing-waning cycles), preserving a complex cut-and-fill history. Figures (a) to (d) show a multi-attribute composition of Envelope and Similarity.

5.8.4. Tie-surfaces and global mean sea level curve

From the tectono-glacial-eustatic (TGE) curve obtained by van der Meer et al., 2022, we propose a qualitative age comparison for each interpreted surface tentatively during the late Cenozoic (Fig. 28a-b) with sea level fall events. Hence, the age ascribed to each surface is ~13.2 Ma (EBS), ~6.8 Ma (ACS1), ~70 Ka (ACS2), and ~18-0 Ka (ACS3), respectively. Figure 28a shows schematically the residual sea level trends curve and its associated amplitude changes (a few to 20 million years). Five major transgressive-regressive sequences are documented for the Neogene-Quaternary, where the surfaces are associated with each end-of-cycle markedly erosive in the shelf.

Nevertheless, can be verified a difference of 2.4 Ma (i.e., 13.2-10.8 Ma) between the assigned age following the van der Meer et al., 2022 TGE curve and the standard age ascribed by other authors (e.g., Viana et al., 1990; Viana et al., 2003; Pelizzon, 2005) for the most basal surface EBS. This one shows up as a widely erosive, with regional expression in the Campos Basin (Gray-marker). We argue this difference can be likely attributed to regional autochthonous tectono-eustatic controls, playing an important role in the evolution of the South Atlantic Ocean portion. van der Meer et al. (2022) discuss the Neogene-Quaternary global sea-level fall due to the pole's continental ice accumulation.

However, with a good correlation between age and sea level fall patterns, the other surfaces ACS1 and ACS2 match with the van der Meer et al. (2022) curve, indicating these two mapped surfaces are related to global sea level fall events – at Tortonian-Messinian quasi-boundary (Upper Miocene), linked to ACS1 (6.8 Ma), and at Upper Pleistocene, linked to ACS2 (70 Ka). In turn, the ACS3 surface is related to the last glacial maximum (LGM), with the sea level regression climax achieved at 18 Ka BP. This event is documented in the Campos Basin by a lowering of approximately 120 m relative to the current level and a displacement of 120 km of the coastal line basinward, installed

at the current continental shelf break. (Corrêa, 1990; Artusi, 2004; Della Giustina, 2006). The subsequent transgressive event of 18–0 Ka occurred suddenly, interpreted by the lack of visible and mappable deposits at this seismic working scale.

Although our interpretations can be reasonably calibrated for the late Cenozoic, the ages proposed here can present some degree of uncertainty and a high likelihood of equally plausible scenarios. Likewise, the consistency of these interpretations should be corroborated with wireline log data and seismic well tie, as well as detailed biostratigraphic analysis (forams and coccoliths) for the Almirante Câmara Canyon. Moreover, according to Viana et al. (1998), this combined analysis shows the seaward extension of erosional events can be mainly associated with relative sea-level lowstand in the Campos Basin.

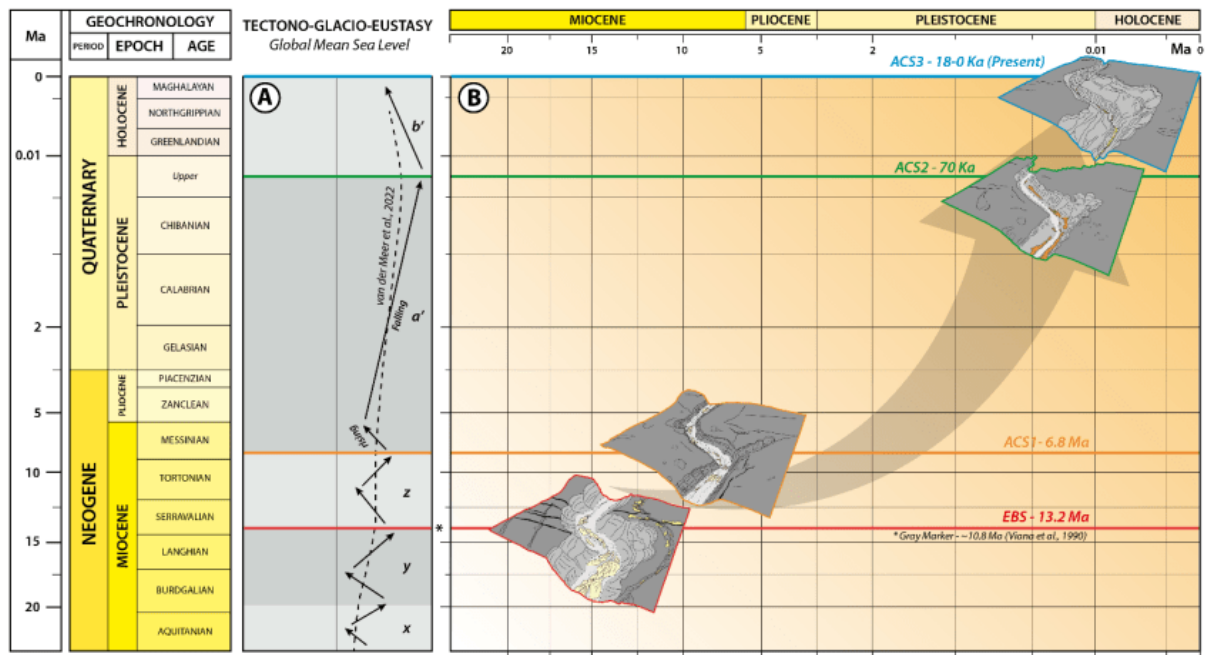


Figure 28 - Neogene-Quaternary tectono-glacial eustatic curve and time-time surface correlation. The horizontal lines (red, orange, green, and blue) assign vertically the age of each surface. a) Curve of residual sea level trends and associated schematic amplitude changes (modified from van der Meer et al., 2022). b) Diagram of time-time correlation. Left-arrows and right-arrows indicate rising sea level and falling sea level, respectively. The letters (x, y, z, a', and b') and shading highlight the unconformity-bound stratigraphic sequences. The dotted line is the long-term (>50Myr) eustatic trend.

5.9. Conclusions

The use of complex seismic attribute analysis enhanced conventional seismic amplitude-based interpretation for the highly complex cut-and-fill history of Almirante Câmara Canyon. The interpretation results show four erosive canyon-valley system surfaces (EBS, ACS1, ACS2, and ACS3) throughout the canyon's evolution. Each one of these surfaces shows an interpretative link with the global sea level curve, which indicates a global sea level fall as the main, but not only, controller of the erosive event. These canyons have ENE-SSW orientation, U-shaped form passing upward to V-shaped form, likely perpendicular to the slope, with relief ranging from 350-540 m and widths of 1-7.1 km. Although the origin of Almirante Câmara Canyon is genetically related to a fall in sea level during the Middle-Upper Miocene, there also appears to be a contemporary relationship between faults activity, those with N-S and NNW-SSE trend that intercept the canyon's mid-portion, at least in the initial stages of the Almirante Câmara Canyon (EBS and ACS1), leading him to an abrupt deflection (roughly 90°). The canyon sediment filling results from stages of erosion and bypass to aggradational filling events of high-frequency cyclicity, at a scale of a single turbidite channel history until the canyon scale itself. Inner-canyon sediment deposited by turbidite channel systems presents thin-bedded turbidite lobes, amalgamated turbidite lobes, and amalgamated bar sand-prone. Mass-flow deposits (MTD) also support the canyon's sediment supply and are present throughout its development. Reflectivity seismic attribute (envelope and similarity) combined with Spectral decomposition and RGB Blending helps to identify and clarify these sandy bodies, showing their stratigraphic and structural wedges in response to tuning-thickness change, acoustic impedance, as well as relative thickening and thinning. Also, RGB Blending has proved to provide substantially more detail and fidelity than full-bandwidth conventional attributes. The bottom currents (contourite deposits) also contribute to sediment supply and the canyon's evolution, thus conferring an asymmetric

transversal profile to the canyon. Canyon's planform geometry assessment shows an approximated fixed and slightly sinuous axis through its evolution. An evolutionary canyon model has been proposed, which is divided into four stages: Stage I (EBS), Stage II (ACS1), Stage III (ACS2), and Stage IV (ACS3). Although the study carried out in this work has not presented direct implications to hydrocarbon exploration, it likewise, can be used as an analogous subsurface environment with potential valid hydrocarbon plays, showing in detail the complexity of superimposed erosive events within a canyon, and the interplay of broad types of depositional elements.

5.10. Acknowledgments

S.A.S. Correa thanks the National Council for Scientific and Technological Development of Brazil – CNPq (grant no. 133110/2017-6) for the Master of Science scholarship and to Seismostratigraphy Laboratory of Universidade Federal do Rio Grande do Sul (UFRGS) Geoscience Institute for the support technical and computational to this research paper. Thanks to dGB Earth Sciences, with special mention to Dr. Paul de Groot, for seismic analysis support and for granting the OpendTect Pro® Academic License. Also, we gratefully acknowledge the support of Shell Brasil Petroleo Ltda for the grant of seismic data and to the Brazilian National Agency of Petroleum, Natural Gas and Biofuels - ANP for their commitment to investment in research and development. The authors are grateful to the reviewers for their constructive comments and revision of the manuscript.

5.11. References

- Abrahão, D., Warme, J.E., 1990. Lacustrine and associated deposits in a rifted continental margin – Lower Cretaceous Lagoa Feia Fm., Campos Basin, Offshore Brazil. In: Katz, B.J. Lacustrine basin exploration, case studies and modern analogs. AAPG, *Memoir* 50, p. 287-305.
- Abreu, V., Sullivan, M., Pirmez, C., Mohrig, D., 2003. Lateral accretion packages (LAPs): an important reservoir element in deep water sinuous channels. *Marine and Petroleum Geology* 20, 631–648.
- Almeida, A. G. & Kowsmann, R. O., 2014. Geomorfologia do Talude Continental e do Platô de São Paulo. In: Kowsmann, R. O. (Ed.). *Geologia e Geomorfologia*. Rio de Janeiro: Elsevier. Habitats Series, v. 1, p. 33-66.
- Alvarenga, R.d.S., Kuchle, J., Iacopini, D., Goldberg, K., Scherer, C.M.d.S., Pantopoulos, G., Ene, P.L., 2021. Tectonic and Stratigraphic Evolution Based on Seismic Sequence Stratigraphy: Central Rift Section of the Campos Basin, Offshore Brazil. *Geosciences*, 11(8), 338. <https://doi.org/10.3390/geosciences11080338>.
- Alves, R. A., 1999. Estudo sismoestratigráfico da bacia do Brasil. Programa de Pós-Graduação em Geologia e Geofísica Marinha, Universidade Federal Fluminense, Dissertação de Mestrado, 88 p.
- Amarante, F.B., Jackson, C.A.-L., Pichel, L.M., Scherer, C.M.S., & Kuchle, J. 2021. Pre-salt rift morphology controls salt tectonics in the Campos Basin, offshore SE Brazil. *Basin Research*, 33, 2837–2861. <https://doi.org/10.1111/bre.12588>.
- Andresen, K.J., Huuse, M., Clausen, O.R., 2008. Morphology and distribution of Oligocene and Miocene pockmarks in the Danish North Sea — implications for bottom current activity and fluid migration. *Basin Research* 20, 445–466. <https://doi.org/10.1111/j.1365-2117.2008.00362.x>
- Artusi, L., 2004. Geologia, geomorfologia e sismoestratigrafia rasa da plataforma continental ao largo da laguna de Araruama – RJ. Rio de Janeiro, Universidade Federal Fluminense. Dissertação de Mestrado. 91p.
- Babonneau, N., Savoye, B., Cremer, M., Klein, B., 2002. Morphology and architecture of the present canyon and channel system of the Zaire deep-sea fan. *Marine and Petroleum Geology*, 194, pp. 445–467. [https://doi.org/10.1016/S0264-8172\(02\)00009-0](https://doi.org/10.1016/S0264-8172(02)00009-0).
-

-
- Bahorich, M., Farmer, S., 1995. 3-D seismic discontinuity for faults and stratigraphic features: The coherence cube. *The Leading Edge* 14(10), pp. 1053-1058. <https://doi.org/10.1190/1.1437077>.
- Baranova, V.V.; Mustaqeem, A., 2010. Using Advanced Seismic Attribute Analysis to Reduce Risk in Frontier Exploration – West Newfoundland Offshore. AAPG International Convention and Exposition, September, 12-15, Canada.
- Barker, P.F., R.L. Carlson, D.A. Johnson, et al., 1983b. Brazil basin. Site 515: Brazil Basin. In: Barker, P.F., R.L. Carlson, D.A. Johnson, et al., (Eds.). Initial reports of the Deep-Sea Drilling Project, 72: Washington, U.S. Government Printing Office, p. 53–154.
- Barker, P.F.; R.T. Buffler; L.P. Gambôa, 1983a. A seismic reflection study of the Rio Grande Rise. In: Initial reports of the Deep-Sea Drilling Project, 72: Washington, U.S. Government Printing Office, p. 499–517.
- Barnes, A.E., 2016. Handbook of Poststack Seismic Attributes. Society of Exploration Geophysicists, 268 p. <https://doi.org/10.1190/1.9781560803324>.
- Bitrus, P. R., Iacopini, D., Bond, C. E. 2016. Defining the 3D geometry of thin shale units in the Sleipner reservoir using seismic attributes. *Marine and Petroleum Geology*, 78, p. 405-425. <https://doi.org/10.1016/j.marpetgeo.2016.09.020>.
- Brouwer, F., 2007. Creating a good Steering Cube. Available in: <http://www2.dgbgroup.com/images/stories/PDF/effectivedipsteeringworkflowusingbgsteering_primerodata.pdf>. Accessed on August 30, 2016.
- Brouwer, F., Huck, A., 2011. An Integrated Workflow to Optimize Discontinuity Attributes from Imaging of Faults. In: Marfurt, K.J., Gao, D., Barnes, A., Chopra, S., Corrao, A., Hart, B., James, H., Pacht, J., Rosen, N.C., (Eds.), *Attributes: New Views on Seismic Imaging – Their Use in Exploration and Production*, 31st Annual GCSSEPM Foundation Bob F. Perkins Research Conference, Houston, Texas, pp. 496-533.
- Bruhn, C., Gomes, J., Lucchese, C., Johann, P., 2003. Campos Basin: Reservoir Characterization and Management - Historical Overview and Future Challenges: In: *Offshore Technology Conference, 2003*, Houston, Texas, OCT No. 15220, Expanded Abstracts, p. 1-14. doi.org/10.4043/15220-MS
- Bulhões, E.M., Amorim, W.N., 2005. Princípio da SismoCamada Elementar e sua aplicação à Técnica Volume de Amplitudes (tecVA). In: 9th International Congress of the Brazilian Geophysical Society, 2005, Salvador.
-

-
- Butler, R.W.H., Turner, J.P., 2010. Gravitational collapse at continental margins: products and processes; an introduction. *Journal of the Geological Society*, 167(3), pp. 569-570. <https://doi.org/10.1144/0016-76492010-003>.
- Castagna, J.P., Sun, S., Seigfried, R.W., 2003, Instantaneous spectral analysis: Detection of low-frequency shadows associated with hydrocarbons: *The Leading Edge*, 22(2), pp. 120–127. <https://doi.org/10.1190/1.1559038>.
- Castro, D.D., 1992. Morfologia da margem continental sudeste-sul brasileira e estratigrafia sísmica do sopé continental. Dissertação de Mestrado, Universidade Federal Rio de Janeiro, Rio de Janeiro, 226 p.
- Chopra, S., 2002. Coherence Cube and beyond. *EAGE, First Break*, 20(1), pp. 27-33. <https://doi.org/10.1046/j.1365-2397.2002.00225.x>.
- Chopra, S., Marfurt, K.J., 2005. Seismic attributes – A historical perspective. *Geophysics*, 70(5), pp. 3SO-28SO. <https://doi.org/10.1190/1.2098670>.
- Chopra, S., Marfurt, K.J., 2007. Seismic attributes for prospect identification and reservoir characterization. *Geophysical Developments Series*, n. 11, 481 p. <https://doi.org/10.1190/1.9781560801900>.
- Cobbold, P., Szatmari, P. 1991. Radial gravity gliding on passive margins. *Tectonophysics*. 188(3/4): 249-289. [https://doi.org/10.1016/0040-1951\(91\)90459-6](https://doi.org/10.1016/0040-1951(91)90459-6).
- Cobbold, P.R., Szatmari, P., Demercian, L.S., Coelho, D., Rossello, E.A., 1995. Seismic experimental evidence for thin-skinned horizontal shortening by convergent radial gliding on evaporites, deep-water Santos Basin. In: Jackson, M.P.A., Roberts, R.G., Snelson, S. (eds.). *Salt tectonics: a global perspective*, AAPG Memoir 65, p. 305–321.
- Cohen, L., 1995, *Time-frequency analysis: theory and applications*. Prentice Hall, Inc., pp. 299.
- Corrêa, I.C.S., 1990. Analyse morphostructurale et evolution paleogeographique de la plateforme continentale Atlantique sud-bresilienne (Rio Grande do Sul - Bresil). Bordeaux, Université de Bordeaux, PhD Tesis ,314p.
- Della Giustina, I.D., 2006. Sedimentacao carbonatica de algas vermelhas coralinaceas da plataforma continental da Bacia de Campos: Um modelo carbonatico analogo para o Terciario. Porto Alegre, Universidade Federal do Rio Grande do Sul, 134p.
- Demercian, L.S., Szatmari, P., Cobbold, P.R. 1993. Style and Pattern of Salt Diapirs due to Thin-Skinned Gravitational Gliding, Campos and Santos Basins, Offshore Brazil. *Tectonophysics*, v. 228, p. 393-433.
-

- Deptuck, M.E., Steffens, G.S., Barton, M., Pirmez, C., 2003. Architecture and evolution of upper fan channel-belts on the Niger Delta slope and in the Arabian Sea. *Marine and Petroleum Geology*, v. 20(6-8), pp. 649–676. doi:10.1016/j.marpetgeo.2003.01.004.
- Deptuck, M.E., Sylvester, Z., Pirmez, C., O'Byrne, C., 2007. Migration-aggradation history and 3-D seismic geomorphology of submarine channels in the Pleistocene Benin-major Canyon, western Niger Delta slope. *Marine and Petroleum Geology* 24, p. 406-433. <https://doi.org/10.1016/j.marpetgeo.2007.01.005>.
- Dias, J.L., Oliveira, J.Q., Vieira, J.C. 1988. Sedimentological and stratigraphic analysis of the Lagoa Feia Formation, rift phase of Campos Basin, offshore Brazil. *Revista Brasileira de Geociências*, v. 18, p. 252-260.
- Dias, J.L., Scarton, J.C., Esteves, F.R., Carminatti, M., Guardado, L.R. 1990. Aspectos da evolução tectono-sedimentar e a ocorrência de hidrocarbonetos na Bacia de Campos. In: Gabaglia, G.P.R., Milani, E.J. (coords.). *Origem e evolução de bacias sedimentares*, PETROBRAS, CENSUD, Rio de Janeiro, p. 333-360.
- Farre, J. A.; McGregor, B. A.; Ryan, W. B. F.; Robb, J. M., 1983. Breaching the shelf break: passage from youthful to mature phase in canyon evolution. In: Stanley, D. J.; Moore, G. T., (Eds.). *The shelf break: critical interface on Continental Margins*. Tulsa: Society of Economic Paleontologists and Mineralogists, 1983. p. 25-39.
- Figueiredo, A.M.F., Martins, C.C. 1990. 20 anos de Exploração da Bacia de Campos e o sucesso nas águas profundas. *Boletim de Geociências da PETROBRAS*, v. 4, n.1, p. 105-123.
- Gambôa, L.A. P.; R.T. Buffler; P.F. Barker, 1983. Seismic stratigraphy and geologic history of the Rio Grande gap and Southern Brazil basin. In: Gambôa, L.A. P.; R.T. Buffler; P.F. Barker (Eds.). *Initial Reports of the Deep-Sea Drilling Project*, 72: Washington, U.S. Government Printing Office, p. 481–498.
- Gilani, S.F., Gomez, L.M., 2015. The application of data conditioning, frequency decomposition and DHI from RGB colour blending in the Gohta discovery (Barents Sea, Norway), Jaipur, SPG India: 11th Biennial International Conference & Exposition, Expanded Abstract. Available in: <https://www.spgindia.org/11_biennial_form/the-application-of-data-conditioning-frequency-decomposition-and-dhi-from-rgb-colour-blending-in-the-gohta-discovery-barents-sea-norway-jaipur-2015.pdf>. Accessed on August 28, 2016.
- Greene, H.G., Clarke, S.H., Kennedy, M.P., 1991. Tectonic evolution of submarine canyons along the California continental margin. In: R. H. Osborne, *From shoreline*
-

- to abyss: contributions in marine geology in honor of Francis Parker Shephard, pp. 231-248. In Spec. Publ. Soc. Econ. Paleontol. Mineral., 46.
- Guardado, L.R.; Gamboa, L.A.P.; Luchesi, C.F., 1989. Petroleum geology of the Campos Basin, a model for a producing Atlantic-type basin. In: Edwards, J. D., Santogrossi, P.A. (eds.). Divergent/Passive Margin Basins. American Association of Petroleum Geology, *Memoir* 48, p. 3-79.
- He, Y., Xie, X., Kneller, B. C., Wang, Z., & Li, X. 2013. Architecture and controlling factors of canyon fills on the shelf margin in the Qiongdongnan Basin, northern South China Sea. *Marine and Petroleum Geology*, 41, 264-276. <https://doi.org/10.1016/j.marpetgeo.2012.03.002>.
- Henderson, J., 2012. Geological Expression: data driven–interpreter guided approach to seismic interpretation. *EAGE, First Break*, 30(3), pp. 95-100.
- Henderson, J., Purves, S.J., Fisher, G., 2008. Delineation of geological elements from RGB color blending of seismic attribute volumes. *The Leading Edge*, 27(3), pp. 342–350. <https://doi.org/10.1190/1.2896625>
- Henderson, J., Purves, S.J., Leppard, C., 2007. Automated delineation of geological elements from 3D seismic data through analysis of multi-channel, volumetric spectral decomposition data. *First Break*, 25(3), pp. 87-93.
- Ho, S., Cartwright, J.A., Imbert, P. 2012. Vertical evolution of fluid venting structures in relation to gas flux, in the Neogene-Quaternary of the Lower Congo Basin, Offshore Angola. *Marine Geology*, 332-334, p. 40-55. <http://dx.doi.org/10.1016/j.margeo.2012.08.011>.
- Höcker, C., Fehmers, G., 2002. Fast structural interpretation with structure-oriented filtering: *The Leading Edge*, 21(3), p. 238–243. <https://doi.org/10.1190/1.1463775>.
- Iacopini, D., Butler, R.W.H., Purves, S., 2012. Seismic imaging of thrust faults and structural damage: a visualization workflow for deepwater thrust belts. *EAGE, First Break*, 5 (30), p.39-46.
- Jaglan, H., Qayyum, F., Huck, H., 2015. Unconventional seismic attributes for fracture characterization. *EAGE, First Break*, v. 33, p. 101-109.
- Kallweit, R.S., Wood, L.C., 1982. The limits of resolution of zero-phase wavelets. *Geophysics*, 47(7), pp. 1035-1046. <https://doi.org/10.1190/1.1441367>.
- Kane, I., Mayall, M., McCaffrey, B., 2013. Internal architecture, bedforms, bedforms and geometry of turbidite channels. A conference held at the Geological Society, London, June 20-21st 2011. *Marine and Petroleum Geology*, 41(1), pp. 1-6. <https://doi.org/10.1016/j.marpetgeo.2012.10.004>.
-

- Kertzus, V., Kneller, B. 2009. Clinoform quantification for assessing the effects of external forcing on continental margin development. *Basin Research*, 21(5), 738-758. <https://doi.org/10.1111/j.1365-2117.2009.00411.x>.
- Liner, C., Zeng, J., Li, P.G.H.K.J., Califf, J., Seales, J., 2010. Application of Cutting-Edge 3D Seismic Attribute Technology to the Assessment of Geological Reservoirs for CO₂ Sequestration. University of Houston, Texas, pp. 85. <https://doi:10.2172/989106>.
- Machado, L.; Kowsmann, R.; Almeida Jr. W.; Murakami, C.; Schreiner, S; Miller, D.; Piauilino, P., 2004. Geometria da porção proximal do sistema deposicional turbidítico moderno da Formação Carapebus, Bacia de Campos; modelo para heterogeneidades de reservatório. *Boletim de Geociências da Petrobrás*, Rio de Janeiro, v. 12, n. 2, p.287-315.
- Machado, L.; Kowsmann, R.; Almeida Jr. W.; Murakami, C.; Schreiner, S; Miller, D.; Piauilino, P., 1997. Geometria da porção proximal do sistema deposicional turbidítico pleistocênico da Formação Carapebus, Bacia de Campos; Modelo para heterogeneidades de reservatório. In: *Simpósio sobre turbiditos*, 1., 1997, Rio de Janeiro. Anais... Rio de Janeiro: PETROBRAS. SEREC. CEN-SUD, p. 104-110.
- Machado, L.; Kowsmann, R.; Almeida Jr. W.; Murakami, C.; Schreiner, S; Miller, D.; Piauilino, P., 1998. Modern turbidite system in the Campos Basin: key to reservoir heterogeneities. In: *American Association of Petroleum Geologists. International Conference & Exhibition*, v. 1, 1998, Rio de Janeiro, Extended Abstracts...Tulsa, Oklahoma: American Association of Petroleum Geologists, 1998, p. 408-409.
- Machado, L.C.R., Miller, D.J., Castro, R.D., Almeida, C.W., Machado, R.P., Almeida Junior, W. 2001. O Trato de sistemas deposicionais marinhos: o caso do moderno da Bacia de Campos. In: *Seminário de Interpretação Exploratória*. 3., 2001, Natal, R.N. SINTEX. Rio de Janeiro: Petrobras. Depex, 2001. 4 p. 1 CD-ROM
- Machado, L.C.R., Viana, A.R., Kowsmann, R.O., Almeida Junior, W. The modern sediment drainage system of the Campos Basin, Brazil. In: *American Association of Petroleum Geologists. Annual Convention, 2002, Houston, Tex.*, [Proceedings of the]... Tulsa, Okla.: American Association of Petroleum Geologists, 2002. p. 9-12, 1 CD-ROM. Paper. 43011
- Marfurt, K.J., Gao, D., Barnes, A., Chopra, S., Corrao, A., Hart, B., James, H., Pacht, J., Rosen, N.C., 2011. Attributes: New Views on Seismic Imaging – Their Use in Exploration and Production. *SEPM Society for Sedimentary Geology*, 31st Annual Conference, v.31. <https://doi.org/10.5724/gcs.11.31>.
-

-
- Mayall, M., Jones, E., And Casey, M., 2006. Turbidite channel reservoirs—key elements in facies prediction and effective development: *Marine and Petroleum Geology*, v. 23, p. 821–841. <https://doi.org/10.1016/j.marpetgeo.2006.08.001>.
- Mayall, M., Stewart, I., 2000. The architecture of turbidite slope channels. In: Weimer, P., Slatt, R.M., Coleman, J., Rosen, N.C., Nelson, H., Bouma, A.H., Styzen, M.J., Lawrence, D.T. (Eds.), *Deep-Water Reservoirs of The World*. Gulf Coast Section SEPM 20th Bob F. Perkins Research Conference, pp. 578-586. <https://doi.org/10.5724/gcs.00.20>.
- McArdle, N.J., Ackers, M.A., 2012. Understanding seismic-thin bed responses using frequency decomposition and RGB blending. *First Break*, 30(12), pp. 57-65. DOI: 10.3997/1365-2397.2012022.
- McHargue, T., Pycrz, M.J., Sullivan, M.D., Clark, J.D., Fildani, A., Romans, B.W., Covault, J.A., Levy, M., Posamentier, H.W., Drinkwater, N.J., 2011. Architecture of turbidite channel systems on the continental slope: Patterns and predictions. *Marine and Petroleum Geology* 28(3), 728–743. <https://doi.org/10.1016/j.marpetgeo.2010.07.008>.
- Meiburg, E., Kneller, B, 2010. Turbidity currents and their deposits. *Annual Review of Fluid Mechanics*, 42, pp. 135–156. <http://dx.doi.org/10.1146/annurev-fluid-121108-145618>
- Mézerai, M.L., Faugères, J.C., A. Figueiredo Jr., A.G., Massé, L., 1993. Contour current accumulation off Vema Channel mouth, Southern Brazil basin: *Sedimentary Geology*, v. 82, no. 1–4, p. 173–188.
- Mitchum Jr., R.M., Vail, P.R., Sangree, J.B. 1977. Seismic Interpretation of Seismic Reflection patterns in Depositional Sequences. In: Payton, C.E. (Ed.). *Seismic Stratigraphy – Application to Hydrocarbon Exploration*. Tulsa, American Association of Petroleum Geologists, Memoir #26, pp.117-133.
- Mizusaki, A.M.P.; Thomaz Filho, A.; Valença, J.G. 1988. Volcano-Sedimentary Sequence of Neocomian age in Campos Basin (Brazil). *Revista Brasileira de Geociências*, v. 18, p. 247-251. <http://doi.org/10.25249/0375-7536.1988247251>.
- Mohriak, W.U.; Hobbs, R., Dewey, J.F., 1990. Basin-forming processes and the deep structure of the Campos Basin, offshore Brazil: *Marine and Petroleum Geology*, v. 7, n. 2, p. 94–122.
- Normark, W.R., Carlson, P.R., 2003. Giant submarine canyons: Is size any clue to their importance in the rock record? *Extreme Depositional Environments: mega end*
-

- members in geologic time. Geological Society of America, pp. 175-190. <https://doi.org/10.1130/0-8137-2370-1.175>.
- Normark, W.R., Piper, D.J.W. 1991. Initiation processes and flow evolution of turbidity currents; implications for the depositional record. In R. H. Osborne (Ed.), From shoreline to abyss; contributions in marine geology in honor of Francis Parker Shepard, p. 207–230. SEPM Special Publication 46.
- Partyka, G., Gridley, J., Lopez, J., 1999. Interpretational applications of spectral decomposition in reservoir characterization. *The Leading Edge*, 18(3), pp. 353-360. <http://dx.doi.org/10.1190/1.1438295>.
- Partyka, G.A., Bush, M.D., Garossino, P.G.A., Gutowski, P.R., 2011. Spectral Decomposition. In: Brown, A. (Ed.), Interpretation of three-dimensional seismic data, 7th edition, AAPG Memoir #42, SEG Investigations in Geophysics, No. 9. <http://dx.doi.org/10.1190/1.9781560802884>.
- Pellizon, M.M., 2005. Caracterização Das Unidades Sísmicas, Processos Sedimentares e Idade Do Cânion Almirante Câmara, Bacia De Campos. Programa de Pós-Graduação em Geologia e Geofísica Marinha, Universidade Federal Fluminense, Dissertação de Mestrado, 84 p.
- Pereira, M.J., Trindade, L.A.F., Gaglianone, P.C. 1984. Origem e evolução das acumulações de hidrocarbonetos na Bacia de Campos. In: SBG, Congresso Brasileiro de Geologia, 33, Rio de Janeiro, Anais, 10, p. 4763- 4777.
- Pérez-Gussinyé, M., Andrés-Martínez, M., Araújo, M., Xin, Y., Armitage, J., & Morgan, J. P., 2020. Lithospheric strength and rift migration controls on synrift stratigraphy and breakup unconformities at rifted margins: Examples from numerical models, the Atlantic and South China Sea margins. *Tectonics*, 39(12), e2020TC006255. <https://doi.org/10.1029/2020TC006255>
- Posamentier, H. W., Erskine, R. D., & Mitchum Jr, R. M. 1991. Models for submarine fan deposition within a sequence-stratigraphic framework. In P. Weimer, & M. H. Link, Seismic facies and sedimentary processes of submarine fans and turbidite systems (pp. 127-136). New York: Springer-Verlag.
- Posamentier, H.W., 2003. Depositional elements associated with a basin floor channel-levee system: case study from the Gulf of Mexico. *Marine and Petroleum Geology* 20, p. 677-690. <https://doi.org/10.1016/j.marpetgeo.2003.01.002>.
-

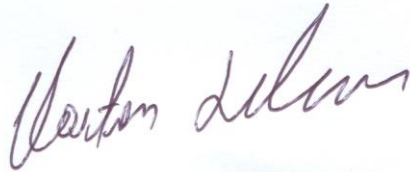
-
- Posamentier, H.W., Kolla, V., 2003. Seismic geomorphology and stratigraphy of depositional elements in deep-water settings. *Journal of Sedimentary Research* 73(3), pp. 367-388. <https://doi.org/10.1306/111302730367>.
- Qayyum, F., de Groot, P., 2012. Seismic Dip – A Key Attribute for Unlocking Reservoirs and Better Understanding Unconventional Resources. *American Oil and Gas Reporter*: Derby, KS, USA.
- Rangel, H.; Martins, F.; Esteves, F.; Feijó, F., 1994. Bacia de Campos: Carta Cronoestratigráfica. *Boletim de Geociências da Petrobras*, Rio de Janeiro, v. 8, n. 1, p. 203-219.
- Reis, A.T., 1994. O grupo sudeste de cânions e sua relação com a progradação do leque São Tomé – RJ. Rio de Janeiro. Observatório Nacional. Dissertação de Mestrado. 123p.
- Scarselli, N., 2020. Chapter 16 - Submarine landslides – architecture, controlling factors and environments. A summary. In: *Regional Geology and Tectonics: Principles of Geologic Analysis (Second Edition)*. N. Scarselli, J. Adam, D. Chiarella, D. G. Roberts, A. W. Bally (Eds.), Elsevier, v.1, pp. 417-439. <https://doi.org/10.1016/B978-0-444-64134-2.00015-8>.
- Schaller, H. Estratigrafia de Bacia de Campos. 1973. In: *Congresso Brasileiro de Geologia* 27, Aracaju. v. 3, p.247-258.
- Shepard, F.P., 1972. Submarine canyons. *Earth Science Reviews*, 8(1), pp. 1-12. [https://doi.org/10.1016/0012-8252\(72\)90032-3](https://doi.org/10.1016/0012-8252(72)90032-3).
- Shepard, F.P., 1981. Submarine canyons: multiple causes and long-time persistence. *AAPG Bull.* 65, pp. 1062-1077.
- Silva, A. 1992. Evolução sedimentar pós-miocênica na área nordeste da bacia de Campos. Rio de Janeiro, Universidade Federal do Rio de Janeiro. Dissertação de Mestrado. 120 p.
- Souza Cruz, C.E., 1995. Estratigrafia e sedimentação de águas profundas do Neogeno da Bacia de Campos. Tese de Doutorado. Universidade Federal do Rio Grande do Sul, 186 p.
- Stow, D.A.V., Mayall, M., 2000. Deep-water sedimentary systems: new models for the 21st century. *Marine and Petroleum Geology*, 17(2), pp.125-135. [http://doi:10.1016/S0264-8172\(99\)00064-1](http://doi:10.1016/S0264-8172(99)00064-1).
- Taner, M.T., Koehler, F., Sheriff, R.E., 1979. Complex Seismic Trace Analysis, *Geophysics*, 44(6), pp. 1041-1063. <http://dx.doi.org/10.1190/1.1440994>.
-

- Tingdahl K.M, 1999. Improving seismic detectability using intrinsic directionality. Earth Sciences Centre, Göteborg University, PhD Thesis, 42p.
- Tingdahl K.M., Bril, A.H., de Groot P.F., 2001. Improving seismic chimney detection using directional attributes. *Journal of Petroleum Science and Engineering*, v. 29: p. 205–211. [https://doi.org/10.1016/S0920-4105\(01\)00090-0](https://doi.org/10.1016/S0920-4105(01)00090-0).
- van der Meer, D.G., Scotese, C.R., Mills, B.J.W., Van den Berg van Saparoea, A.-P., Sluijs, A., van de Weg, R.M.B., 2022. Long-Term Phanerozoic Global Mean Sea Level: Insights from Strontium Isotope Variations and Estimates of Continental Glaciation. *Gondwana Research*, 111, p. 103-121. <https://doi.org/10.1016/j.gr.2022.07.014>.
- Vernejo, L., Trincherro, E. 2015, Application of amplitude volume technique attributes, their variations, and impact. *The Leading Edge*, 34(10), pp. 1246-1253. <http://dx.doi.org/10.1190/tle34101246.1>.
- Viana, A.R., Almeida, W., Machado, L.C. 1999. Different styles of canyon infill related to gravity and bottom current processes: examples from the upper slope of the SE Brazilian margin. 6th International Congress of the Brazilian Geophysical Society; Rio de Janeiro, Brasil. Rio de Janeiro: Sociedade Brasileira de Geofísica. Expanded Abstract 01499. <https://doi.org/10.3997/2214-4609-pdb.215.sbgf014>.
- Viana, A.R., Figueiredo Jr., A. G.; Faugères, J.C., Lima, J.A.M.; Gonthier E., Brehme I.; Zaragosi S., 2003. The São Tomé Deep-Sea Turbidite System (Southern Brazil Basin): Cenozoic Seismic Stratigraphy and Sedimentary Processes. *AAPG Bulletin*, V. 87, No. 5 (May 2003), pp. 873-894.
- Viana, A.R.; Faugères, J.C., Stow, D.A.V., 1998. Bottom-current-controlled sand deposits – a review of modern shallow – to deep-water environments. *Sedimentary Geology*, v.115, p. 53-80.
- Viana, A.R.; Kowsmann, R.O.; Castro, D.D., 1990. A discordância do Mioceno Médio/Superior: Um Marco regional no talude da bacia de Campos. In: 36º Congresso da Sociedade Brasileira de Geologia, Natal. Anais... Natal, SBG.1: p. 313-323.
- Winter, W.R.; Jahnert, R.J.; França, A.B., 2007. Bacia de Campos. *Boletim de Geociências da Petrobras*, Rio de Janeiro, v. 15, n. 2, p. 511-529.
- Yilmaz, Ö., 2001. Migration. In: Yilmaz, Ö., (Ed). *Seismic Data Analysis: Processing, Inversion and Interpretation of Seismic Data*, Investigations in Geophysics, no.10, 2001. p. 436-654. <https://doi.org/10.1190/1.9781560801580>.
-

ANEXO I
Título da Dissertação:
“MODELO DEPOSICIONAL E EVOLUÇÃO BASEADOS EM ATRIBUTOS SÍSMICOS DO CANYON ALMIRANTE CÂMARA: NEÓGENO AO QUATERNÁRIO DA BACIA DE CAMPOS, BRASIL”
Área de Concentração: Estratigrafia
Autor: Samuel Aparecido da Silva Corrêa
Orientador: Prof. Dr. Juliano Kuchle
Examinador: Prof. Dr. Claiton Marlon dos Santos Scherer
Data: 13/03/2024
Conceito: A
PARECER:
<p>A dissertação analisada trata-se de um trabalho de boa qualidade onde o autor constrói um modelo evolutivo deposicional do Canyon Almirante Câmara para o intervalo de estudo Neógeno-Quaternário, tendo como base exclusivamente dados sísmicos. Através da análise espectral e do uso combinado de atributos sísmicos complexos, foi possível mapear a geometria, elementos arquiteturais, distribuição, e padrão de preenchimento dos depósitos arenosos internos ao Canyon Almirante Câmara ao longo da sua evolução. Com base nisso, o mestrando propôs uma evolução estratigráfica do Canyon Almirante Câmara, estabelecendo-se quatro fases de erosão/ incisão e preenchimento de alta frequência, denotando uma evolução complexa de sobreposição de vários cânions ao longo do Neógeno e Quaternário. O capítulo do estado da arte está bem escrito, a bibliografia utilizada é bastante atualizada, cobrindo de forma satisfatória os diferentes assuntos abordados na dissertação. Entretanto, acredito que a temática abordada no estado da arte está bastante ampla, envolvendo desde uma revisão sobre canyon submarino até atributos sísmicos. Isso fez com que a revisão conceitual fosse superficial. Talvez a melhor forma de abordagem tivesse sido o autor ter focado na temática de canyon submarino, abordando de forma mais abrangente e profunda o tema.</p> <p>O artigo está bem escrito, sólido e inovativo, reconstruindo o modelo deposicional e o padrão de preenchimento de Canyon Almirante Câmara. Os objetivos são claros e bem definidos e a metodologia adequada, estando muito bem detalhada no texto (abrange 10 páginas). As figuras são de excelente qualidade, apresentando um caráter elucidativo e complementar ao texto, sendo um dos pontos fortes da dissertação. A definição das superfícies limítrofes das diferentes fases de preenchimento do canyon, bem como as suas anatomias e as características deposicionais associadas, estão bem fundamentadas e as interpretações estão de uma forma geral sustentadas nos dados apresentados. Cabe, entretanto, ressaltar como ponto fraco do modelo o fato de não existir nenhum dado de rocha associado para dar uma sustentação maior as interpretações litológicas efetuadas. Não existiam poços testemunhados que</p>

perfurassem o canyon? Quais as litologias desses poços? Eram arenitos conforme prevê o modelo sísmico? Outra questão altamente especulativa, refere-se a amarração das quatro superfícies (EBS, ACS1, ACS2 e ACS3) identificadas a fases de rebaixamento eustático, tendo sido atribuídas idades de 13, 2 Ma, 6,8Ma, 70Ka e 18Ka, respectivamente. Entretanto, os autores não mostram datações bioestratigráficas do intervalo de estudo que suporte minimamente essas interpretações.

Como conclusão, considero a dissertação de mestrado de muito boa qualidade, estando o Samuel e o orientador, Dr. Juliano Kuchle, de parabéns.




Assinatura:

Data: 13/03/2024

Ciente do Orientador:


Ciente do Aluno:

ANEXO I	
Título da Dissertação:	
“MODELO DEPOSICIONAL E EVOLUÇÃO BASEADOS EM ATRIBUTOS SÍSMICOS DO CANYON ALMIRANTE CÂMARA: NEÓGENO AO QUATERNÁRIO DA BACIA DE CAMPOS, BRASIL”	
Área de Concentração: Estratigrafia	
Autor: Samuel Aparecido da Silva Corrêa	
Orientador: Prof. Dr. Juliano Kuchle	
Examinadora: Dra. Francyne Bochi do Amarante	
Data: 12/03/2024	
Conceito: A	
PARECER:	
<p>O trabalho do Samuel está excelente. Além de estar muito bem escrito, o aluno cumpriu os objetivos propostos no trabalho, aplicando uma metodologia adequada e sofisticada. As figuras são pertinentes e ilustram muito bem os resultados e discussões (e são lindas!). O tema estudado é relevante atualmente e tenho certeza que o artigo será aceito para publicação em uma revista internacional. Minha única crítica é que faltaram dados de poços para confirmar as interpretações sedimentológicas de preenchimento do cânion nos resultados e discussões (item 5.8.3). De qualquer forma, mesmo excluindo-se as interpretações sedimentológicas, o trabalho é importante e apresenta um grande avanço no entendimento da evolução do Canyon Almirante Câmara.</p>	
Assinatura: 	Data: 12 de março de 2024
Ciente do Orientador:	
Ciente do Aluno:	

ANEXO I
Título da Dissertação:
“MODELO DEPOSICIONAL E EVOLUÇÃO BASEADOS EM ATRIBUTOS SÍSMICOS DO CANYON ALMIRANTE CÂMARA: NEÓGENO AO QUATERNÁRIO DA BACIA DE CAMPOS, BRASIL”
Área de Concentração: Estratigrafia
Autor: Samuel Aparecido da Silva Corrêa
Orientador: Prof. Dr. Juliano Kuchle
Examinadora: Dra. Junia Casagrande
Data: 01/04/2024
Conceito: B
PARECER:
<p>A monografia de dissertação de mestrado do candidato Samuel Aparecido da Silva Corrêa apresenta as condições necessárias para seu título de mestre em Geociências. O tema de pesquisa é relevante e traz ineditismo em relação à base de dados e ao modelo deposicional proposto. A metodologia de pesquisa adotada e a base de dados são adequados para atingir os objetivos apresentados. Em especial, a metodologia de mapeamento sísmico e análise de atributos sísmicos foi executada de maneira robusta, com bom embasamento teórico, assim, atingindo plenamente os objetivos específicos da pesquisa.</p> <p>Em relação ao objetivo geral da pesquisa “construir um modelo evolutivo deposicional do Canyon Almirante Câmara” considero que o mesmo foi atingido através da identificação e caracterização das diferentes fases evolutivas do canyon. Entretanto, julgo que a pesquisa se favoreceria de uma revisão mais aprofundada da literatura específica sobre sistemas deposicionais de águas profundas, principalmente no que diz respeito à gênese dos tipos de depósitos e evolução estratigráfica de canyons e canais submarinos. Isto teria auxiliado o autor a realizar interpretações mais assertivas e contextualizadas em relação aos processos deposicionais e erosivos associados aos depósitos identificados na análise de atributos sísmicos (mais detalhes no PDF anotado) evitando, assim, algumas deficiências conceituais.</p> <p>Em relação ao objetivo específico de correlacionar as superfícies mapeadas à uma curva eustática global, julgo que o objetivo foi atingido. O autor reconhece que a metodologia aplicada é simplificada, mas reforço aqui que para ser cientificamente aceita, apesar de especulativa, necessita de maior respaldo da literatura. A geração de superfícies erosivas em canyons não é necessariamente controlada por variações relativas do nível do mar. Desta forma, o autor deve ponderar todas as possibilidades e defender sua hipótese.</p> <p>Outras sugestões de melhoria:</p>

- O capítulo 3 (Síntese de resultados), apresenta considerações sobre a discussão final da pesquisa, entretanto isto é mostrado antes dos resultados serem apresentados ao leitor. Sendo assim, esta seção poderia ser deslocada para o final da dissertação como um capítulo de considerações finais.
- Atentar para sentenças em que o autor traz dados, mas não cita a literatura (ver pdf anotado).
- Na seção “Geological setting” do artigo científico sugiro revisar a literatura utilizada a fim de corrigir algumas inconsistências terminológicas e re-escrever o parágrafo sobre a tectônica de sal (ver pdf anotado).
- Atentar para interpretações feitas sem mostrar as devidas evidências que suportam estas interpretações (por exemplo, sugerir que a morfologia do canyon é controlada por falhas e citar uma figura onde isso não é demonstrado, ver no PDF).
- Na parte de metodologia do artigo científico citar qual tipo de dado sísmico está sendo utilizado (PSDM ou PSTM) e calcular a resolução vertical do dado.
- A análise estratigráfica foi baseada primeiramente na análise de atributos sísmicos em planta. Entretanto, seções sísmicas transversais e longitudinais ao canyon poderiam trazer maior robustez ao modelo estratigráfico proposto. As seções sísmicas apresentadas devem ser incluídas em um mapa de localização.
- Os rótulos nos mapas de atributos do artigo científico não estão muito legíveis, sugiro aumentar a fonte.
- Relações com anomalias de amplitude e litologia, e conteúdo de frequência com espessuras, são apresentadas. Como não há dado de poço para comprovar essas relações, sugiro embasar essas interpretações com exemplos da literatura.
- O controle estrutural do canyon está descrito na seção de discussão, entretanto, se trata de resultados. Sugiro criar uma nova seção nos resultados a cerca deste tópico.
- O artigo científico está, no geral, bem escrito, entretanto, se beneficiaria de revisão do inglês para substituição de alguns termos e re-escrita em alguns parágrafos para maior clareza (ver pdf anotado).
- Atentar para um vínculo mais direto com o texto e a figura (nem sempre a figura mostra claramente o que o autor cita no texto, ver pdf anotado).
- Atentar para não apresentar interpretações antes das evidências ou embasamento teórico no texto (ver pdf anotado).

Documento assinado digitalmente

Assinatura: 

JUNIA CASAGRANDE

Data: 01/04/2024 17:21:10-0300

Verifique em <https://validar.iti.gov.br>

Data:01/04/2024

Ciente do Orientador:

Ciente do Aluno: